Dr-1195

ANL-75-3

Part I

1
3-10-75

ANL-75-3

Part I

RADIOLOGICAL AND ENVIRONMENTAL RESEARCH DIVISION ANNUAL REPORT

Radiation Physics

July 1973—June 1974

ARGONNE NATIONAL LABORATORY, ARGONNE, ILLINOIS

Prepared for the U. S. ENERGY RESEARCH AND DEVELOPMENT ADMINISTRATION under Contract W-31-109-Eng-38

DISCLAIMER

The facilities of Argonne National Laboratory are owned by the United States Government. Under the terms of a contract (W-31-109-Eng-38) between the U. S. Energy Research and Development Administration, Argonne Universities Association and The University of Chicago, the University employs the staff and operates the Laboratory in accordance with policies and programs formulated, approved and reviewed by the Association.

MEMBERS OF ARGONNE UNIVERSITIES ASSOCIATION

The University of Arizona
Carnegie-Mellon University
Case Western Reserve University
The University of Chicago
University of Cincinnati
Illinois Institute of Technology
University of Illinois
Indiana University
Iowa State University
The University of Iowa
Kansas State University
The University of Kansas
Loyola University
Marquette University
Michigan State University
The University of Michigan
University of Minnesota
University of Missouri
Northwestern University
University of Notre Dame
The Ohio State University
Ohio University
The Pennsylvania State University
Purdue University
Saint Louis University
Southern Illinois University
The University of Texas at Austin
Washington University
Wayne State University
The University of Wisconsin

Printed in the United States of America
Available from
National Technical Information Service
U. S. Department of Commerce
5285 Port Royal Road
Springfield, Virginia 22161
Price: Printed Copy $5.45; Microfiche $2.25

ANL-75-3
Part I
Biology and
Medicine
UC-48

ARGONNE NATIONAL LABORATORY
9700 South Cass Avenue
Argonne, Illinois 60439

RADIOLOGICAL AND ENVIRONMENTAL RESEARCH DIVISION ANNUAL REPORT

Radiation Physics

July 1973 through June 1974

R. E. Rowland, Division Director
Mitio Inokuti, Section Head

Preceding Report: ANL-8060, Part I, July 1972–June 1973

FOREWORD

In the past year, the Radiation Physics Section has enhanced its strength considerably. With improved technical capabilities in all three areas — electron scattering by molecules, photoabsorption and photoionization processes, and pertinent theoretical studies — we now approach closer than ever before our eventual goal: the elucidation of elementary mechanisms of radiation actions.

A highlight of the electron-scattering program is the initial operation of the electron energy-loss spectrometer (as described in paper 13 of this report). After some effort directed toward its technical perfection, this apparatus will generate important data for years to come. Another apparatus that uses a trapped-electron technique has exhibited unprecedented versatility in the study of electron-molecule collisions; different modes of operation of this single instrument enable one to study resonances in low-energy electron-molecule interactions (papers 30–32, 35, and 36), to measure the excitation functions of individual excited states (paper 33), and even to clarify the intricacies of ionizing collisions of electrons near the ionization threshold (paper 34).

Studies on photon interactions with molecules have likewise been successful. The absolute measurement of photoabsorption and photoionization cross sections in the far vacuum-ultraviolet region is now well under way (papers 17 and 18). We consider it a unique advantage to conduct both electron energy-loss analyses and photoabsorption measurements in the same group; cross-checking of the oscillator strength from the two independent sources often helps us assess the data reliability and sometimes offers a new insight into the physics involved (papers 14–18). The photoelectron analysis has produced significant results on partial photoionization cross sections (papers 21 and 22).

Theoretical studies have been extended in several ways. First, there were serious attempts to improve theories that connect various radiation-chemical yields to basic cross-section data (papers 1–3). Second, analyses

of the secondary-electron data (papers 4–6) now make possible a realistic assessment of this crucial element in the theoretical prediction of primary yields. Third, the application of a multiple-scattering method to molecular electronic continua has demonstrated its power in systematic calculations of cross sections for photoionization and electron scattering of molecules (papers 28 and 29). Finally, we have extended the scope of our research to include the spectroscopy of highly stripped ions (paper 41), a subject of increasing importance because of the advent of heavy-ion accelerators and also because of its relevance to controlled thermonuclear research.

We are proud of having played major roles in two important meetings. Together with the Health Physics Division of the Oak Ridge National Laboratory, we organized the Symposium on the Jesse Effect and Related Phenomena, Gatlinburg, Tennessee, November 1973. The Symposium honored Dr. W. P. Jesse, a pioneer in radiation physics and an earlier head of the group from which this Section has evolved, and provided an opportunity for fruitful discussion among workers in diverse fields ranging from basic radiation physics to vacuum-ultraviolet laser technology. We were especially honored to have Dr. Jesse at the Symposium, but were saddened by his death only about three months later. A full record of the Symposium was published in Radiation Research, August 1974. The Section also helped to organize a full-day symposium on the basic physics of the interactions with matter as a part of the Vth International Congress of Radiation Research, Seattle, Washington, July 1974. The symposium was dedicated to the memory of the late Professor R. L. Platzman, who was an early leader of our group, and whose tradition in radiation research will continue to influence our activities for years to come.

****

The papers in this report are ordered according to subjects treated. Papers 1–3 deal with theories of primary yields, 4–6 concern secondary-electron spectra, and 7–16, collisions of fast charged particles. Papers 17–27 mainly treat photoionization processes, papers 28–36, low-energy electron collisions, papers 37–40, energy transfer from an excited species to another molecule, and papers 41–47, other problems.

TABLE OF CONTENTS

Radiation Physics

Mitio Inokuti, Section Head

THEORY OF THE IONIZATION YIELD IN GASES UNDER ELECTRON IRRADIATION*

Mitio Inokuti

The total number $N_i(T)$ of ionizations that an incident electron of kinetic energy T causes in a pure gas obeys an integral equation known as the Fowler equation. The present work shows that its solution closely approximates $N_i(T) = (T - U)/W_a$ for T exceeding several multiples of the first ionization energy I, where U and W_a are constants having the energy dimension. Simple formulas express U and W_a in terms of various cross sections for electron inelastic collisions with a gas molecule. In particular, $U - I$ represents the average kinetic energy of a subionization electron.

Introduction

The total ionization in a gas plays a dual role in radiation research. First, the possibility of its accurate measurements makes the total ionization an important and now well-recognized basis of dosimetry.[1-3] Second, its microscopic interpretation provides an excellent opportunity of linking radiation physics and chemistry with basic atomic physics. Ions are a major product from any gas under irradiation, and chiefly (though not exclusively) stem from initial processes of radiation action, i.e., from individual collisions of energetic particles with molecules.[4] Thus, quantitative prediction of the total ionization yield represents a prototype study in our Section's endeavors toward full elucidation of initial radiation-chemical yields in general.[5]

Suppose an electron of kinetic energy T enters a gas and produces a total of $N_i(T)$ electrons until all electrons become thermalized. Then the ionization yield may be expressed in terms of the ratio $W(T) = T/N_i(T)$, the average energy absorbed per ion pair formed. Any theoretical calculation must include[4] two ingredients: first, the determination of a set of cross sections for all energy-loss processes and secondary-electron production upon electron collision with molecules, and second, some method of bookkeeping of various

*Part of this work was presented at the Vth International Congress of Radiation Research, Seattle, July 1974 [abstract published in Radiat. Res. 59, 230 (1974)].

ionization events.

As for the first ingredient, recent years have seen considerable progress in the physics of electron collisions, although our knowledge remains incomplete and imprecise in many respects. Indeed, much of our Section's effort is being devoted to obtaining extensive and reliable data of electron-collision cross sections from both theory and experiment. Work on the second ingredient has been continuing for many years since the initial papers by Bethe[6] and by Bagge[7] but has barely attained the richness and maturity that should match the current knowledge of pertinent cross-section data. Enhanced efforts toward a bookkeeping solution, therefore, seem to be urgent, not only for a balanced development of our understanding of radiation effects, but also for a realistic assessment of the accuracy with which cross-section data should be known for this purpose.

With the above views in mind, our Section has recently embarked on a series of studies on the theory of W values.[8,9] This article describes an elementary method of bookkeeping and the succeeding article[8] presents systematics of W for monatomic gases uncovered by use of the method.

An Approximate Solution of the Fowler Equation in the Simplest Case

The most straightforward method of bookkeeping uses an integral equation for $N_i(T)$ due to Fowler.[10] Let $\sigma_i(T)$ be the cross section for an electron with kinetic energy T ionizing a molecule in a gas which we assume to be pure. The ionization may result from various values of energy transfer E from an electron to the molecule. Suppose for simplicity that the molecule has a single ionization-threshold energy I, and that the transfer of energy $E > I$ to the molecule always results in an ion, a primary electron now with energy $T - E$, and a secondary electron with energy $E - I$. The (differential) cross section $d\sigma_i(E,T)/dE$ for energy transfer E from an electron of initial energy T characterizes that ionization process. Obviously we have

$$\sigma_i(T) = \int_I^{\frac{1}{2}(T+I)} \frac{d\sigma_i(E,T)}{dE}\, dE , \qquad (1)$$

where the upper limit of integration implies the customary convention that one calls the more energetic of the two electrons the primary, and the less energetic the secondary; in classical terms, when the incident electron transfers most of its energy to an atomic electron, the former nominally becomes the "secondary" and the latter becomes the "primary." Let $\sigma_n(T)$ be the cross section for an electron with kinetic energy T exciting a discrete state n whose excitation energy (measured from the ground state) is E_n. The sum

$$\sigma_{tot}(T) = \sigma_i(T) + \Sigma_n \sigma_n(T) \tag{2}$$

is the total inelastic-scattering cross section for an electron of kinetic energy T. For convenience, we introduce probabilities of each event per inelastic collision:

$$p_n(T) = \sigma_n(T)/\sigma_{tot}(T) \ , \tag{3}$$

$$p_i(T) = \sigma_i(T)/\sigma_{tot}(T) \ , \tag{4}$$

and

$$dp_i(E,T)/dE = \left[d\sigma_i(E,T)/dE\right] /\sigma_{tot}(T) \ . \tag{5}$$

Obviously, one has

$$\Sigma_n p_n(T) + p_i(T) = 1 \ . \tag{6}$$

Then, elementary consideration shows that $N_i(T)$ satisfies the Fowler equation

$$N_i(T) = p_i(T) + \Sigma_n p_n(T)\, N_i(T - E_n) + \int_I^{\frac{1}{2}(T+I)} dE \ \frac{dp_i(E,T)}{dE} \left[N_i(T-E) + N_i(E-I)\right] \ . \tag{7}$$

As soon as the coefficients $p_n(T)$, $p_i(T)$, and $dp_i(E,T)/dE$ are known, one can in principle solve Eq. (7) by starting with

$$N_i(T) = 0 \qquad \text{for } T < I \ , \tag{8}$$

and by ascending in T. Thus, in the initial step, one finds that

$$N_i(T) = p_i(T) \qquad \text{for } I \le T < I + E_1 \ , \tag{9}$$

where E_1 is the first excitation potential of the gas.

The foregoing formulation rigorously applies to a gas with a single ionization potential; modifications to account for pre-ionization, several ionization potentials, and multiple ionization are straightforward though somewhat cumbersome to describe in full detail, as we shall see in the next section. In the present section we shall presume that the single-ionization schematization [Eq. (7)] is adequate, at least as a first approximation.

Equation (7) has been numerically solved in several examples.[11-19] Inspection of these authors' results impresses one with a few striking features of the solution $N_i(T)$ as a function of incident energy T, as seen in an example for He (Figure 1). It is true that $N_i(T)$ for T not greatly exceeding I shows in general an erratic trend that clearly reflects a complicated behavior of the cross sections, $\sigma_i(T)$ and $\sigma_n(T)$. But $N_i(T)$ closely approximates a linear function of T as soon as T exceeds a few multiples of I, and the asymptotic slope corresponds to W^{-1} at high T. Furthermore, if one extrapolates the high-T (asymptotic) linear behavior back to lower T, one invariably finds that the asymptote intercepts the T axis at some point $T = U > 0$. In the example of He, shown in Figure 1, the intercept energy U is about 12 eV.

Then it is natural to look for an approximate analytical solution of the form

$$N_i(T) \cong (T - U)/W_a \tag{10}$$

for T exceeding several multiples of I, where W_a and U are constants (both having the dimension of energy) to be determined optimally, i.e., so that the right-hand side of Eq. (10) may best approximate the true solution $N_i(T)$ in some sense.

If one inserts Eq. (10) into Eq. (7), one gets

$$(T - U)/W_a = p_i(T) + \Sigma_n (T - U - E_n) p_n(T)/W_a$$

$$+ (T - I - 2U) p_i(T)/W_a \ . \tag{11}$$

Rearranging terms and taking note of Eq. (6), one can readily solve the above equation for W_a to obtain

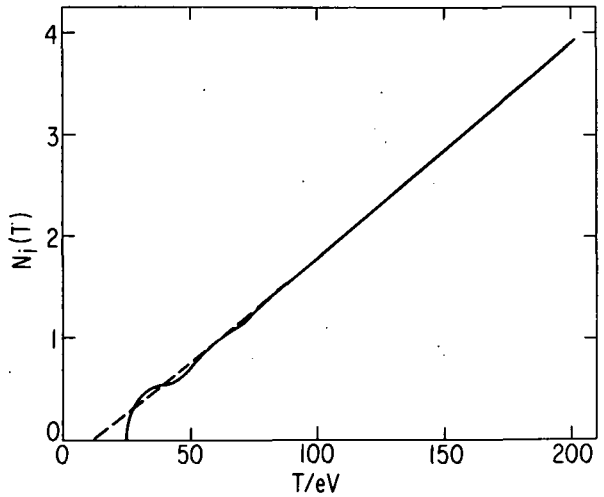

FIG. 1.--An example of the numerical solution of the Fowler equation. The number $N_i(T)$ of ions produced in helium by an electron of initial energy T is plotted as a function of T. The data were taken from Miller.[14] The broken straight line shows an extrapolation of the asymptotic behavior and intercept with the horizontal axis at about $T = U = 12$ eV.

$$W_a = \Sigma_n E_n p_n(T)/p_i(T) + I + U \ . \tag{12}$$

Admittedly this equation is not rigorously valid because the right-hand side depends upon T, whereas W_a is a constant by assumption. In other words, Eq. (10) does not represent an exact solution. Yet this logical inconsistency is not at all serious in practice. The T dependence of the first term at sufficiently great T is very weak. More precisely, it is given for an electron of velocity $v = \beta c$ according to the Bethe theory[6,20,21] by

$$\frac{\Sigma_n E_n p_n(T)}{p_i(T)} = \frac{R f_{ex}\{\ln[\beta^2/(1-\beta^2)] - \beta^2\} + \tilde{C}_{ex}}{M_i^2\{\ln[\beta^2/(1-\beta^2)] - \beta^2\} + C_i} \ , \tag{13}$$

where f_{ex} is the total oscillator strength for discrete excitation, M_i^2 is the squared dipole-matrix element for ionization measured in units of the squared Bohr radius, R is the Rydberg energy, and $\tilde{C}_{ex}$ and C_i are constants. Thus, it is justifiably understood hereafter that the right-hand side of Eq. (12) is to be evaluated at a great value of T, say greater than 10 keV, and it may be assumed that the result is insensitive to the T value.

More importantly, Eq. (12) remains incomplete as a prescription for evaluating W_a until one knows how to determine U. A method of determination of U emerges from the following critique of our procedure.

So long as T greatly exceeds I (and, therefore, every E_n), as well as all E at which $dp_i(E,T)/dE$ is appreciable, it is reasonable to insert the assumed asymptotic form Eq. (10) into terms $N_i(T)$, $N_i(T-E_n)$, and $N_i(T-E)$ in Eq. (7). But it is an unreasonable approximation to use Eq. (10) in the last term $N_i(E-I)$ of Eq. (7) because the argument $E-I$ is not necessarily much greater than I, but may even be smaller than I. Thus, our use of Eq. (10) in Eq. (11) must have caused some errors, chiefly originating in the last term $N_i(E-I)$; the major inconsistency that resulted from the use of Eq. (10) in Eq. (7) is the difference

$$D = \int_I^{\frac{1}{2}(T+I)} dE \, \frac{dp_i(E,T)}{dE} \, N_i(E-I)$$

$$- \int_I^{\frac{1}{2}(T+I)} dE \, \frac{dp_i(E,T)}{dE} \, (E-I-U)/W_a \, . \qquad (14)$$

To obtain an estimate of D, one should first recall Eq. (8) and recognize that the first integral really extends over the interval $2I < E < \frac{1}{2}(T+I)$. In this interval it should not be grossly wrong to replace $N_i(E-I)$ by $(E-I-U)/W_a$ because the argument $E-I$ at least exceeds I (though not many multiples of I). Thus, a first estimate of D is

$$D_1 = - \int_I^{2I} dE \, \frac{dp_i(E,T)}{dE} \, (E-I-U)/W_a \, . \qquad (15)$$

Demanding that $D_1 = 0$ leads to

$$U = E_{i1} - I \, , \qquad (16)$$

where

$$E_{i1} = \int_I^{2I} dE\, E\, \frac{dp_i(E,T)}{dE} \Big/ \int_I^{2I} dE\, \frac{dp_i(E,T)}{dE} \tag{17}$$

is the average energy transfer for those ionizing collisions for which $I < E < 2I$, i.e., for which the ejected electron is energetically incapable of further ionization. Substituting Eq. (16) into Eq. (12), one obtains

$$W_a = \Sigma_n E_n p_n(T)/p_i(T) + E_{i1} \ , \tag{18}$$

an expression to be used in the numerical work of the next report.[8]

Parenthetically, it may be noted that the use of Eq. (9) in a similar argument gives a better estimate of D as

$$D_2 = -\int_I^{2I+E_1} dE\, \frac{dp_i(E,T)}{dE}\, (E-I-U)/W_a + \int_{2I}^{2I+E_1} dE\, \frac{dp_i(E,T)}{dE}\, p_i(E-I) \ . \tag{19}$$

Again demanding that $D_2 = 0$, one obtains

$$U = E'_{i1} - r W_a - I \ , \tag{20}$$

where

$$E'_{i1} = \int_I^{2I+E_1} dE\, E\, \frac{dp_i(E,T)}{dE} \Big/ \int_I^{2I+E_1} dE\, \frac{dp_i(E,T)}{dE} \ , \tag{21}$$

and

$$r = \int_{2I}^{2I+E_1} dE\, \frac{dp_i(E,T)}{dE}\, p_i(E-I) \Big/ \int_I^{2I+E_1} dE\, \frac{dp_i(E,T)}{dE} \ . \tag{22}$$

Combining Eq. (20) with Eq. (12) and solving for W_a, we obtain

$$W_a = (1+r)^{-1} [\Sigma_n E_n p_n(T)/p_i(T) + E'_{i1}] \ . \tag{23}$$

This expression is undoubtedly more accurate than Eq. (18) but is far more complicated to use numerically. I shall defer further treatment of Eqs. (20)-(23) until another occasion.

Instead, let us examine some consequences of the first estimate given by Eqs. (16)–(18).

To test the accuracy of my theory I have evaluated U of Eq. (16) using the current data of $dp_i(E,T)/dE$, mostly summarized by Kim.[22,23] The resulting U may be compared with the intercept of the asymptotic $N_i(T)$ obtained by various authors through numerical solution of Eq. (7). Table 1 presents this comparison. The satisfactory agreement of the U values from Eq. (17) with the literature values demonstrates the correctness of the theory. [Notice also that U values show no obvious correlation with I. Thus, the relation $N_i(T) \propto T - I$, casually alluded to by Erskine[12] and also claimed by Herring and Merzbacher,[13] is grossly misleading. Presumably that claimed relation is a consequence of the particular set of cross-section data used by these authors.[13] Knipp et al.[11] certainly considered Eq. (10) as an approximate solution but failed to identify the optimal choice of U.]

Equation (18) permits a simple intuitive interpretation. The first term on the right-hand side obviously is the average energy wasted per ion pair in exciting discrete levels of gaseous molecules. The second term, E_{i1}, represents the average energy needed in an ionization event. Clearly an electron must spend at least I to cause an ionization: the difference $E_{i1} - I = U$ is the average kinetic energy of an electron no longer capable of further ionization and closely approximates (though slightly exceeds) the average energy of a subexcitation electron. The recent work of Douthat[24] and of Fano and Spencer[25] corroborates this interpretation.

A relation of my theory with Fano's pioneering work[26] must be pointed out. Through an ingenious and intuitive argument he wrote down as an expression for W at high T [his Eq. (3)]

$$W_F = \{\Sigma_n E_n p_n(T) + E_{i1} p_{i1}(T) + I p_{i2}(T)\}/p_i(T) , \tag{24}$$

where

$$p_{i1}(T) = \int_I^{2I} dE \, \frac{dp_i(E,T)}{dE} \tag{25}$$

is the probability that an ionizing collision creates a secondary electron that is no longer capable of further ionization, and

$$p_{i2}(T) = p_i(T) - p_{i1}(T) . \tag{26}$$

TABLE 1. Values of U in Eq. (10)

Species	U in eV evaluated by Eqs. (16) and (17)	Numerical solution of the Fowler equation U in eV	Author(s)
H	3	4	Knipp et al.[11] Dalgarno and Griffing[15]
He	9.5	12	Miller[14] Douthat[24]
H_2	14	15	Jones[17] Gerhart[18]
Ar	11	11	Eggarter[19]

It is appropriate to compare Fano's W_F with W_a because both are supposed to give the asymptotic W value at high T. Note that Eq. (24) can be recast in the form

$$W_F = \Sigma_n E_n p_n(T)/p_i(T) + I + (E_{i1} - I)\, p_{i1}(T)/p_i(T) \ . \tag{27}$$

Comparison with Eqs. (12) and (16) shows that Fano's expression corresponds to choosing for U

$$U_F = (E_{i1} - I)\, p_{i1}(T)/p_i(T) \ , \tag{28}$$

By the definition of $p_{i1}(T)$ [Eq. (25)] U_F is always smaller than U of Eq. (16), and, therefore, W_F is also smaller than W_a of Eq. (18). In other words, Fano's theory underestimates the energy wasted in producing subexcitation electrons. Indeed, his result for He (38 eV) is considerably smaller than the accurate values 45 to 46 eV obtained by Miller[14] and by Alkhazov.[16] To avoid misunderstanding, I note here that Fano never discussed the intercept U of the asymptotic $N_i(T)$ with the T axis; Eq. (27) for U_F was given solely for close comparison with the present treatment.

Finally, a practical significance of the present result may be indicated. Equation (10) gives an average energy per ion pair

$$W(T) \cong (1 - U/T)^{-1} W_a \ , \tag{29}$$

an expression for T-dependent W valid at $T >> I$. Evaluation of U by Eqs. (16) and (17) is straightforward once the secondary-electron data for $dp_i(E,T)/dE$ are at hand; otherwise U can be reasonably inferred from photoionization cross sections by Kim's method.[22,23] If one substitutes W_a in Eq. (29) an experimental W value at high T (which is known for many gases), then one obtains a prediction for W(T) at lower values at T, i.e., for a quantity of vital importance that is beginning to be experimentally accessible only recently.[27-29]

Further work in this direction is in progress.

The Fowler Equation in a Generalized Form

The treatment in the previous Section was limited, deliberately for clarity of presentation, to an ideal gas having a single ionization energy. For any real gas, one must face at least three complications: a) the dissociation occurring in competition with pre-ionization (or autoionization) as emphasized by Platzman,[30,31] b) the presence of many ionization thresholds corresponding to different (vibrational and electronic) states of an ion, and c) the possibility of multiple ionization in a single electron collision. Let us consider how these complications can be incorporated into the Fowler equation and its approximate solution.

It is simple to account for complication a). For this purpose, any non-ionizing collision may be grouped together with discrete excitations because it gives rise to no new electron. Therefore, one can simply incorporate all non-ionizing collisions into the second term $\Sigma_n p_n(T)\, N_i(T-E_n)$ on the right-hand side of Eq. (7). The only new features are that E_n may now exceed the first ionization energy and that the summation may, in effect, include integration over a continuous spectrum of E_n. This modification clearly necessitates no appreciable change of the treatment of the last Section, and, therefore, we merely stipulate in what follows that the term $\Sigma_n p_n(T)\, N_i(T-E_n)$ includes contributions from all non-ionizing collisions. (Likewise, contributions from pure vibrational and rotational excitations may be included, but they are usually negligible at high T.)

It is also easy to see the influence of complication b) upon the Fowler equation. Different ionization thresholds I_k, where $k = 1,2,3,\ldots$, merely cause the third (integral) term to be replaced by a simple sum of terms having the same analytic structure.

Complication c), in contrast, is somewhat more tedious to treat. Suppose that an electron of kinetic energy T collides with a molecule and that three electrons of energies T_1, T_2, and T_3 emerge with probability $\pi^{(2)}(T_1,T_2,T_3;T)$ per inelastic collision. Let the threshold energy for the

double-ionization process be $I^{(2)}$. Then the total double-ionization probability $p_i^{(2)}(T)$ per inelastic collision is

$$p_i^{(2)}(T) = \iiint dT_1\, dT_2\, dT_3\, \pi^{(2)}(T_1, T_2, T_3; T) \tag{30}$$

where the integral is taken with the condition

$$T_1 + T_2 + T_3 = T - I^{(2)} . \tag{31}$$

The same process gives rise to new terms of the form

$$2p_i^{(2)}(T) + \iiint dT_1 dT_2\, dT_3\, \pi^{(2)}(T_1, T_2, T_3; T)\,[N_i(T_1) + N_i(T_2) + N_i(T_3)]$$

in the right-hand side of the Fowler equation, Eq. (7).

With the above preamble it may be appropriate now to introduce a generalized Fowler equation that incorporates complication a) implicitly, as well as complications b) and c) explicitly. Suppose that an electron of energy T causes an m-fold ionization resulting in m+1 electrons having energies $T_1, T_2, \ldots, T_{m+1}$. This m-fold ionization may leave the resulting ion in any of its quantum states to be designated by label k; each ion state thus has an ionization threshold $I_k^{(m)}$. The probability (per inelastic collision) of the above-described process may be written as $\pi_k^{(m)}(T_1, \ldots T_{m+1}; T)$. The total probability (per inelastic collision) of m-fold ionization leaving the ion in its kth state is then

$$\int \ldots \int dT_1 \ldots dT_{m+1} \pi_k^{(m)}(T_1, \ldots T_{m+1}; T) = p_{ik}^{(m)}(T) . \tag{32}$$

The total probability of m-fold ionization regardless of the ion state is

$$\sum_k p_{ik}^{(m)}(T) = p_i^{(m)}(T) . \tag{33}$$

Finally, the gross ionization, or the expectation value of the number of ejected electrons per inelastic collision is

$$\sum_m m\, p_i^{(m)}(T) = p_{ig}(T) , \tag{34}$$

and the total probability of an ionization event per inelastic collision is

$$\sum_m p_i^{(m)}(T) = p_i(T) \ . \tag{35}$$

Then, the Fowler equation in a general form becomes

$$N_i(T) = \sum_m p_i^{(m)}(T) + \sum_n p_n(T)\, N_i(T - E_n)$$

$$+ \sum_m \sum_k \int dT_1 \ldots \int dT_{m+1} \pi_k^{(m)}(T_1, \ldots, T_{m+1}; T) \sum_{\mu=1}^{m+1} N_i(T_\mu) \tag{36}$$

where the $(m+1)$-fold integral in the last term is subject to the energy-conservation relation

$$\sum_{\mu=1}^{m+1} T_\mu = T - I_k^{(m)} \ . \tag{37}$$

Inserting again Eq. (10) into Eq. (36) and using Eqs. (6), (32), (33), (34), (35), and (37), one obtains

$$W_a = \sum E_n p_n(T)/p_{ig}(T) + I_{AV} + U \ , \tag{38}$$

where an average ionization energy I_{AV} is defined by

$$I_{AV} = \sum_m \sum_k I_k^{(m)} p_{ik}^{(m)} / \sum_m \sum_k p_{ik}^{(m)}(T)/p_{ig}(T) \ . \tag{39}$$

The argument leading to the determination of U proceeds in the same way as we arrived at Eq. (17). The first estimate D_1 for the inconsistency arising from the use of Eq. (10) now becomes

$$D_1 = \sum_m \sum_k \int dT_1 \ldots \int dT_{m+1} \pi_k^{(m)}(T_1, \ldots, T_{m+1}; T)$$

$$\sum_{\mu=1}^{m+1} (T_\mu - U)/W_a \ , \tag{40}$$

where the $(m+1)$-fold integral is to be taken over the domain defined by

$$\sum_{\mu=1}^{m+1} T_\mu = T - I_k^{(m)} \tag{41}$$

and

$$T_\mu < I_1^{(1)} \quad \text{for every } \mu \quad , \tag{42}$$

$I_1^{(1)}$ being the first ionization threshold for single ionization. Again demanding $D_1 = 0$, one obtains an expression for an optimal U, similar to Eqs. (16) and (17). In other words, U remains to represent approximately the average energy of a subexcitation electron.

We have thus seen that the three complications necessitate no fundamental modification of the theory at all.

Concluding Remarks

The present theory should be a significant improvement over the Fano theory, and yet both theories are equally easy to apply. Numerical consequences of the two theories for many monatomic gases are examined in the following article.[8]

We have seen the key role of E_{i1} of Eq. (17), or more fundamentally, of $dp_i(E,T)/dE$ for $I < E < 2I$, in theory of W(T). As Kim[22,23] points out in many instances, current secondary-electron measurements suffer from considerable uncertainties precisely in that interval. I sincerely wish to see the measurements improved in this respect.

It is desirable to compare closely the present theory with other approximate bookkeeping methods[32–35] based on continuous slowing-down approximations. Work in this direction is in progress.

Finally, the yield of initial species[4,5,14,17–19,33] other than ions (e.g., a particular excited state or a dissociation product) should be amenable to an analysis similar to the present treatment. Extension of the work in this direction will establish a close link of various cross-section data with radiation chemistry.

Acknowledgements

Much of the present work was stimulated by conversations with Dr. E. Eggarter. I thank Professor U. Fano, Dr. J. L. Dehmer, Dr. R. P. Saxon, and Dr. D. A. Douthat for valuable comments on an earlier manuscript.

References

1. J. W. Boag. Quantities, Units, and Measuring Methods of Ionizing Radiation, Proc. Symp. Rome, April 1958, Ed. F. Fossati (Ulrico Heopli, Milan, 1959), p. 100.
2. J. Booz and H. G. Ebert. Strahlentherapie 120, 7 (1963).
3. G N. Whyte. Radiat. Res. 18, 265 (1963).
4. R. L. Platzman. Int. J. Appl. Radiat. Isotopes 10, 116 (1961).
5. M. Inokuti. Physical Mechanisms in Radiation Biology, Proc. Conf. Airlie, Virginia, 11–14 October 1972, Ed. R. D. Cooper and R. W. Wood. U.S. Atomic Energy Commission Report CONF-721001 (1974), p. 51.
6. H. Bethe. Ann. Physik (Leipzig) 5, 325 (1930).
7. E. Bagge. Ann. Physik (Leipzig) 30, 72 (1973).
8. M. Inokuti, J. L. Dehmer, and R. P. Saxon. Paper 2, this report.
9. D. A. Douthat. Paper 3, this report.
10. R. H. Fowler. Proc. Cambridge Phil. Soc. 21, 531 (1923).
11. J. K. Knipp, T. Eguchi, M. Ohta, and S. Nagata. Prog. Theor. Phys. (Kyoto) 10, 24 (1953).
12. G. A. Erskine. Proc. Roy. Soc. (London) A224, 362 (1954).
13. J. R. Herring and E. Merzbacher. J. Elisha Mitchell Sci. Soc. 73, 267 (1957).
14. W. F. Miller. Ph.D. Thesis, Purdue University (1957), unpublished.
15. A. Dalgarno and G. W. Griffing, Proc. Roy. Soc. (London) A248, 415 (1958).
16. G. D. Alkhazov. Zh. Tekh. Fiz. 41, 2513 (1971). [English trans. Soviet Phys. — Tech. Phys. 16, 1995 (1972).]
17. W. M. Jones. J. Chem. Phys. 59, 5688 (1973).
18. D. E. Gerhart. Comprehensive optical and collision data for radiation action. I. H_2. J. Chem. Phys., in press.
19. E. Eggarter. Comprehensive optical and collision data for radiation action. II. Ar. J. Chem. Phys., in press.
20. H. Bethe. Handbuch der Physik 24/1, Ed. H. Geiger and K. Scheel. Springer Verlag, Berlin, 1933, Ch. 4, p. 273.
21. M. Inokuti. Rev. Mod. Phys. 43, 297 (1971).
22. Y.-K. Kim. Argonne National Laboratory Radiological and Environmental Research Division Annual Report, July 1972–June 1973. ANL-8060, Part I, p. 55.
23. Y.-K. Kim. Paper 4, this report.
24. D. A. Douthat. Radiat. Res., in press.

25. U. Fano and V. L. Spencer. Int. J. Radiat. Phys. Chem., in press.
26. U. Fano. Phys. Rev. 70, 44 (1946).
27. A. Cole. Radiat. Res. 38, 7 (1969).
28. D. Srdoč. Nucl. Instr. Methods 108, 327 (1973).
29. J. A. R. Samson, University of Nebraska. Personal communication.
30. R. L. Platzman. J. Phys. Radium 21, 853 (1960).
31. R. L. Platzman. Radiat. Res. 17, 419 (1962).
32. R. L. Peterson and A. E. S. Green. J. Phys. B 1, 1131 (1968).
33. A. E. S. Green and J. H. Miller. Physical Mechanisms in Radiation Biology, Proc. Conf. Airlie, Virginia 11–14 October 1972, Ed. R. D. Cooper and R. W. Wood. U.S. Atomic Energy Commission Report CONF-721001 (1974), p. 68.
34. S. P. Khare. J. Phys. B 3, 971 (1970).
35. R. Shingal, B. B. Srivastava, and S. P. Khare. Ionizing collisions of electrons with molecular hydrogen. To be published.

SYSTEMATICS OF THE IONIZATION YIELD IN MONATOMIC GASES UNDER ELECTRON IRRADIATION*

Mitio Inokuti, J. L. Dehmer, and Roberta P. Saxon†

We have applied the Fano theory and the theory of the foregoing article to all atoms in the first two rows of the periodic table. Results show significant systematics hitherto little explored.

Introduction

As an initial application of the theory of the foregoing article,[1] we have chosen to study all monatomic gases in the first two rows of the periodic table. The motivation for this choice is manyfold.

First, the W value of monatomic gases has so far remained unknown,[2] except for rare gases and mercury vapor.[3] On the basis of the data on rare gases alone, one might quickly hazard a naive assumption that the ratio W/I would be about 1.7 for all atoms. As we shall demonstrate below, W, as well as W/I, actually shows great variations from one atom to another, and clearly reflects the atomic shell structure.

Second, despite readily understandable obstacles in its direct measurement, the total ionization in monatomic gases (other than rare gases) has practical significance in some applications such as discharge and plasma formation. In particular, the total ionization in the sodium vapor is pertinent to some aspects of liquid-metal breeder reactors such as boiling phenomena and radiation monitoring.

Third, basic data for monatomic gases are conveniently available for use. Specifically in the present work we have used a comprehensive set of spectral data generated in our earlier work.[4] Also, monatomic gases are simpler to treat theoretically than polyatomic gases because of the absence

---

*Part of this work was presented at the Vth International Congress of Radiation Research. See abstract published in Radiat. Res. 59, 230 (1974).

†Presidential Intern, RER Division, February 1972–February 1973. Present address: Stanford Research Institute, Menlo Park, California 94025.

of molecular internal degrees of freedom; it is a good approximation in monatomic gases to assume that any energy transfer exceeding the first ionization threshold results in ionization, while that is not so in polyatomic gases.[5,6]

Expressions for W

We recapitulate below some of the defintions and formulas of the foregoing article.[1]

An electron of kinetic energy T excites an atom to its discrete state n at excitation energy E_n below the first ionization threshold I with the probability $p_n(T)$ per inelastic collision. The same electron ionizes the atom with the probability $p_i(T)$ per inelastic collision. This probability is an integral of the differential ionization probability $dp_i(E,T)/dE$ for a specified energy transfer E over the interval $I < E < \frac{1}{2}(T+I)$.

The theory of the foregoing article[1] gives the average energy W(T) per ion pair generated by an incident electron of kinetic energy $T \gg I$ as

$$W(T) = (1 - U/T)^{-1} W_a \ . \tag{1}$$

Under the assumption of a single ionization threshold, U and W_a are evaluated by

$$U = E_{i1} - I \ , \tag{2}$$

and

$$W_a = \sum_n E_n p_n(T)/p_i(T) + E_{i1} \ , \tag{3}$$

where

$$E_{i1} = \int_I^{2I} dE E \frac{dp_i(E,T)}{dE} \Big/ p_{i1}(T) \ , \tag{4}$$

and

$$p_{i1}(T) = \int_I^{2I} dE \frac{dp_i(E,T)}{dE} \ . \tag{5}$$

The Fano theory[7] gives for W(T) at high T

$$W_F = [\sum_n E_n p_n(T) + E_{i1} p_{i1}(T) + I p_{i2}(T)] / p_i(T) \ , \tag{6}$$

where E_{i1} and $p_{i1}(T)$ are the same as above and

$$p_{i2}(T) = p_i(T) - p_{i1}(T) \ . \tag{7}$$

We may consider W_F as being on the same footing as W_a because both represent an asymptotic value of W(T) as $T \to \infty$.

Choice of Cross Sections

We follow Fano[7] in assigning the probabilities $p_n(T)$, $p_i(T)$, and $dp_i(E,T)/dE$ at $T \gg I$. According to the Bethe theory[8,9] all inelastic collisions of an electron with an atom may be classified into two kinds: glancing (or dipole) interactions, and hard (or knock-on) collisions. The former is quantitatively described by the relevant oscillator strength, and the latter may be reasonably evaluated by use of the Rutherford formula with modifications to account for the electron binding to the atom. In the following brief sketch we shall use several notations and concepts from Inokuti's review article[10] on the Bethe theory.

Notice first that the Bethe expression for all inelastic-scattering cross sections has a universal factor $4\pi a_0^2 R/T$ (where a_0 is the Bohr radius and R is the Rydberg energy), and that this factor drops out in the probabilities $p_n(T)$, $p_i(T)$, and $dp_i(E,T)/dE$. In the present article we shall presume that T is much greater than the first ionization threshold but is still small enough to allow the use of nonrelativistic formulas.

For $T \gg I$, the first term of Eq. (3) or Eq. (6) may be written as

$$\frac{\Sigma_n E_n p_n(T)}{p_i(T)} = \frac{R f_{ex} \ln (4\tilde{c}_{ex} T/R)}{M_i^2 \ln (4c_i T/R)} \ . \tag{8}$$

In the denominator of the right-hand side of the above equation

$$M_i^2 = \int_I^\infty (R/E)\,(df/dE)\,dE \tag{9}$$

is the integral of the dipole matrix element squared for ionization, and c_i is defined by

$$M_i^2 \ln c_i = \int_I^\infty (R/E)\,(df/dE) \ln c_E\, dE \ , \tag{10}$$

where df/dE is the density of the dipole oscillator strength per unit interval of the energy transfer E and c_E is the second parameter that characterizes the Bethe expression and depends upon the generalized oscillator strength (see Sect. 4.1 of Ref. 10). In the numerator of Eq. (8)

$$f_{ex} = \Sigma_n f_n \tag{11}$$

is the total oscillator strength for discrete excitation and $\tilde{c}_{ex}$ is defined by

$$f_{ex} \ln \tilde{c}_{ex} = \Sigma_n f_n \ln c_n \ , \tag{12}$$

where c_n is the analog of c_E for discrete excitation. Note that $\ln \tilde{c}_{ex}$ is the average of $\ln c_n$ with weight f_n, while $\ln c_i$ is the average of $\ln c_E$ with weight (R/E) (df/dE). To keep this distinction in mind, we let the notation $\tilde{c}_{ex}$ carry the tilde.

Similarly, E_{i1} of Eq. (4) may be written for T >> I as

$$E_{i1} = \frac{R f_{i1} \ln (4\tilde{c}_{i1}\, T/R)}{M_{i1}^2 \ln (4c_{i1}\, T/R)} \ , \tag{13}$$

where

$$M_{i1}^2 - \int_I^{2I} (R/E)\,(df/dE)\, dE \ , \tag{14}$$

$$M_{i1}^2 \ln c_{i1} = \int_I^{2I} (R/E)\,(df/dE) \ln c_E\, dE \ , \tag{15}$$

$$f_{i1} = \int_I^{2I} (df/dE)\, dE \ , \tag{16}$$

$$f_{i1} \ln \tilde{c}_{i1} = \int_I^{2I} (df/dE) \ln c_E\, dE \ . \tag{17}$$

Again observe the difference between c_{i1} and $\tilde{c}_{i1}$.

Rigorous evaluation of all the c's requires complete knowledge of the generalized oscillator strength. In the present work we follow Fano's

choice[7]

$$\ln \tilde{c}_{ex} = \ln (R/I) \ , \tag{18}$$

$$\ln c_i = \ln (R/I) + ZR/(IM_i^2) \ , \tag{19}$$

$$\ln \tilde{c}_{i1} = \ln (R/I) + Z \ln 2/f_{i1} \ , \tag{20}$$

$$\ln c_{i1} = \ln (R/I) + ZR/(2IM_{i1}^2) \ , \tag{21}$$

where Z is the atomic number.

Substituting Eqs. (18)–(21) into Eqs. (8) and (13) and using the result in Eq. (3), we obtain

$$\frac{W_a}{R} = \frac{f_{ex}\lambda}{M_i^2\lambda + ZR/I} + \frac{f_{i1}\lambda + Z \ln 2}{M_{i1}^2\lambda + (RZ/2I)} \ , \tag{22}$$

where

$$\lambda = \ln (4T/I) \ . \tag{23}$$

Similarly, Fano[7] obtained from Eq. (6)

$$\frac{W_F}{R} = \frac{[f_{ex} + f_{i1} + (I/R)(M_i^2 - M_{i1}^2)]\lambda + Z(\frac{1}{2} + \ln 2)}{M_i^2\lambda + ZR/I} \ . \tag{24}$$

We can now evaluate Eqs. (22) or (24) as soon as we know f_{ex}, f_{i1}, M_{i1}^2, and M_i^2, quantities that depend on the spectral distribution of the dipole oscillator strength only. We have used the spectral distribution[4] obtained from the Hartree-Slater model for all atoms in the first two rows of the periodic table and computed the four spectral properties. Table 1 presents these values, and Table 2 presents W_a values from Eq. (22), as well as W_F values from Eq. (24), both evaluated for T = 10 keV. Because both W_a and W_F are insensitive to T exceeding several keV, we may consider them virtually the same as the W value for electrons with any higher energies.

Figure 1 shows a plot of W_a and W_F against the atomic number Z. It also includes experimental W values[11,12] for He, Ne, and Ar, as well as theoretical values obtained by solving the Fowler equation numerically.[13-15] The W_a value is greater than the W_F value of each atom, as it should be, and

TABLE 1. Values of Spectral Properties Pertinent to the W Value[a]

Atom	f_{ex}	f_{i1}	f_i	M_{ex}^2	M_{i2}^2	M_i^2
H	0.5650	0.335	0.4350	0.7166	0.279	0.2834
He	0.4935	0.8995	1.5065	0.3229	0.3917	0.4992
Li	0.7760	0.0673	2.2240	5.3703	0.1162	0.4946
Be	1.3644	0.1500	2.6356	5.1660	0.1708	0.5048
B	1.7321	0.4654	3.7332	0.8499	0.7018	1.3613
C	1.0202	0.8752	4.9798	0.6322	0.9434	1.7741
N	0.2981	1.6317	6.7018	0.4336	1.5211	2.4661
O	0.2636	1.6404	7.7364	0.3081	1.1648	2.1734
F	0.2372	1.6050	8.7628	0.2307	0.9057	1.9444
Ne	0.2236	1.5429	9.7764	0.1805	0.7131	1.7601
Na	0.9796	0.0025	10.0204	6.3414	0.0042	1.2427
Mg	1.8909	0.0073	19.1091	7.6758	0.0110	0.9429
Al	0.7804	1.8601	12.2196	3.1944	4.6420	5.4789
Si	1.1211	2.1871	12.8789	3.0340	3.8918	4.6720
P	1.2204	2.7162	13.7796	2.4529	3.6726	4.3999
S	1.8518	3.3517	14.8148	1.8552	3.5891	4.2721
Cl	1.3375	3.7803	15.6625	1.3953	3.2461	3.8907
Ar	4.7100	4.7100	17.0418	1.0412	3.4329	4.0444

[a] All the data (except those for hydrogen) are based on the Hartree-Slater model.[4] For completeness, this table includes the total dipole matrix element squared for discrete excitation

$$M_{ex}^2 = \Sigma_n (R/E_n) ,$$

a quantity that has not been used in the present work.

is closer to experiment for He, Ne, and Ar. The difference $W_a - W_F$ is appreciable for the first-row atoms, and is especially significant for neon. For the second-row atoms, W_a differs only little from W_F. Figure 2 shows a substantial discrepancy for Ar between experiment on the one hand and either W_a or W_F on the other hand. This discrepancy is in part attributable to the cross-section assignment, as opposed to the bookkeeping method. We shall soon clarify this point by re-evaluation of W_a and W_F from more accurate cross-section data by Eggarter.[15] [Such a re-evaluation was done for Ne by use of the accurate spectral distribution adopted by Saxon;[16] the result is W_a = 32.5 eV and W_F = 27.9 eV. Because the Saxon distribution is rather close to the Hartree-Slater-model distribution, W values naturally come out likewise; the discrepancy still remaining between W_a and experiment is probably attributable to our schematic treatment of hard collisions [Eqs. (18)–(21)].

With these qualifications in mind, we still emphasize that the marked Z-dependence seen in Figure 1 is realistic. The W values show prominent maxima for fully closed shells (Z = 2, 10, and 18), and secondary maxima for

TABLE 2. Values of W_a [Eq. (22)] and W_F [Eq. (24)] Evaluated for T = 10 keV[a]

Atom	W_F in eV	W_a in eV	W_F/I	W_a/I
H	35	36	2.6	2.7
He	39.4	41.7	1.68	1.78
Li	14.3	15.6	2.60	2.84
Be	24.1	25.9	2.94	3.17
B	14.8	18.4	2.22	2.76
C	15.7	17.4	1.75	1.94
N	14.7	16.1	1.28	1.41
O	18.0	20.5	1.27	1.44
F	21.4	25.1	1.26	1.48
Ne	25.0	29.9	1.25	1.50
Na	8.8	10.1	1.72	1.96
Mg	14.9	16.5	2.16	2.40
Al	6.7	7.0	1.37	1.43
Si	8.5	10.0	1.45	1.53
P	12.1	12.8	1.45	1.53
S	14.7	15.5	1.43	1.50
Cl	18.0	19.1	1.46	1.55
Ar	19.9	21.1	1.37	1.46

[a] To compute the ratios W_a/I and W_F/I for each atom (except hydrogen), we used for logical consistency the ionization energy I given by the Hartree-Slater model,[4] rather than the spectroscopic value.

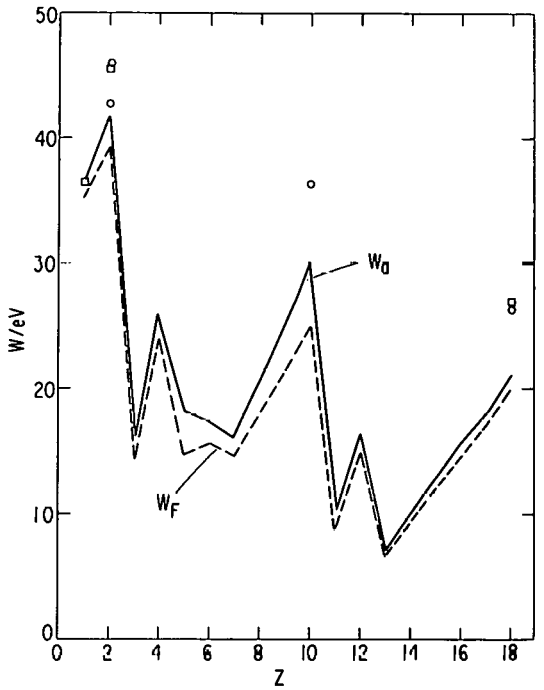

FIG. 1.--Values of W_a and W_F plotted against Z. Better theoretical results (shown by squares) for H by Dalgarno and Griffing[13] for He by Miller,[14] and for Ar by Eggarter,[15] as well as representative experimental values (shown by circles) for He, Ne, and Ar, are included for comparison. For He, the greater of the two experimental values is due to Bortner and Hurst[11] and the lesser is due to Jesse and Sadauskis.[12]

nominally closed shells (Z = 4 and Z = 12).

There are systematic variations also in the ratios W_a/I and W_F/I, as seen in Figure 2. These ratios tend to be smallest in the neighborhood of rare gases — a behavior understandable from their substantial fraction of the oscillator strength at high E in the continua. The maxima of the ratios for Be and Mg, in contrast, must be due to the strong oscillator strength for the resonance transition in these atoms. The above trend qualitatively explains the Jesse measurement,[3] W/I = 2.27 for Hg, an atom in the same column of the

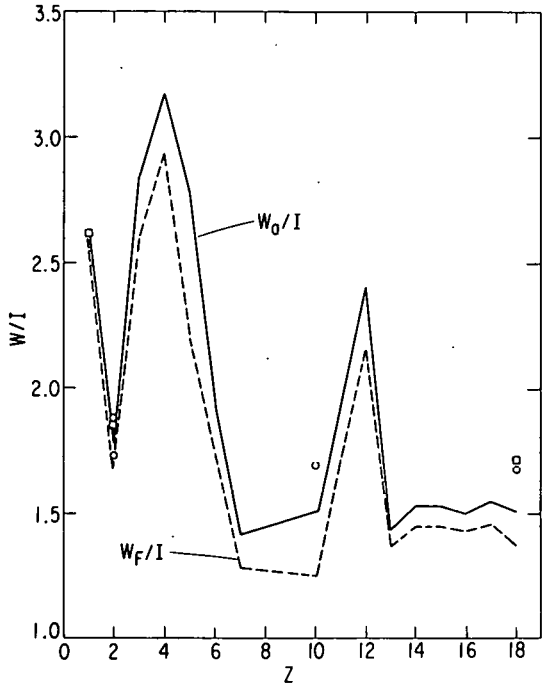

FIG. 2.--The ratios W_a/I and W_F/I plotted against Z. To compute these ratios for each atom (except hydrogen), we used the ionization energy given by the Hartree-Slater model.[4] However, data points for better theoretical results[11-13] (shown by squares) and for experimental results[11,12] (shown by circles) correspond to the ratios obtained by use of the spectroscopic ionization energy.

periodic table as Be and Mg.

The last point was indeed made by Fano,[7] who cited lithium as an example, and also by Platzman,[2] who referred to alkali-metal atoms in general (in his footnote on p. 122). Now that experimental data, e.g., summarized by Marr[17] and by Hudson and Kieffer,[18] on df/dE are at hand, one should be able to treat this point more quantitatively and realistically than we have done in the present work. We plan to report additional work on this aspect in the future.

Outlook

Although we have made substantial progress, much remains to be done. Our plans for work in the immediate future include the following.

First, we can easily improve the assignment of the c values beyond those of Eqs. (18)—(21). The improvement will make full use of the general properties known about c_n and c_E (e.g., the sum rule[19] of Inokuti, Kim, and Platzman), and will also take advantage of Kim's analyses[20,21] of data on $dp_i(E,T)/dE$.

Second, the approximate solution of the Fowler equation can be readily applied to molecules after some modifications.[1] So long as the cross section

assignment by the Fano method is justified, we can then calculate W values by use of experimental data on the spectral distribution, which are now available in the literature for many basic molecules such as O_2, N_2, and CH_4 and H_2O.

Acknowledgements

We thank Professor U. Fano and Dr. D. A. Douthat for numerous discussions and valuable comments throughout the present work.

References

1. M. Inokuti. Paper 1, this report.
2. R. L. Platzman. Int. J. Appl. Radiat. Isotopes 10, 116 (1961).
3. W. P. Jesse. J. Chem. Phys. 55, 3603 (1971).
4. J. L. Dehmer, M. Inokuti, and R. P. Saxon. Paper 9, this report. See also Argonne National Laboratory Radiological and Environmental Research Division Annual Report, July 1972–June 1973. ANL-8060, Part I, pp. 100 and 102.
5. R. L. Platzman. J. Phys. Radium 21, 853 (1960).
6. R. L. Platzman. Radiat. Res. 17, 419 (1962).
7. U. Fano. Phys. Rev. 70, 44 (1946).
8. H. Bethe. Ann. Physik 5, 325 (1930).
9. H. Bethe. Handbuch der Physik, Ed. H. Geiger and K. Scheel. Springer Verlag, Berlin, 1933, Vol. 24/1, p. 273.
10. M. Inokuti. Rev. Mod. Phys. 43, 297 (1971).
11. T. E. Bortner and G. S. Hurst. Phys. Rev. 93, 1236 (1954).
12. W. P. Jesse and J. Sadauskis. Phys. Rev. 90, 1120 (1953).
13. A. Dalgarno and G. W. Griffing. Proc. Roy. Soc. (London) A248, 415 (1958).
14. W. F. Miller. A Theoretical Study of Excitation and Ionization by Electrons in Helium and of the Mean Energy per Ion Pair for Electrons in Helium. Ph.D. Thesis, Purdue University, 1956, unpublished. See also Bull. Am. Phys. Soc. 1, 202 (1956).
15. E. Eggarter. Comprehensive Optical and Collision Data for Radiation Action. II. Ar. J. Chem. Phys., in press.
16. R. P. Saxon. Phys. Rev. A 8, 839 (1973).
17. G. V. Marr. Photoionization Processes in Gases. Academic Press, New York, 1967.
18. R. D. Hudson and L. J. Kieffer. Atomic Data 2, 205 (1971).
19. M. Inokuti, Y.-K. Kim, and R. L. Platzman. Phys. Rev. 164, 55 (1967).
20. Y.-K. Kim. Argonne National Laboratory Radiological and Environmental Research Division Annual Report, July 1972–June 1973. ANL-8060, Part I, p. 55.
21. Y.-K. Kim. Paper 4, this report.

CALCULATIONS OF ELECTRON DEGRADATION SPECTRA

D. A. Douthat*

We are extending recent calculations of degradation spectra in helium in order to test the sensitivity of the spectra with regard to the selection of cross-section data.

The degradation spectrum (DGS) of particles in an irradiated medium is just the distribution in kinetic energy of free particles in the medium. The DGS is perhaps the most fundamental piece of information in a description of the complete radiation field acting on the system. Recent studies[1-4] have focussed on electron degradation spectra, and a few complete spectra now exist.

In view of the labor required to assemble the necessary data for the calculation of spectra (a complete set of inelastic-collision cross sections over a broad energy range) the sensitivity of calculated degradation spectra with regard to the various cross sections is important. The Spencer-Fano method,[5] which is valid for energies greatly in excess of the ionization energy, is based on the insensitivity of spectra with regard to the detailed form of small energy losses and consequently requires knowledge only of the stopping power and the "hard" collision cross section. Klots and Wright[1] found the continuous slowing-down approximation to be accurate to within about 10% for all energies for their model cross sections.

We are currently calculating electron degradation spectra for gaseous helium using various "model" cross sections in an effort to answer the following questions: 1) How sensitively do calculated spectra depend on the input data? 2) What constraints should approximate cross sections meet in order to enhance the reliability of the resulting spectra? and 3) What is the best "prescription," given the currently (limited) available data (e.g., cross sections, mean excitation energy, mean energy per ion pair), for the

*Kennedy-King College, Chicago, Illinois. Consultant, RER Division, Argonne National Laboratory.

calculation of degradation spectra? Optimally, of course, spectra are calculated from a complete set of inelastic-collision cross sections which are, in turn, based on a survey of all existing data, but such sets are available[6–10] only for He, H_2, and Ar.

The construction of model cross sections and analysis of results will be done in collaboration with Dr. Y.-K. Kim and Dr. Mitio Inokuti.

References

1. C. E. Klots and H. Wright. Int. J. Radiat. Phys. Chem. 2, 191 (1970).
2. G. D. Alkhazov. Zh. Tekh. Fiz. 41, 2513 (1971) [English translation: Sov. Phys. — Tech. Phys. 16, 1995 (1972)].
3. L. C. Emerson, R. D. Birkhoff, V. E. Anderson, and R. H. Ritchie. Phys. Rev. B 7, 1798 (1973).
4. D. A. Douthat. Radiat. Res., in press.
5. L. V. Spencer and U. Fano. Phys. Rev. 93, 1172 (1954).
6. W. F. Miller. Ph.D. Thesis, Purdue University (1956), unpublished.
7. A. T. Jusick, C. E. Watson, L. R. Peterson, and A. E. S. Green. J. Geophys. Res. 72, 3943 (1967).
8. G. D. Alkhazov. Zh. Tekh. Fiz. 40, 97 (1970). [English translation Sov. Phys. — Tech. Phys. 15, 66 (1970)].
9. D. E. Gerhart. To be published in J. Chem. Phys.
10. E. Eggarter. To be published in J. Chem. Phys.

ENERGY DISTRIBUTION OF SECONDARY ELECTRONS. I. CONSISTENCY OF EXPERIMENTAL DATA*

Yong-Ki Kim

The energy distribution of secondary electrons ejected by fast charged particles from free atoms and molecules should show certain qualitative features according to theory. Recent electron-impact data by Opal, Beaty, and Peterson[1] indeed exhibit these features clearly. The spectrum of fast secondaries tends to agree better with the Mott cross section than with the binary-encounter theory with the corrections for the initial momentum distribution of bound electrons. A method is proposed for extraplating the secondary-electron spectra to ranges where experiment becomes difficult (e.g., for very slow and very fast secondary electrons). With this method, secondary-electron spectra can be put easily on an absolute scale, provided that reliable total ionization cross sections are available. The method applies also to the analysis of experimental data on electrons ejected by fast heavy particles, such as protons and alpha particles.

Reference

1. C. B. Opal, E. C. Beaty, and W. K. Peterson. Atomic Data 4, 209 (1972).

---

*Abstract of a paper published in Radiat. Res. 61, 21–35 (1975). See also Bull. Am. Phys. Soc. 19, 82 (1974) and Argonne National Laboratory Radiological and Environmental Research Division Annual Report, July 1972-June 1973. ANL-8060, Part I, p. 55.

SECONDARY-ELECTRON SPECTRA*

Yong-Ki Kim

A simple but powerful method for constructing a consistent set of secondary-electron spectra is illustrated through its application to H_2O and N_2. For N_2, recommended spectra for incident-electron energies of 50 eV to 10 keV are presented in Figure 1. The area under each curve has been normalized to σ_{ion} for corresponding incident energies T. The expected position and width (but not the amplitude) of KLL Auger peaks are indicated. The area under the Auger peaks should be proportional to the sum of the total cross sections for ionization and excitation of K electrons. The spectra between the ionization threshold and R/E = 0.832 (W = 0.77 eV) would depend on the energy resolution owing to the sharp autoionization peaks and rapidly changing ionization efficiency in that region. The shaded area is proportional to the number of secondary electrons with kinetic energies less than the first ionization potential, viz., 15.58 eV.

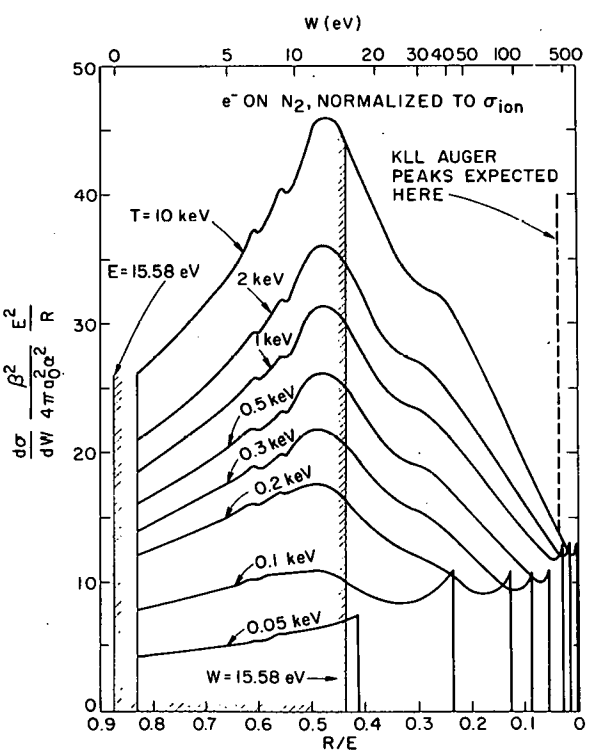

FIG. 1.--Secondary-electron spectra of N_2 for electron impact. $d\sigma/dW$ = energy distribution of secondary electrons; W = kinetic energy of the secondary electron; E = W + first ionization potential; T = incident electron energy; R = Rydberg energy (13.6 eV); α = fine structure constant; β = incident electron speed/speed of light; a_0 = Bohr radius (0.529 Å); σ_{ion} = total ionization cross section.

In the construction of the recommended spectra for N_2, the electron-impact data of Opal, Beaty, and Peterson[1] have been revised through renormalization and extrapolation over some ranges of variables not covered in their data. The spectrum for T = 10 keV in Figure 1 is a theoretical prediction based on the revised experimental data for lower incident-electron energy.

Reference

1. C. B. Opal, E. C. Beaty, and W. K. Peterson. Atomic Data 4, 209 (1972).

---

*Summary of a paper presented at the Fifth International Congress of Radiation Research, Seattle, July 14–20, 1974.

SECONDARY ELECTRONS EJECTED FROM He BY PROTONS AND ELECTRONS*

Y.-K. Kim and Tetsushi Noguchi†

Experimental data on the energy distribution of secondary electrons ejected from He by fast protons[1] and electrons[2] are shown in Figure 1 to exhibit the following features expected from the Rutherford theory and the Born approximation: a) the energy distribution of slow secondary electrons resembles in shape that deduced from the photoionization cross section; b) the energy distribution for fast secondary electrons converges to that predicted by the Rutherford theory for proton impact and by the Mott theory for electron impact; c) the cross sections for fast protons are very similar to those for electrons with the same velocity as the protons. Comparison of the secondary-electron spectra with the optical data[3] in Figure 1 indicates that some minor but systematic corrections on the experimental data are necessary. The corrected experimental data are consistent with the total ionization cross section.[4]

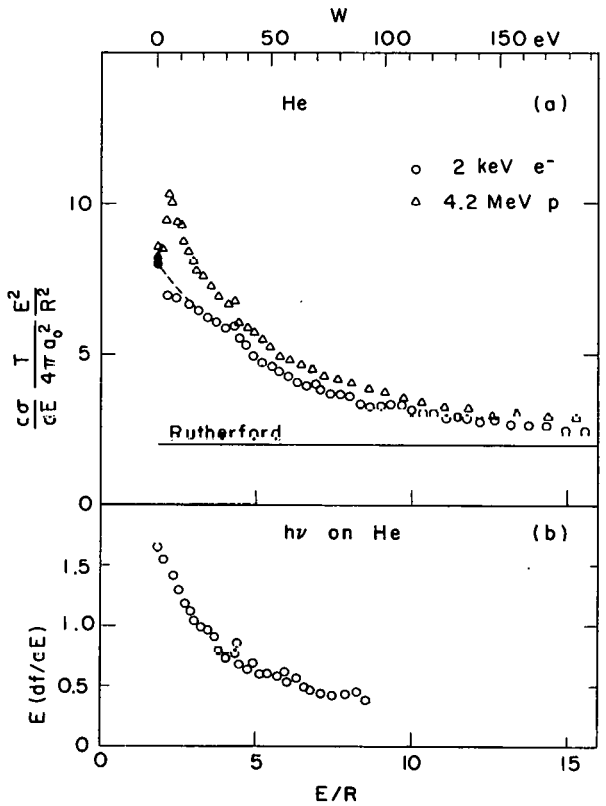

FIG. 1.--(a) Secondary-electron spectrum of He as a function of energy transfer from 4.2-MeV protons[1] (Δ) and 2-keV[2] (o). The corresponding Born cross sections[5] for the ejection of zero-kinetic-energy electrons by protons (Δ) and electrons (o) are shown also. (b) Photoabsorption data[3] as a function of photon energy. The dashed curve in (a) indicates the secondary-electron spectrum theoretically adjusted to the shape of the optical data in (b) as well as to the Born cross section at the ionization threshold. The horizontal line represents the Rutherford cross section. $d\sigma/dE$ = secondary electron energy distribution; E = energy transfer; W = kinetic energy of secondary electrons; $T = \frac{1}{2}mv^2$, where m is the electron mass and v is the incident particle speed; R = Rydberg energy (13.6 eV); a_0 = Bohr radius (0.529 Å); df/dE = differential dipole oscillator strength.

References

1. N. Stolterfoht. Hahn-Meitner Institut für Kernforschung, Berlin. Private communication, 1973.
2. C. B. Opal, E. C. Beaty, and W. K. Peterson. Atomic Data 4, 209 (1972).
3. J. A. R. Samson. Advances Atom. Mol. Phys. 2, 177 (1966).
4. Y.-K. Kim and M. Inokuti. Phys. Rev. A 3, 665 (1971).
5. Y.-K. Kim and M. Inokuti. Phys. Rev. A 7, 1257 (1973).

---

*Summary of a paper to appear in Int. J. Radiat. Phys. Chem.

†Student Associate, September 1973–March 1974.

ATOMIC FORM FACTOR AND INCOHERENT-SCATTERING FUNCTION OF Ar*

M. Naon,† M. Cornille,‡ and Yong-Ki Kim

The atomic form factor and the incoherent-scattering function of Ar calculated from the Bethe-Goldstone method are presented. The results include electron correlation effects in the M shell, as well as those between L and M shells. The form factor calculated from the Hartree-Fock wavefunction agrees within 2% with the result from the Bethe-Goldstone method for a wide range of momentum transfer. However, the correlation effects reduce the incoherent-scattering function for small momentum transfers ($\lesssim$ 1 a.u.) by $\sim$ 20% from the Hartree-Fock values.

*Abstract of a paper to be submitted to J. Phys. B.

†Centre de Mécanique Ondulatoire Appliqée, 23 Rue du Maroc, 75019, Paris, France.

‡Centre Européan de Calcul Atomique et Moléculaire, Bâtiment 506, 91405, Campus d'Orsay, France.

TOTAL CROSS SECTIONS FOR INELASTIC SCATTERING OF CHARGED PARTICLES BY ATOMS AND MOLECULES. VIII. SYSTEMATICS FOR ATOMS IN THE FIRST AND SECOND ROW*

Mitio Inokuti, Roberta P. Saxon,† and J. L. Dehmer

The Bethe theory gives an asymptotic formula for the total cross section σ_{tot} for inelastic scattering of fast charged particles. For a (structureless) particle of charge ze and (nonrelativistic) velocity v, it is written as

$$\sigma_{tot} = 4\pi a_0^2 z^2 \, (R/T) \, M_{tot}^2 \ln (4c_{tot} T/R) \, ,$$

where R is the Rydberg energy, a_0 is the Bohr radius, and $T = \frac{1}{2} mv^2$, m being the electron mass. Two quantities, M_{tot}^2 and $\ln c_{tot}$, depend upon the internal dynamics of the atom. We have performed comprehensive calculations of these quantities for neutral atoms He through Ar by use of independent-particle models, and also have studied the influence of electron correlations for several atoms.

Our calculations reveal certain systematics of M_{tot}^2 and $\ln c_{tot}$ as functions of the atomic number Z. Because M_{tot}^2 is expressed as the ground-state expectation value of the squared sum of atomic-electron ccordinates, the trend of M_{tot}^2 follows the size of the atom, governed by its shell structure (Figure 1). The quantity $\ln c_{tot}$ also varies with the atomic size, but within a fairly modest range (Figure 2). Hence, the variation of σ_{tot} at fixed v from one atom to another is chiefly governed by M_{tot}^2.

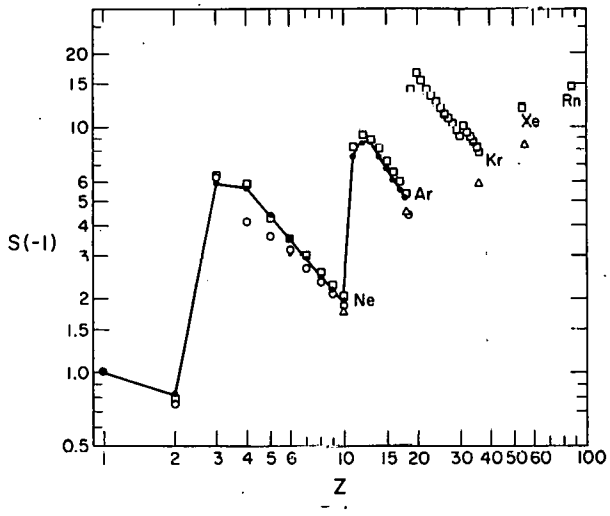

FIG. 1.--The total dipole matrix element squared $M_{tot}^2 \equiv S(-1)$ as a function of atomic number Z. The dots connected with heavy lines represent the Hartree-Slater values obtained in the present work, the squares the Hartree-Fock values from the literature, and the circles more accurate theoretical values also from the literature. The values indicated by the triangles stem from experimental oscillator-strength distributions.

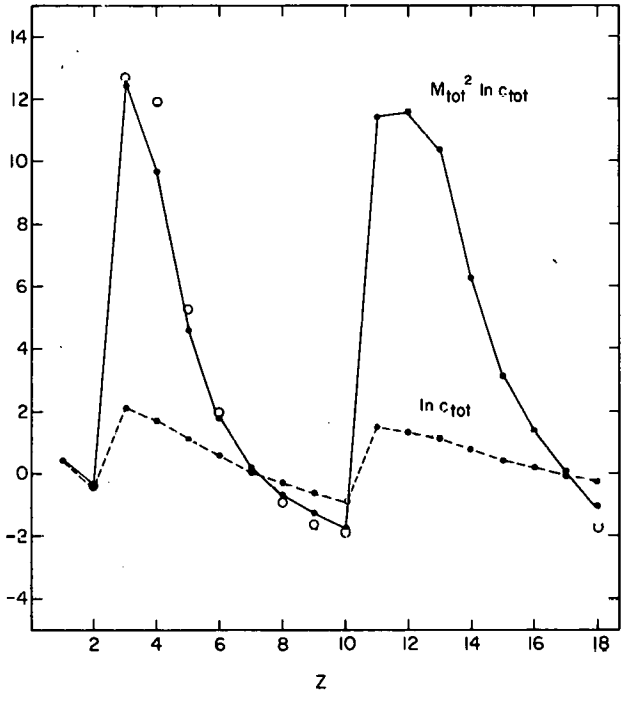

FIG. 2.--The quantities $M_{tot}^2 \ln c_{tot}$ and $\ln c_{tot}$ as functions of atomic number Z. The dots represent values based solely on independent-particle models, and the circles values including some configuration-interaction effects.

---

*Abstract of a paper to appear in Int. J. Radiat. Phys. Chem.

†Presidential Intern, Radiological and Environmental Research Division, February 1972–February 1973. Research Associate, Chemistry Division March–October 1973. Present address: Stanford Research Institute, Menlo Park, California 94025.

ATOMIC PERIODICITY AS MANIFESTED IN THE OSCILLATOR-STRENGTH SUMS*

J. L. Dehmer, Mitio Inokuti, and R. P. Saxon†

The moments $S(\mu)$ of various order of μ for dipole oscillator-strength distribution of atoms pertain to numerous phenomena ranging from optical dispersion to charged-particle collisions. We have surveyed literature data and have conducted comprehensive calculations using a Hartree-Slater model for all atoms with $Z \leqq 18$. The general behavior of $S(\mu)$ as a function of μ naturally classifies atoms into three groups. This is illustrated in Figure 1. The first group, which we call "tight" atoms (i.e., rare gases), has $S(\mu)$ that monotonically increases with μ, a behavior characteristic of heavy concentration of the oscillator strength at high excitation energies. The second group is composed of "loose" atoms (e.g., alkalis), and, in contrast, has $S(\mu)$ with a prominent minimum near $\mu = -1$. An almost linear decline of log $S(\mu)$ for $\mu < -1$ indicates the dominance of the strong resonance transition. Finally, the third group of atoms in the middle of the periodic table exhibits an intermediate trend, in part similar to the loose atoms and in part similar to the tight atoms.

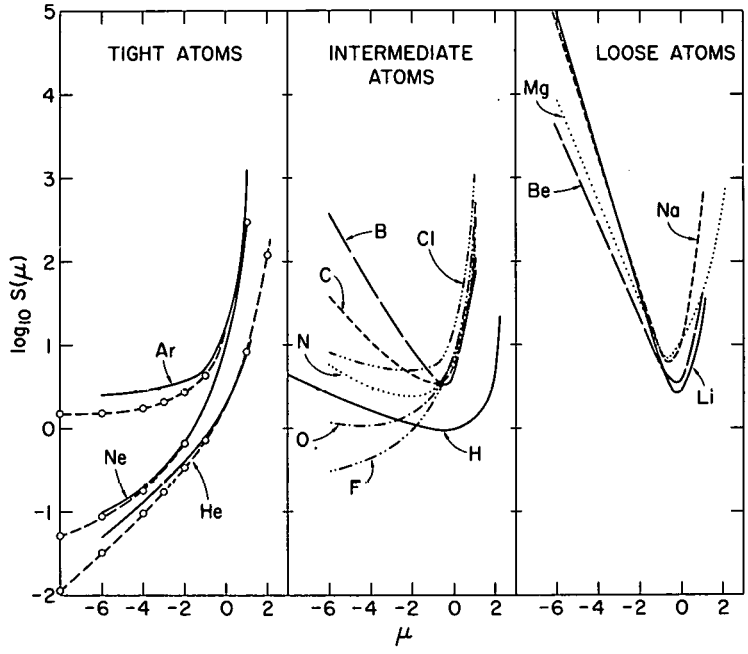

FIG. 1.--The moment $S(\mu)$ for each atom as a function of μ. Note that the vertical scale is logarithmic. The open circles connected by broken lines show semiempirical or otherwise better values for He, Ne, and Ar. The curve for H is rigorous. All the other curves are based upon the oscillator strength distribution for the Herman-Skillman model.

*Abstract of a paper to be presented at the Annual Meeting of the Division of Electron and Atomic Physics of the American Physical Society, Chicago 2–4 December 1974. Full account to be submitted to Phys. Rev. A.

†Presidential Intern, RER Division, February 1972–February 1973. Present address: Stanford Research Institute, Menlo Park, California 95025.

SYSTEMATICS OF MOMENTS OF DIPOLE OSCILLATOR-STRENGTH DISTRIBUTIONS. EXTENSION TO ATOMS OF THE THIRD ROW

J. L. Dehmer and J. D. Hanson*

An ongoing program to study systematics in the Z dependence of moments of the dipole oscillator-strength distributions is being extended to the atoms of the third row, K through Kr. The present work employs the realistic atomic potentials tabulated by Herman and Skillman.[1] Details of the calculation are specified elsewhere.[2–4]

Our earlier study of the first two rows have shown dramatic periodic variations with Z of moments of the oscillator-strength distribution. In particular, we observed that the rare gases, which are the atoms most easily treated experimentally, usually represent extremities of this periodic variation. The principal objective of the present extension of this work is to map out the behavior of these moments along the transition metal series where the 3d subshell is filling.

TABLE 1. Values of the Dipole Oscillator Strength Moments $S(\mu)$ and $L(\mu)$ for Krypton Based on the Herman-Skillman Potential

μ	$S(\mu)$	$L(\mu)$
-6	7.381	-1.126
-5	6.466	-7.205×10^{-1}
-4	5.918	-3.810×10^{-1}
-3	5.700	-5.004×10^{-2}
-2	5.869	4.635×10^{-1}
-1	7.337	3.750
0	$3.604 \times 10^{+1}$	$1.150 \times 10^{+2}$
1	$6.015 \times 10^{+3}$	$4.286 \times 10^{+4}$
2	$2.348 \times 10^{+6}$	$1.628 \times 10^{+7}$

We report preliminary results for Kr here. The moments $S(\mu)$ and $L(\mu)$ for $-6 < \mu < 2$ are presented in Table 1. For $\mu \leq 0$ the accuracy is $< 0.1\%$. The accuracy declines for $\mu = 1$ ($\sim 1\%$) and $\mu = 2$ (5 to 10%) due to truncation at high energy (~ 500 Ryd) in the calculation of inner shell oscillator-strength distributions.

References

1. F. Herman and S. Skillman. Atomic Structure Calculations. Prentice-Hall, Inc., Englewood Cliffs, New Jersey, 1963.
2. J. L. Dehmer and R. P. Saxon. Radiological and Environmental Research Division Annual Report, July 1972–June 1973. ANL-8060, Part I, p. 102.
3. M. Inokuti, R. P. Saxon, and J. L. Dehmer. Int. J. Radiat. Phys. Chem. in press.
4. J. L. Dehmer, M. Inokuti, and R. P. Saxon. Phys. Rev. A, to be published.

* Appointee, Undergraduate Research Participation Program, Fall 1974, from Kalamazoo College, Kalamazoo, Michigan 49001.

ELECTRON DENSITIES OF ATOMS, AND CROSS SECTIONS FOR SCATTERING OF FAST CHARGED PARTICLES*

Mitio Inokuti and Michio Matsuzawa †

The cross section σ for elastic scattering of a particle of charge z and of high incident energy k^2 (Ryd) by a neutral atom of atomic number Z is written as $\sigma = \pi z^2 (Ak^{-2} + Bk^{-4} + \ldots)$, and the Born approximation gives[1] $A = 8 \int_0^\infty |F(K) - Z|^2 K^{-3} dK$, $B = -Z^2$, where F(K) is the form factor. The same A can be expressed directly in terms of the electron density $\rho(r)$ as

$$A = \frac{4}{3} \iint \rho(r)\, \rho(r')\, R^2 \ln R \, d\vec{r}\, d\vec{r'} - \frac{8}{3} Z \int \rho(r)\, r^2 \ln r \, d\vec{r} \,,$$

where $R = |\vec{r} - \vec{r'}|$. In the cross section for inelastic scattering, the coefficient of the leading $k^{-2} \ln k$ term is the dipole matrix element squared.[1] The coefficient of the k^{-2} term is given by a formula analogous to the one above for A, except that $\rho(r)$ now signifies an appropriate transition density.

Reference

1. H. Bethe. Ann. Physik (Leipzig) 5, 325 (1930).

---

*Abstract of a paper presented at the Annual Meeting of the Division of Electron and Atomic Physics of the American Physical Society, Chicago, 2–4 December 1974. An account of the work will also appear in the Proceedings of the International Symposium on Electron and Photon Interactions with Atoms in Honor of Ugo Fano, Stirling, Scotland, 16–19 July 1974.

†Visiting Scientist 1972–1973. Present address: The University of Electro-Communications, Chifu-shi, Tokyo, Japan.

ELASTIC SCATTERING OF FAST ELECTRONS BY ATOMS. I. HELIUM TO NEON*

Mitio Inokuti and M. R. C. McDowell†

The total elastic-scattering cross section for electrons on neutral atoms is evaluated in the first Born approximation via tabulated values of the form factors. The cross section at energy k^2 Rydbergs is expressed as $\sum_{j=1}^{3} a_j(Z)\, k^{-2j}$, values of the coefficients $a_j(Z)$ being given for $1 \le Z \le 10$. The theoretical results are compared with experiment for helium, neon, and lithium. For lithium, comparisons are also made with Glauber and polarization-Glauber models. A simple model is presented for low-energy total cross sections in lithium, and its predictions compared with experiment. Elastic differential cross sections for helium and neon are briefly discussed.

---

*Abstract of a paper published in J. Phys. B. 7, 2382 (1974).

†Mathematics Department, Royal Holloway College, Englefield Green TW20 OEX, England.

ELECTRON ENERGY-LOSS SPECTROMETER. PROGRESS REPORT II

R. H. Huebner, David Spence, and O. J. Steingraber

The operational characteristics of the electron energy-loss spectrometer have been studied. Preliminary electron energy-loss spectra for molecular nitrogen have been obtained at several scattering angles.

Introduction

Previously we have reported the design[1] and construction details[2] of the electron energy-loss spectrometer (EELS). Mechanical assembly of this new apparatus was complete at the time of the last progress report, and major subsystem components had been tested. However, at that time, neither the electron monochromator nor the energy analyzer had been tested. Progress on the operation of these components and the completed system is reported here.

In September 1973 an electron beam was obtained from the monochromator and collected in a Faraday cup. The beam intensity was optimized for the lens element voltages expected from design considerations, although the energy spread of the beam was not determined. A beam current of about 5×10^{-8} A was measured at the collision region for a cathode emission current of 25 μA.

Electrical connections to the energy analyzer were completed in January 1974 after modifications to the electrostatic shields and the installation of an electron collector behind a small hole in the analyzer hemisphere. This collector is located on the beam axis of the entrance leg of the analyzer and is used in aligning the beam. Other connections were made to several lens elements to permit detection of the beam at critical points along its path. With these modifications a procedure was established for passing the beam through the electron-optical system.

With the beam properly aligned, its energy distribution could be measured by applying a linear bias voltage to the analyzer. A typical energy distribution obtained in these tests is shown in Figure 1. At present our energy resolution has been limited to about 200 meV full width at half maximum (FWHM),

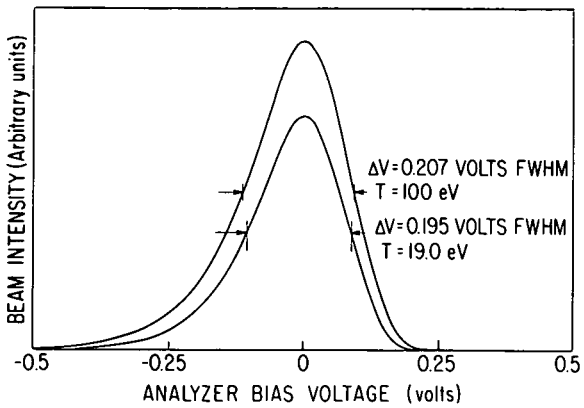

FIG. 1.--Measured energy distributions of the EELS electron beam for incident energies of 10 and 100 eV.

which is a factor of 4 greater than our design objective. Some additional modifications may be necessary for high-resolution work. However, beam stability and current are sufficient for preliminary energy-loss studies.

Tests of the system operating in the energy loss mode have been most encouraging. By shielding the collision region from stray electric fields with a molybdenum wire mesh and adjusting the system for maximum beam intensity, we successfully obtained our first energy-loss spectra. In Figure 2 we show spectra of molecular nitrogen obtained for an 80-eV incident beam at several scattering angles. The peak observed at zero energy loss is due to elastically scattered electrons. Even with modest energy resolution ($\sim$ 300 meV FWHM), distinct energy loss peaks characteristic of N_2 are apparent.

Actually the observed peaks in Figure 2 are composites of several unresolved vibrational bands: for example, the intense peak at 12.9 eV is made up of 6 peaks spaced less than 0.1 eV apart.[3] However, the general shape of the spectrum and peak positions closely match the early data of Lassettre and co-workers.[4,5]

It is also interesting to note the trend of these spectra as the scattering angle is increased from 6° to 15°. First, the intensity of the inelastic features decreases relative to the intensity of the elastic-scattering peak as the angle is increased. This is expected, since the inelastic-scattering cross section is usually more strongly peaked in the forward direction than the elastic-scattering cross section. Second, the forbidden transition at 9.2 eV, the Lyman-Birge-Hopfield bands of N_2, increases relative to the dipole allowed features at 12.9 and 14.0 eV as the scattering angle is increased.

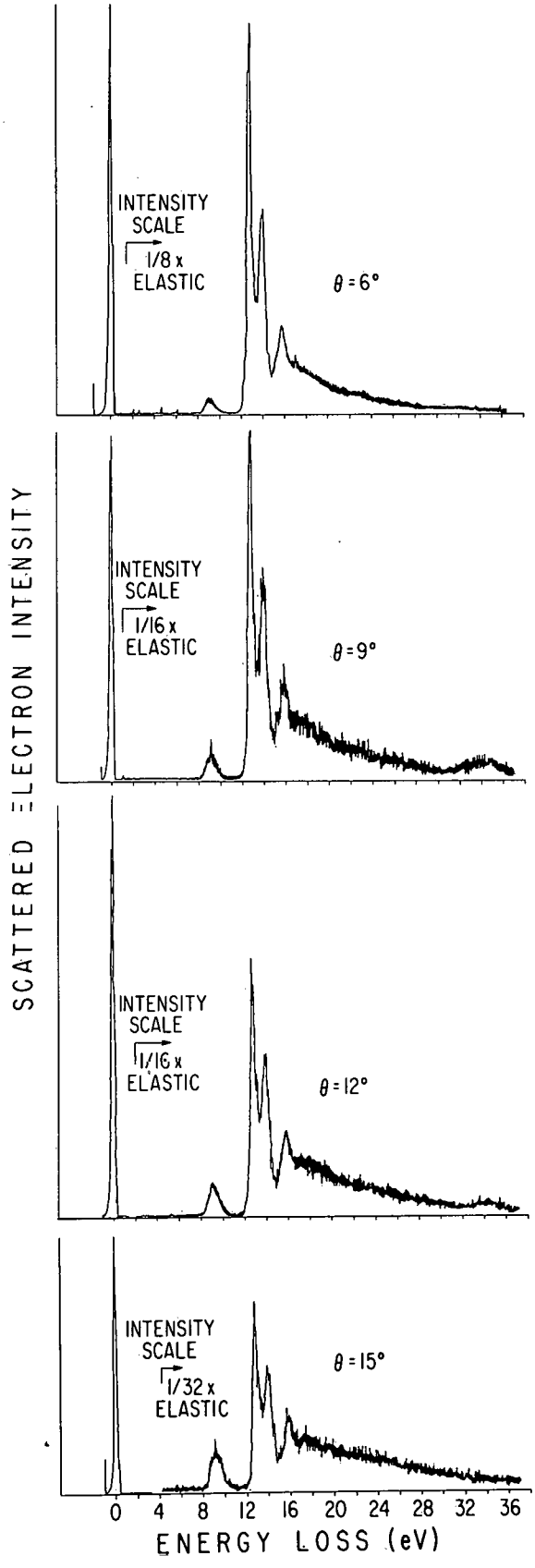

FIG. 2.--Energy-loss spectra of N_2 obtained for 100-eV incident electrons at the indicated scattering angles. The inelastic scattering intensity is relative to the elastic scattering peak intensity at each angle.

This behavior is the same as that first observed by Lassettre and Krasnow[6] and demonstrates the different angular dependence expected between dipole allowed and forbidden transitions.

Another interesting feature is the occurrence of a broad maximum at an energy loss of about 34 eV in the ionization continuum of N_2 at scattering angles of 9° and 12°. This maximum is not apparent in either the 6° or 15° spectra. For the present experimental conditions, this angular range corresponds to momentum transfer values $[(Ka_0)^2]$ between 0.37 and 0.50 in atomic units. Qualitatively this can be understood by noting the generalized oscillator strength (GOS) measurements of Silverman and Lassettre.[7] They observed that between energy losses of 24.5 and 34.2 eV in N_2 the GOS changes from a monotonically decreasing function of $(Ka_0)^2$ to a function that first increases to a maximum before declining. In fact, their data show that the GOS for a 34.2-eV energy loss rises above the GOS at 24.5 eV for values of $(Ka_0)^2$ above 0.40. Although the GOS values they determined for 500-eV incident electrons should not be precisely the same for the 80-eV incident electrons used in this study, the similarity between the two observations suggests a close relationship.

These preliminary results indicate the EELS capability for energy loss measurements. Further tests are underway to test EELS operation for incident energies of 100 eV and above. Attention is also being given to ways of improving instrumental energy resolution.

References

1. D. Spence and R. H. Huebner. Radiological and Environmental Research Division Annual Report, July 1971–June 1972. ANL-8060, Part I, p. 45.
2. R. H. Huebner, D. Spence, and O. J. Steingraber. Radiological and Environmental Research Division Annual Report, July 1972–June 1973. ANL-8060, Part I, p. 74.
3. V. D. Meyer, A. Skerbele, and E. N. Lassettre. J. Chem. Phys. 43, 805 (1965).
4. A. Skerbele and E. N. Lassettre. J. Chem. Phys. 42, 395 (1965).
5. E. N. Lassettre, F. M. Glaser, V. D. Meyer, and A. Skerbele. J. Chem. Phys. 42, 3429 (1965).
6. E. N. Lassettre and M. E. Krasnow. J. Chem. Phys. 40, 1248 (1964).
7. S. M. Silverman and E. N. Lassettre. J. Chem. Phys. 42, 3420 (1965).

APPARENT OSCILLATOR-STRENGTH DISTRIBUTIONS DERIVED FROM ELECTRON ENERGY-LOSS MEASUREMENT: METHANE AND n-HEXANE*

R. H. Huebner, C. H. Fergurson,† R. J. Celotta,‡ and S. R. Mielczarek‡

High-quality "calibration" spectra of methane and n-hexane have shown[1] the possibility of quantitative analysis by electron energy-loss spectroscopy. These spectra were taken for 100-eV incident electrons with the NBS model AN-1 electron-impact spectrometer,[1,2] which recorded electrons scattered within 20 milliradians of the incident direction. Research-grade gases with stated purity of 99.99% were used without further purification. The energy-loss spectra were obtained by digitally recording the intensity of inelastically scattered electrons in 10-meV intervals. Each spectrum was swept between two selected energy-loss points, alternately for increasing and decreasing energy loss, so that effects due to pressure and electron-beam fluctuations would be averaged out.

Two corrections were made to the data. First, the count rate was adjusted to allow for a 20-nsec dead time of the counting circuitry, and thus to assure linearity of the measured intensity. Second, approximately equal parts of helium and the sample gas were introduced simultaneously into the apparatus, and the energy-loss scale was calibrated to the position of the $2^1P \leftarrow 1^1S$ transition in helium at 21.21 eV. From the full width at half maximum of this transition, we determined the energy resolution to be 39 meV and 42 meV, respectively, for the methane and n-hexane.

Apparent oscillator-strength distributions were derived from the data by a procedure[3,4] that corrects for the finite angular acceptance of the apparatus

---

*A preliminary version was presented at the IV International Conference on Vacuum-Ultraviolet Radiation Physics, Hamburg, July 22–26, 1974 and will be published by Vieweg-Pergamon.

†Undergraduate Research Participant from Illinois College, Jacksonville, Ill. sponsored by the Center for Educational Affairs, Argonne National Laboratory.

‡National Bureau of Standards, Washington, D.C. 20234.

and normalizes the distribution to an optical value at one value of the energy loss. To test this procedure, we first compared the result for methane with the energy-loss data of Harshbarger and Lassettre.[5] Their data pertain to 500-eV incident electrons scattered at zero degrees. Both sets of derived oscillator-strength distributions were normalized to an optical value of 0.1749 eV^{-1} at 10.33 eV measured by Watanabe et al.[6] and are compared in Figure 1. The distribution obtained from these two independent measurements agree well within experimental accuracy between 8.0 and 14.0 eV. Thus, the same limiting shape of the oscillator-strength distribution is reached even though the Born approximation is unlikely to hold equally well for incident energies of 100 and 500 eV. Further, we obtain an integrated f value of 0.290 for the first optically allowed transition (8.55 to 10.95 eV) that agrees closely with 0.277 ± 0.035 given by Harshbarger and Lassettre.[5] The latter value was obtained by normalization to the oscillator strength of the $2^1P \leftarrow 1^1S$ transition in helium and so provides an independent verification of the normalization chosen in the present work.

The values presented in Hudson's review[7] of photoabsorption data, along with other optical measurements,[8] are compared with the NBS/ANL oscillator-strength distribution in Figure 2. In the energy region shown, the agreement is good. Where particular sets of optical values differ from the present results, we feel that the electron-impact values are more reliable.

Our apparent oscillator-strength distribution yields an oscillator strength sum of 0.754 for all transitions below the ionization potential[9] of 12.615 eV and 1.376 for all processes below 14.0 eV. This distribution is also consistent with recent sum-rule calculations[10] based mainly on a summary of photoabsorption data.

Electron energy-loss data for n-hexane are shown in Figure 3. The data were normalized at 10.067 eV to the df/dE value of 0.89 eV^{-1} from the optical measurements of Raymonda and Simpson.[11] Their values and those of Lombos et al.[8] are compared with the electron-impact results in Figure 3. The apparent oscillator strengths for n-hexane are not as reliable as those for methane, owing to the large uncertainty in the optical value used for

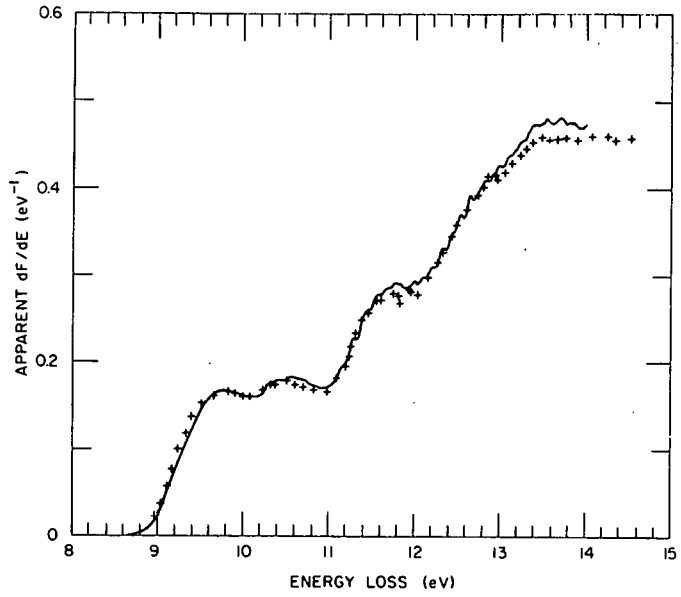

FIG. 1.--Apparent oscillator-strength distribution of methane derived from electron energy-loss data (+, Ref. 5; solid line, present work).

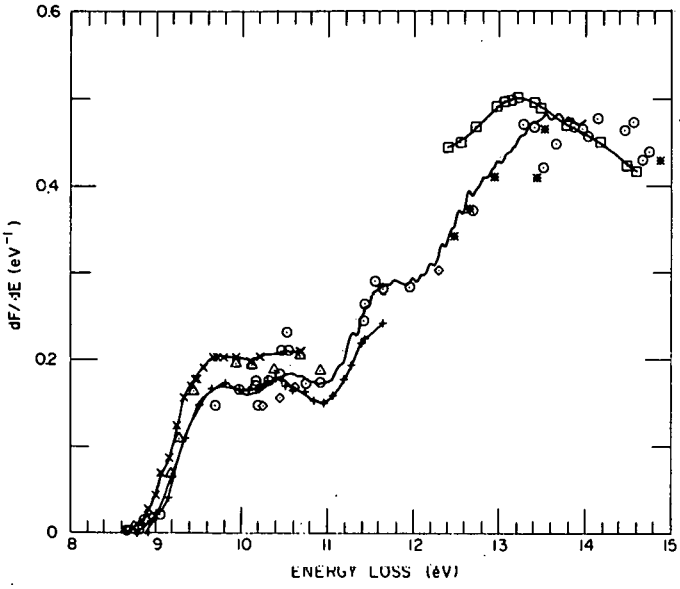

FIG. 2.--Apparent oscillator-strength distribution of methane compared with optical measurements. (Refs. 7 and 8). Solid line, present work; ◇, Wilkinson and Johnson; +, Watanabe et al. △, Laufer and McNesby; ⊙, Ditchburn; ▭, Metzger and Cook; *, Rustgi; x, Lombos et al. (See Refs. 7 and 8).

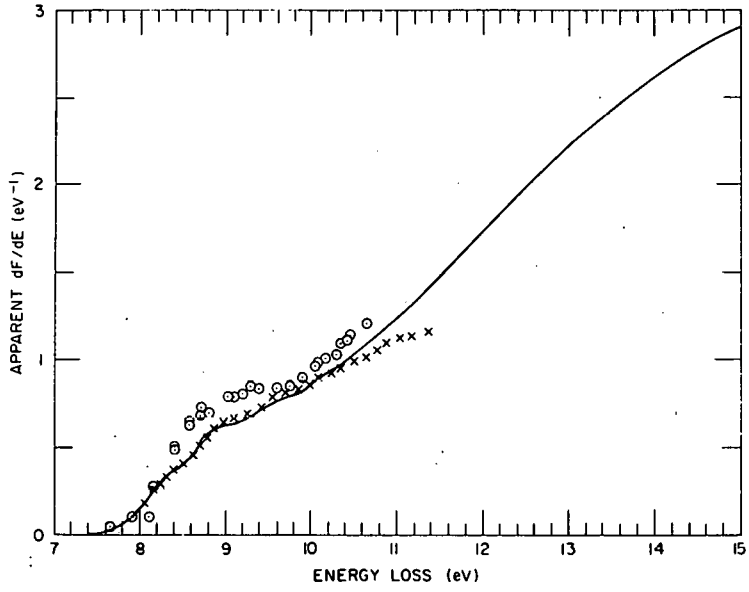

FIG. 3.--Apparent oscillator-strength distribution of n-hexane compared with optical measurements. Solid line, present work; x from Ref. 11; ⊙ from Ref. 8.

normalization. But the relative shapes of the distributions are in satisfactory agreement. The present results yield an integrated oscillator strength of 1.34 for the region below the ionization potential[12] of 10.18 eV and a value of 10.39 for the entire spectrum below 15.00 eV.

References

1. R. J. Celotta, S. R. Mielczarek, and C. E. Kuyatt. Electron Spectroscopy for Gas Analysis. National Bureau of Standards Report No. 10915 (1972).
2. J. A. Simpson. Record, Xth Symp. Electron Ion and Laser Beam Technology, Ed. L. Marton, San Francisco Press, 1969, p. 345.
3. R. H. Huebner and R. J. Celotta. Radiological and Environmental Research Division Annual Report, July 1971–June 1972. ANL-7960, Part I, p. 49.
4. R. H. Huebner, R. J. Celotta, S. R. Mielczarek, and C. E. Kuyatt. J. Chem. Phys. 59, 5434 (1973).
5. W. R. Harshbarger and E. N. Lassettre. J. Chem. Phys. 58, 1505 (1973).
6. K. Watanabe, M. Zelikoff, and E. C. Y. Inn. Geophys. Res. Pap. No. 21 (Geophys. Res. Directorate) Air Force Cambridge Research Center Tech. Rep. No. 53-23 (1953).
7. R. D. Hudson. Rev. Geophys. Space Phys. 9, 305 (1971).
8. B. A. Lombos, P. Sauvageau, and C. Sandorfy. J. Mol. Spectry. 24, 253 (1967).
9. W. A. Chupka and J. Berkowitz. J. Chem. Phys. 54, 4256 (1971).
10. J. Berkowitz, M. Inokuti, and J. C. Person. Abstracts, VIII International Conf. Phys. Electronic and Atomic Collisions, Belgrade, Yugoslavia, 16–23 July 1973, Ed. B. C. Čobić and M. V. Kurepa. Institute of Physics, Belgrade, 1973, p. 561.
11. R. W. Raymonda and W. T. Simpson. J. Chem. Phys. 47, 430 (1967).
12. K. Watanabe, T. Nakayama, and J. Mottl. J. Quant. Spectry. Radiative Transfer 2, 369 (1962).

DIPOLE OSCILLATOR-STRENGTH DISTRIBUTIONS DERIVED FOR SEVERAL HYDROCARBONS FROM ELECTRON ENERGY-LOSS SPECTRA*

R. H. Huebner, R. J. Celotta, † S. R. Mielczarek, † and C.E. Kuyatt †

An important input for calculating the radiation-chemical yields of primary products is the dipole oscillator-strength distribution of the molecular target. Such distributions can be obtained not only from photoabsorption measurements, but also from electron energy-loss spectra by a method described in detail elsewhere.[1,2] We have derived relative oscillator strengths for a number of hydrocarbons from energy-loss spectra measured for 100-eV incident electrons scattered in the forward direction. After these data are normalized to an optical value at one energy, the electron-impact values are found in good agreement with optical values for other energies below 15 eV.

Besides the results presented elsewhere in this report[3] for methane and n-hexane, we have obtained the apparent oscillator strength distribution for benzene. Figure 1a shows the benzene data normalized at 11.39 eV to a df/dE value of 0.6424 eV^{-1} obtained by Person.[4] Other optical values[4,5] are included for comparison. This normalization yields an integrated f value of 0.779 for the strong $^1E_{1u} \leftarrow {}^1A_{1g}$ transition between 6.525 and 7.75 eV. This is 15% lower than optical values of 0.91 and 0.88 measured by Yoshino et al.[5] and Hammond and Price,[6] respectively. If the electron-impact values are increased by 15%, we obtain the distribution shown in Figure 1b. Recent optical data obtained by Koch and Otto[7] with a synchrotron light source are also shown. This change in normalization improves the agreement between the electron-impact and optical data below 9 eV. However, between 9.5 and 10.5 eV and above 12 eV the electron values are larger than the optical. A more extensive comparison is shown in Figure 2 where all of the optical data[4,5,8–10] available between 9 and 15 eV are included. Although the optical data show a considerable spread about the electron data in the

---

* Summary of a paper presented at the Vth International Congress on Radiation Research, Seattle, Washington, July 1974.

† National Bureau of Standards, Washington, D.C.

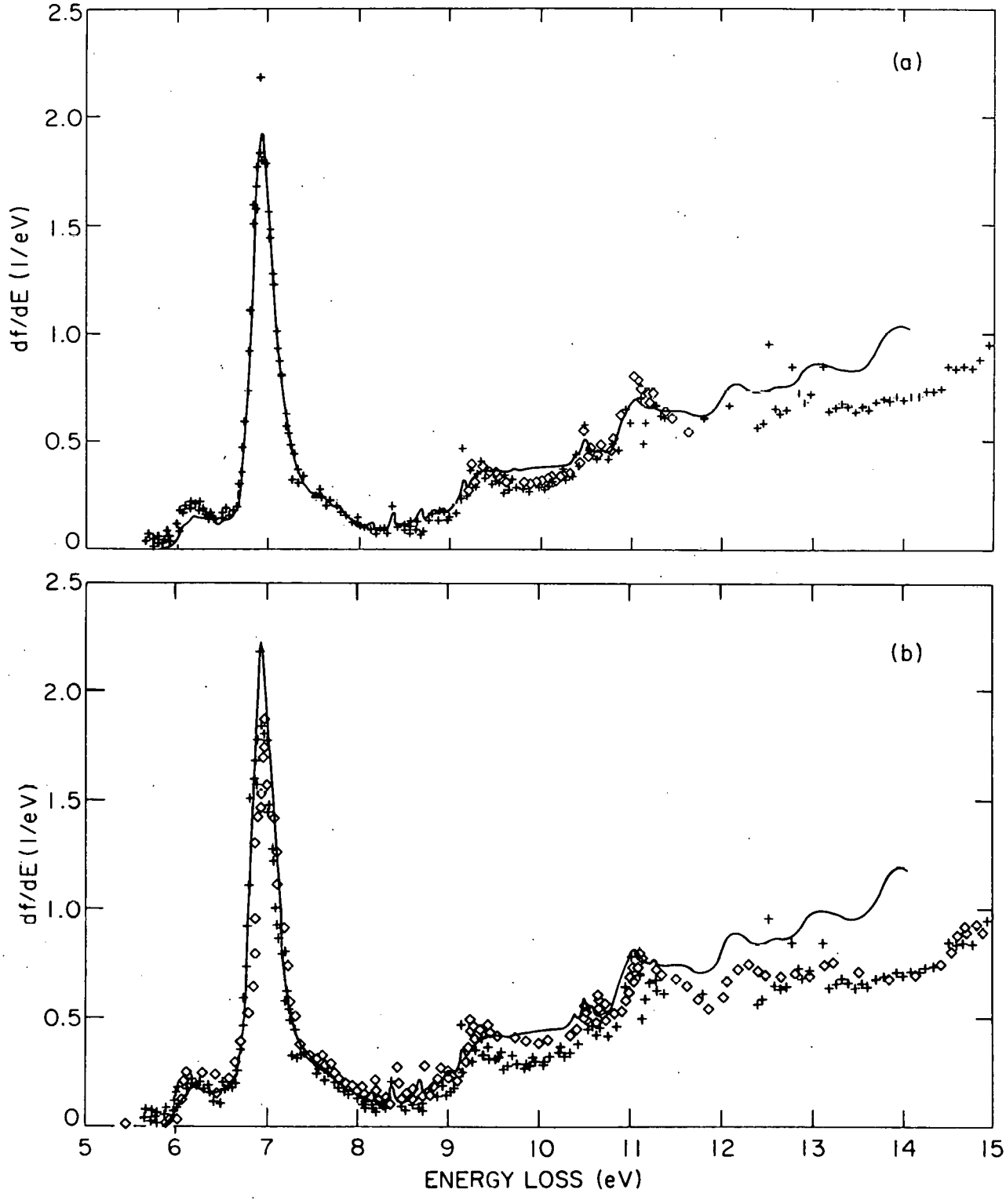

FIG. 1.--The oscillator-strength distribution for benzene: (a) electron impact values (solid line) normalized at 11.39 eV are compared with optical data of Ref. 4 (diamonds) and Ref. 5 (crosses); (b) electron impact values (solid line) normalized to give an integrated f value of 0.90 for the transition at 6.9 eV are compared with optical values of Ref. 5 (crosses) and Ref. 7 (diamonds).

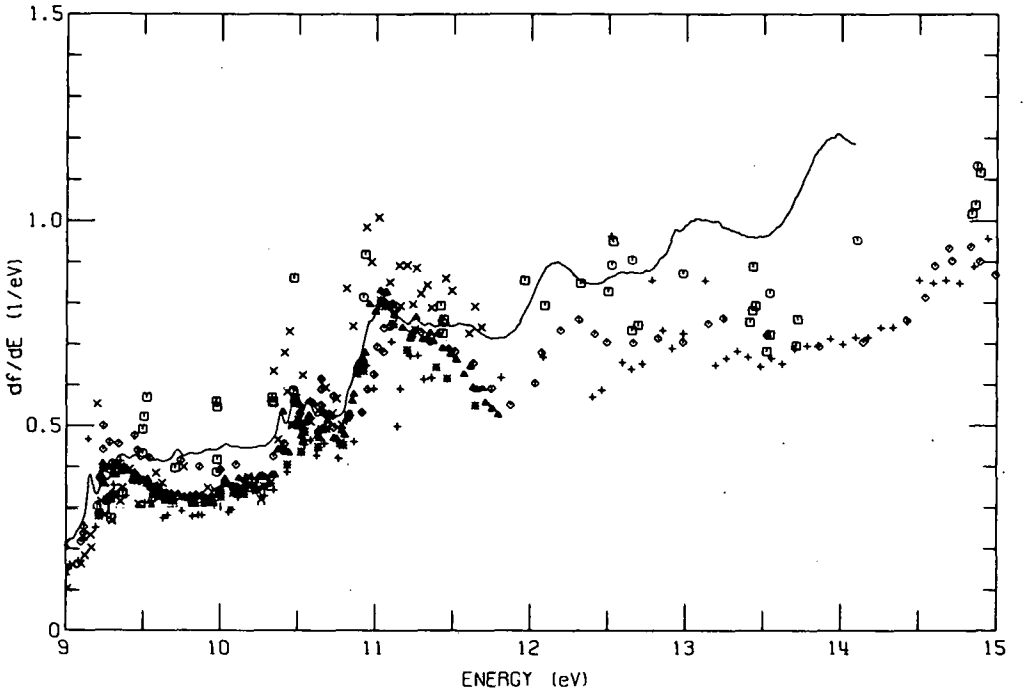

FIG. 2.--Comparison of electron-impact oscillator-strength distribution of Fig. 1b (solid line) with optical values of Ref. 4 (*), Ref. 5 (+), Ref. 7 (diamond), Ref. 8 (triangle), Ref. 9 (square and circle), and Ref. 10 (X).

9.5- to 10.5-eV region, the usually more reliable measurements of Person[4] and Samson[8] lie 30% below the electron-impact curve. Such a large difference has not been previously noticed in similar comparisons for other polyatomic molecules.[1] The cause of this difference is not understood.

Above 11.5 eV the values derived from energy-loss data are higher than most of the optical data. Also, some of the structure, e.g., the sharp rise between 13.5 and 14.0 eV, is absent in the optical data. A similar unexplained rise was observed by Skerbele and Lassettre[11] for 300-eV electrons incident on benzene. It is possible that optically forbidden excitations may contribute increased intensity to the energy-loss spectrum in this region, although we are aware of no supporting evidence for this contention. It may also be that the energy-loss spectrum may be somewhat distorted for these large energy losses. On the other hand, the optical values may be too low as the result, for example, of photoexcited fluorescence in the sample. Recent sum-rule calculations[12] based on a summary of photoabsorption data yield a total f sum that is about 9.5% below the theoretically expected value of Z = 42 for the benzene molecule.

This supports the suggestion that the optical measurements are too low, although it is uncertain whether this is limited to specific regions or spread over the entire photoabsorption spectrum.

The present analysis suggests that further studies in the 9.5- to 10.5-eV region and in the region above 11.5 eV are needed before the dipole oscillator-strength distribution of benzene can be regarded as firmly established.

References

1. R. H. Huebner and R. J. Celotta. Argonne National Laboratory Radiological and Environmental Research Division Annual Report, July 1971–June 1972. ANL-7960, Part I, p. 49.
2. R. H. Huebner, R. J. Celotta, S. R. Mielczarek, and C. E. Kuyatt. J. Chem. Phys. 59, 5434 (1973).
3. R. H. Huebner, C. H. Fergurson, R. J. Celotta, and S. R. Mielczarek. Apparent Oscillator-Strength Distributions Derived from Electron Energy-Loss Measurements. Methane and n-Hexane. This report.
4. J. C. Person. J. Chem. Phys. 43, 2553 (1965).
5. M. Yoshino, J. Takeuchi, and H. Suzuki. J. Phys. Soc. Japan 34, 1039 (1973).
6. V. J. Hammond and W. C. Price. Trans. Faraday Soc. 51, 605 (1955).
7. E. E. Koch and A. Otto. Int. J. Radiat. Phys. Chem. To be published.
8. J. A. R. Samson. Planetary Atmosphere Studies III. Summary Report; Experimental Results of Vacuum Ultraviolet Spectroscopy. GCA Technical Report No. 61-15-N (December 1961).
9. S. M. Bunch, G. R. Cook, M. Ogawa, and A. W. Ehler. J. Chem. Phys. 28, 740 (1958).
10. K. Goto. Sci. Light 11, 116 (1962).
11. A. Skerbele and E. N. Lassettre. J. Chem. Phys. 42, 395 (1965).
12. J. Berkowitz, ANL Physics Division. Private communication.

APPARENT OSCILLATOR STRENGTHS FOR MOLECULAR OXYGEN*

R. H. Huebner, R. J. Celotta,† S. R. Mielczarek,† and C. E. Kuyatt†

Oxygen, the second most abundant molecule in the atmosphere, plays an important role in a variety of combustion and atmospheric photochemical processes. Thus, the microscopic processes of energy absorption by O_2 are of considerable interest, not only from a fundamental, but also from a practical viewpoint. An apparent oscillator strength distribution for O_2 (Figure 1) was derived[1,2] from the energy loss spectrum of 100-eV electrons scattered within 20 milliradians of the incident direction. These data are compared with optical data of Watanabe[3] in Figures 2 and 3. Integrated f values of the order of 10^{-5} for the v' = 2 to v' = 20 vibrational members of the Schumann-Runge bands agree closely with high-resolution photoabsorption measurements[4-8] (Table 1). Vibrational peaks superimposed on the Schumann-Runge continuum, previously assigned[9] to the $(3s\sigma_g)^3\Pi_g$ Rydberg state, contribute 0.46% of the total oscillator strength of 0.1616 obtained for the Schumann-Runge bands and continuum. Oscillator strengths in the remainder of the spectrum are given in Table 2. These data yield f sums of 0.1978 and 0.3833 for all transitions below 12.07 and 14.09 eV, respectively.

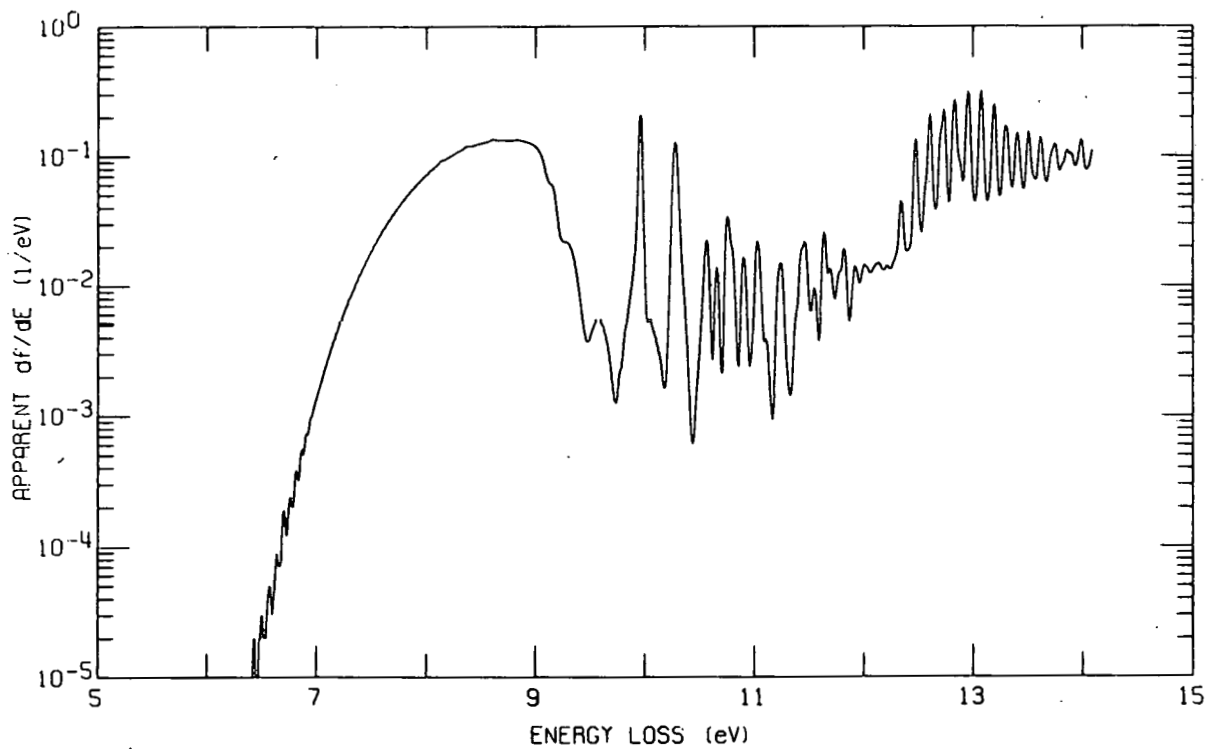

FIG. 1.--Apparent oscillator strength distribution for O_2.

TABLE 1. Oscillator Strengths of the Schumann-Runge Bands of O_2

$\nu' - \nu''$	Band origin, eV	Optical values					Electron values
		Bethke[4]	Halmann[5]	Farmer et al.[7]	Ackerman et al.[6]	Hasson et al.[8]	This work
0 – 0	6.121				3.45×10^{-10}	3.3×10^{-10}	
1 – 0	6.204				3.9×10^{-9}	3.5×10^{-9}	2.7×10^{-8}
2 – 0	6.287	2.3×10^{-8}	2.6×10^{-8}	2.69×10^{-8}	2.38×10^{-8}	1.99×10^{-8}	6.2×10^{-8}
3 – 0	6.366	7.4×10^{-8}	8.2×10^{-8}	1.54×10^{-7}	9.9×10^{-8}	6.8×10^{-8}	5.6×10^{-8}
4 – 0	6.443	2.74×10^{-7}	2.4×10^{-7}	7.11×10^{-7}	3.21×10^{-7}		2.97×10^{-7}
5 – 0	6.516	7.28×10^{-7}	7.48×10^{-7}	2.80×10^{-6}	8.52×10^{-7}		7.39×10^{-7}
6 – 0	6.586	1.73×10^{-6}	1.77×10^{-6}	4.40×10^{-6}	1.91×10^{-6}		1.70×10^{-6}
7 – 0	6.652	3.56×10^{-6}	4.24×10^{-6}	8.15×10^{-6}	3.81×10^{-6}		3.50×10^{-6}
8 – 0	6.714	6.75×10^{-6}	6.59×10^{-6}	1.22×10^{-5}	6.68×10^{-6}		6.85×10^{-6}*
9 – 0	6.772	1.07×10^{-5}	1.13×10^{-5}	1.50×10^{-5}	1.06×10^{-5}		1.05×10^{-5}
10 – 0	6.825	1.56×10^{-5}	1.42×10^{-5}	2.05×10^{-5}	1.57×10^{-5}		1.60×10^{-5}
11 – 0	6.873	2.16×10^{-5}		2.74×10^{-5}	2.09×10^{-5}		2.26×10^{-5}
12 – 0	6.916	2.81×10^{-5}		3.58×10^{-5}	2.53×10^{-5}		2.88×10^{-5}
13 – 0	6.953	3.17×10^{-5}		3.66×10^{-5}	2.88×10^{-5}		3.41×10^{-5}
14 – 0	6.985	3.24×10^{-5}		3.69×10^{-5}	3.03×10^{-5}		3.77×10^{-5}
15 – 0	7.011	3.26×10^{-5}		3.77×10^{-5}	2.92×10^{-5}		3.73×10^{-5}
16 – 0	7.032	3.16×10^{-5}		3.31×10^{-5}	2.59×10^{-5}		3.53×10^{-5}
17 – 0	7.048	2.94×10^{-5}		3.16×10^{-5}	2.23×10^{-5}		3.03×10^{-5}
18 – 0	7.061			2.03×10^{-5}	1.83×10^{-5}		2.72×10^{-5}
19 – 0	7.070			1.74×10^{-5}	1.44×10^{-5}		1.98×10^{-5}
20 – 0	7.077			1.35×10^{-5}			1.64×10^{-5}

*A 10% correction to the 8 – 0 band was made to account for an estimated contamination of less than 1 ppm of mercury vapor from the diffusion pumps.

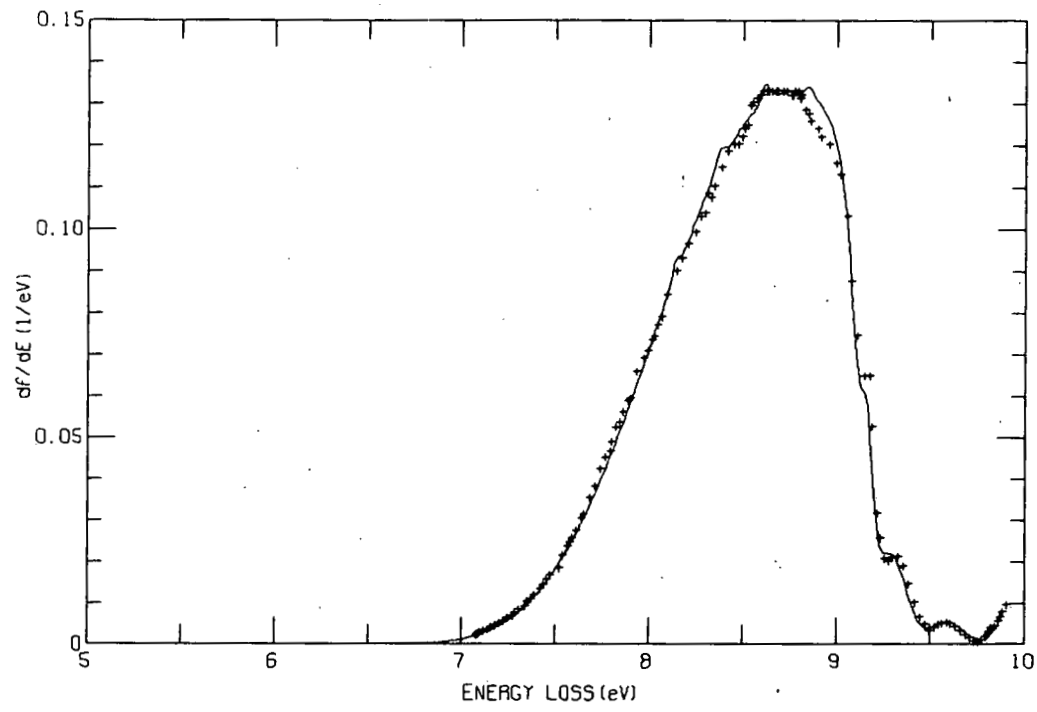

FIG. 2.--Comparison of oscillator strengths in the Schumann-Runge region of O_2: (solid line) electron impact values; (crosses) optical data of Watanabe.[3]

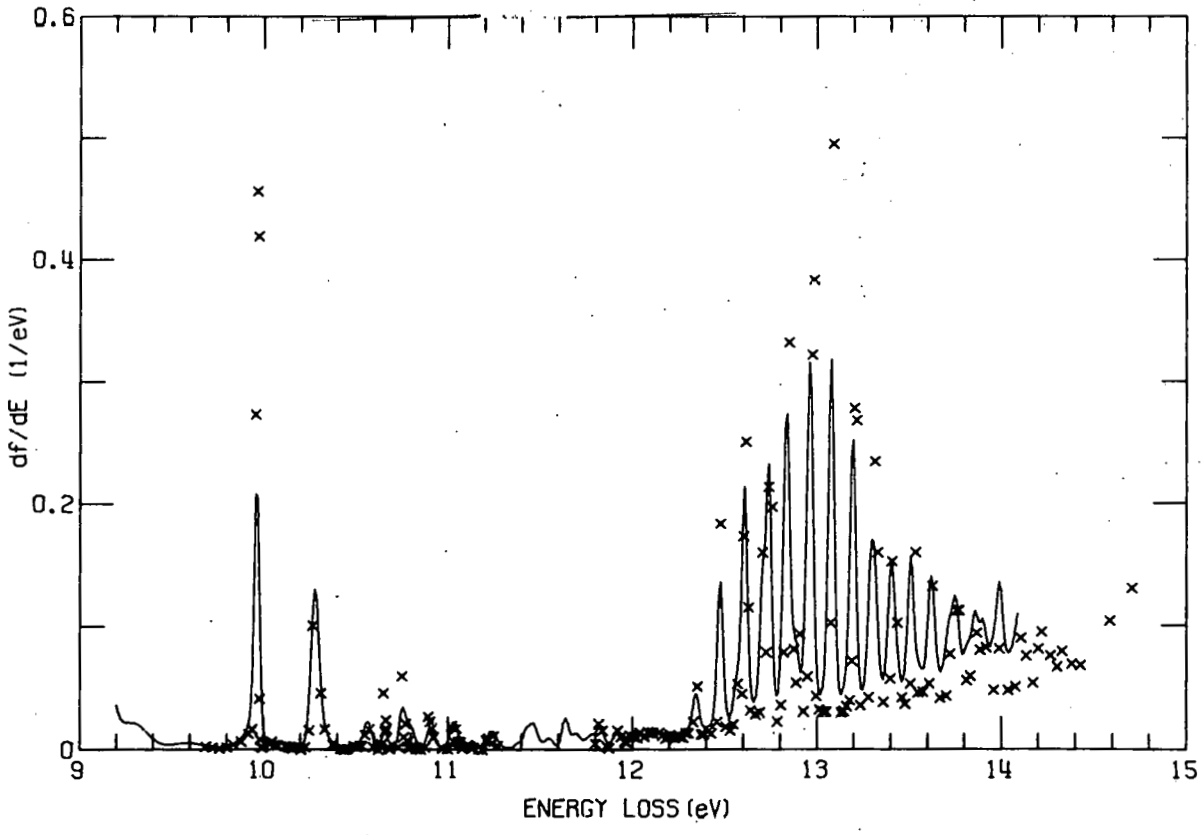

FIG. 3.--Comparison of oscillator strengths in the 9- to 15-eV region of O_2: (solid line) electron impact values; (crosses) optical data of Watanabe.[3]

TABLE 2. Oscillator Strengths for Transitions in O_2 from 9.58 to 14.04 eV

E_m, eV	E_1, eV	E_2, eV	f-value	Identification
9.58	9.48	9.74	1.01×10^{-3}	
9.96	9.74	10.18	10.24×10^{-3}	longest band
10.28	10.18	10.44	8.04×10^{-3}	second band
10.57	10.44	10.62	1.47×10^{-3}	third band
10.66	10.62	10.71	6.50×10^{-4}	a
10.76	10.71	10.86	2.42×10^{-3}	a
10.90	10.86	10.96	9.00×10^{-4}	b
11.03	10.96	11.17	1.59×10^{-3}	b,c
11.24	11.17	11.33	1.10×10^{-3}	c
11.46	11.33	11.52	2.10×10^{-3}	d
11.55	11.52	11.59	5.02×10^{-4}	(?)
11.64	11.59	11.74	2.05×10^{-3}	d
11.82	11.74	11.87	1.63×10^{-3}	d
many	11.87	12.10	2.83×10^{-3}	
many	12.10	12.24	1.02×10^{-3}	
12.34	12.24	12.40	3.79×10^{-3}	H
12.48	12.40	12.53	7.25×10^{-3}	H
12.61	12.53	12.66	11.76×10^{-3}	H, H'
12.74	12.66	12.78	14.38×10^{-3}	H, H'
12.84	12.78	12.91	17.24×10^{-3}	H'
12.96	12.91	13.02	16.41×10^{-3}	M, H'
13.08	13.02	13.13	15.67×10^{-3}	M
13.20	13.13	13.25	13.90×10^{-3}	M
13.30	13.25	13.36	11.86×10^{-3}	M, M'
13.41	13.36	13.46	9.87×10^{-3}	M, M'
13.51	13.46	13.57	10.33×10^{-3}	M'
13.62	13.57	13.67	9.52×10^{-3}	M'
13.75	13.67	13.79	11.66×10^{-3}	M', (?)
13.86	13.79	13.94	14.24×10^{-3}	J
13.99	13.94	14.04	10.27×10^{-3}	J

References

1. R. H. Huebner and R. J. Celotta. Argonne National Laboratory Radiological and Environmental Research Division Annual Report, July 1971–June 1972. ANL-7960, Part I, p. 49.
2. R. H. Huebner, R. J. Celotta, S. R. Mielczarek, and C. E Kuyatt. J. Chem. Phys. 59, 5434 (1973).
3. K. Watanabe. Advances Geophys. 5, 153 (1958).
4. G. W. Bethke. J. Chem. Phys. 31, 669 (1959).
5. M. Halmann. J. Chem. Phys. 44, 2406 (1966).
6. M. Ackermann, F. Biaume, and G. Kockarts. Planet. Space Sci. 18, 1639 (1970).
7. A. J. D. Farmer, W. Fabian, B. R. Lewis, K. H. Lokan, and G. N. Haddad. J. Quant. Spectry. Radiative Transfer 8, 1739 (1968).
8. V. Hasson, G. R. Hebert, and R. W. Nicholls. J. Phys. B 3, 1188 (1970).
9. D. C. Cartwright, W. J. Hunt, W. Williams, S. Trajmar, and W. A. Goddard, III. Phys. Rev. A 8, 2436 (1973).

---

*Summary of a paper to be presented at the Annual Meeting of the Division of Electron and Atomic Physics of the American Physical Society, Chicago, 2–4 December 1974.

†National Bureau of Standards, Washington, D.C.

ABSORPTION CROSS SECTIONS FOR GASES IN THE EXTREME ULTRAVIOLET REGION: C_2H_4, $C(CH_3)_4$, CH_3OH, C_2H_5OH, c-C_6H_{12}, C_6H_6, $CH_3C_6H_5$, AND CCl_4

James C. Person and Paul P. Nicole

Absorption cross sections or differential oscillator strengths measured with the double ion chamber are presented for ethylene, neopentane, methanol, ethanol, cyclohexane, benzene, toluene, and carbon tetrachloride. In all cases the upper energy limit is 21.2 eV and the lower energy limit is between 8.8 and 12.7 eV. The comparison of the present data with electron energy-loss data is discussed, along with some possible assignments of the spectral features observed.

Introduction

One valuable input for theoretical radiation physics is the oscillator-strength distribution. As the differential oscillator strength df/dE is directly porportional to the absorption cross section σ, absorption data are a natural starting point in the construction of an oscillator-strength distribution. Unfortunately, many of the existing absorption data are unreliable and large discrepancies in the results obtained by different workers are common. However, the double ion chamber[1] has proved to be a reliable apparatus for σ determinations, as it is unaffected by low energy photons which may result from scattered light or from emission produced in the sample. We are presently using this technique to measure σ values over a wide range of photon energy E (for E values above the ionization potential of the sample), and we report values for $E \leq 21$ eV. The preliminary σ values are given for ethylene, 2,2-dimethyl propane (neopentane), methanol, ethanol, cyclohexane, benzene, toluene, and carbon tetrachloride; and the df/dE values derived from the σ values are compared with relative df/dE values derived from electron energy-loss experiments for methanol, ethanol, and benzene.

Experimental

The apparatus, consisting of a light source, monochromator, and double ion chamber, has previously been described.[2,3] A hydrogen-discharge

lamp was used for energies up to 13.3 eV, and a high-pressure helium lamp was used for $12.5 \leq E \leq 21.2$ eV. The double ion chamber has been modified by inserting a stainless-steel end plate between the exit slit and the start of the front chamber. The plate has a rectangular hole 0.53×0.25 cm (divided into $0.18- \times 0.25$-cm open areas by wires 0.002 cm in diameter) to pass the incoming light beam. The introduction of this plate has shortened the front chamber to 7.39 cm, and the rear chamber is 21.07 cm long. The rear chamber has a tungsten mesh (98% transparent) on each end, and the end plates, the cylindrical walls, and the repeller plates in each chamber are all connected to a positive potential (typically 17 to 23 eV) to provide the collecting field for the positive ions. Thus, the new end plate provides a more uniform field in comparison with that given by the interior of the slit assembly.

The gas pressure was measured using an MKS Baratron Type 77H-1 capacitive manometer, using the calibration supplied by the manufacturer. The ethylene, neopentane, cyclohexane, benzene, and toluene were all Phillips Petroleum Company research grade, with stated purities of 99.88 mol % or greater. The alcohols were the same as used previously,[3,4] and the CCl_4 was Fisher Scientific Company, certified A.C.S. grade. All samples were degassed before use, but there were no checks of sample purity.

Data Analysis

A small correction for scattered light was made by subtracting the ion currents measured at E values where the lamp does not emit (24.8 eV for the helium lamp and 17.0 eV for the hydrogen lamp). In some cases, the hydrogen-lamp data were corrected by a linear interpolation between scattered-light measurements at a high energy and at a low energy, below the ionization potential of the sample.

The relative responses of the electrometers used to measure the ion currents were recalibrated, and tests of this calibration and of the relative length of the two cells were done by measuring σ as a function of pressure over a wide range of pressures. These tests revealed that some of our earlier data were analyzed incorrectly,[2,3] and corrections as large as 5 to 10% may

be necessary. The tests also indicate that any residual error in the cell lengths or calibration factors would not introduce an error in σ larger than 1 to 2%.

Results and Discussion

The data are presented in Figures 1–5, either as σ, or as df/dE. Most of the data were taken at wavelength intervals of 0.4 Å ($\Delta E \approx 0.01$ eV), and three points were averaged — this tends to reduce the energy resolution (the monochromator bandpass was 0.9 Å FWHM). For each gas, only one pressure was used with each light source, but results with other gases indicate that the σ values are reproducible to 1 to 3%. The energy scale has been adjusted to match the peaks of various emission lines so that the E values should be within 0.01 eV.

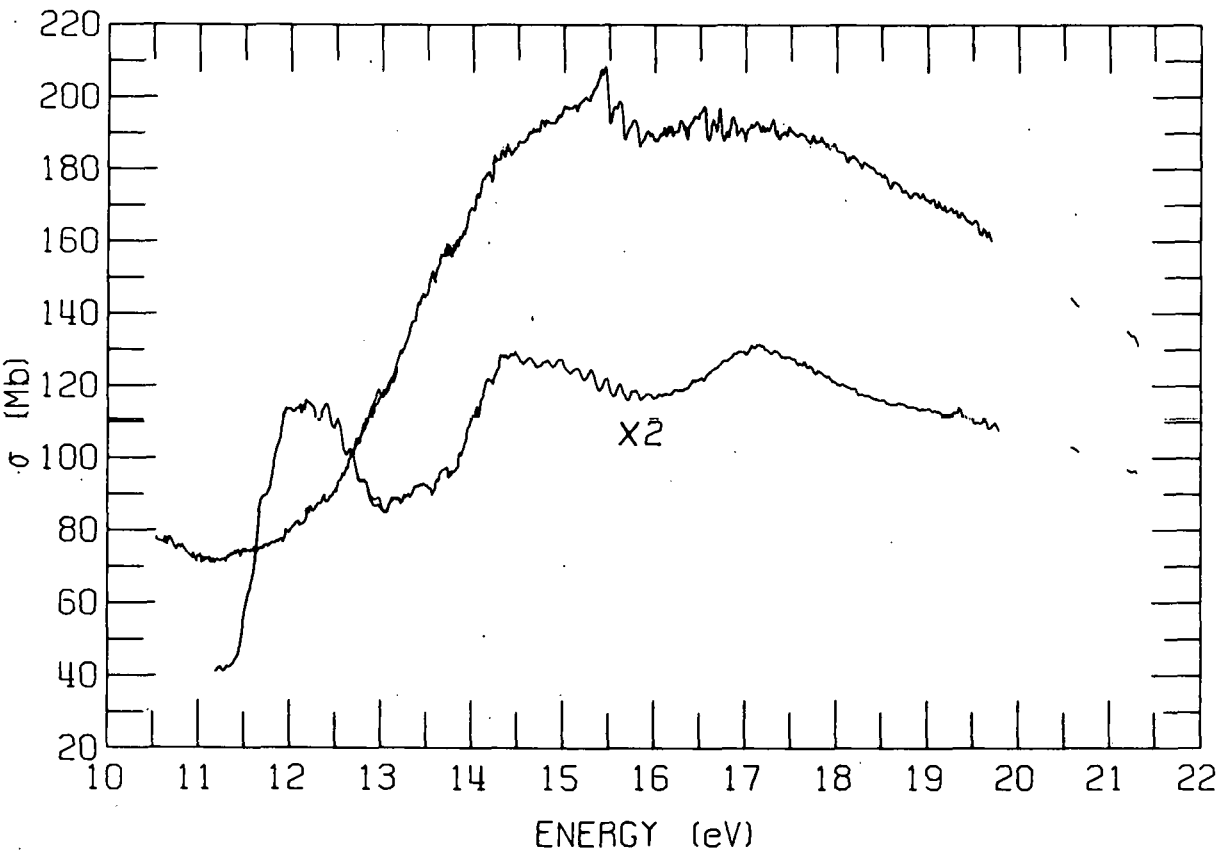

FIG. 1.--Absorption cross sections for ethylene and 2,2-dimethylpropane (neopentane). The cross sections for ethylene have been multiplied by 2 before plotting, and the resultant values give the curve that is lower except for a peak around 12 eV.

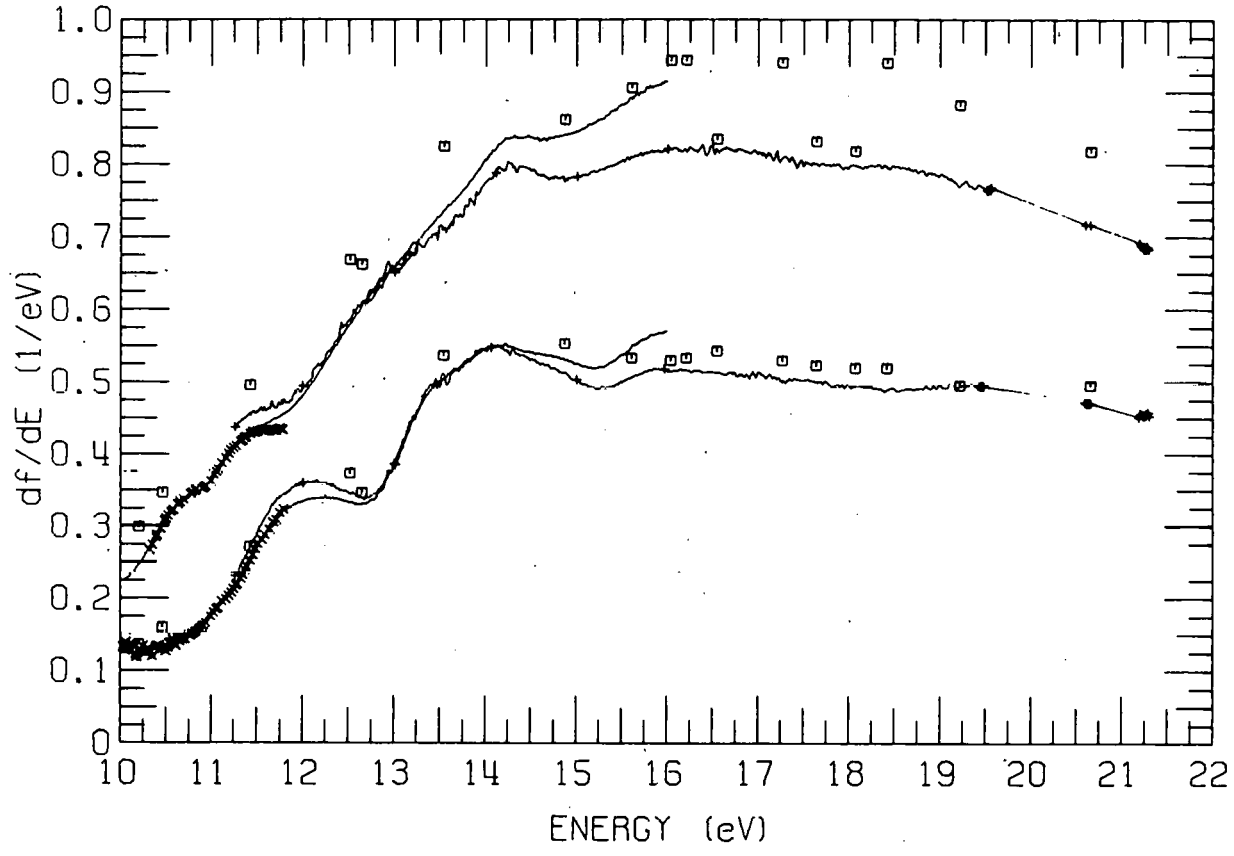

FIG. 2.--Oscillator-strength distributions for methanol (lower curves) and ethanol (upper curves). The present data are plotted as a line with some + marks on it for E < 19.5 eV. Above 19.5 eV our data are plotted as +'s connected by straight lines. The EELS data from Refs. 7 and 8 are plotted as lines from 10 to 16 eV. The data of Ref. 15 are plotted as squares, and our previous data (Ref. 4) are plotted as X's.

The results are preliminary in the sense that further experiments are needed to check sample purity, pressure calibration, and reproducibility at different gas pressures. For most of the samples there are two sets of data for energies near 13 eV, and the comparison of the two lines indicates the effects of different scattered-light corrections, and differing regions of low-light intensity in the lamp.

The data for ethylene are shown in Figure 1; note that the σ value has been multiplied by two in order to plot on the same scale as 2,2-dimethyl propane. Also, the data around 20.5 and 21.2 eV are represented as short lines, not connected with the remaining data. Figure 2 presents the data for CH_3OH and C_2H_5OH, illustrating how the methyl substitution has increased

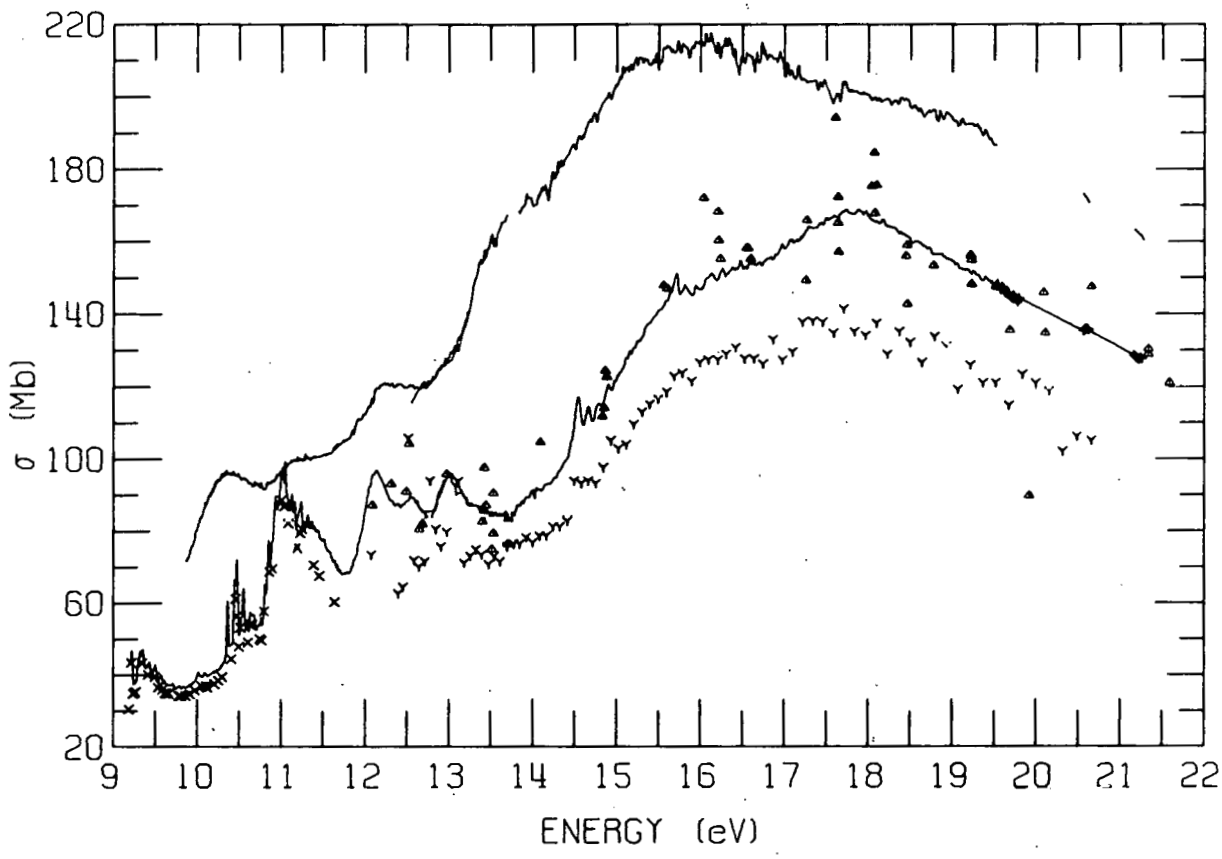

FIG. 3.--Absorption cross sections for cyclohexane (upper curve) and benzene (lower curve and points). The present data are plotted as lines except that points for benzene with E > 19.5 eV are shown as +'s connected by lines. The data of Refs. 6, 16, and 17 are plotted as X's, triangles, and Y's, respectively, but only the data for E > 12 eV are shown in the last two cases.

the oscillator strength. The value of σ in Mb units (1 Mb = 10^{-18} cm^2) can be found by dividing the df/dE values by 0.009112. In Figure 2 the experimental points are plotted as +'s for E > 19.5 eV, as they also are in the benzene data in Figure 3. The upper line in Figure 3 shows how the six additional electrons in cyclohexane have increased the absorption in comparison with benzene. These data will be useful in predicting the distribution of energy deposition by ionizing radiation in benzene-cyclohexane mixtures. Figure 4 shows the low-energy data for benzene in more detail, and Figure 5 gives the data for two other solvents, toluene and CCl_4.

We have previously reported data for four of the sample gases measured using a cell with LiF windows and a photomultiplier to measure the light absorption for E < 11.8 eV. Our old results are lower by 3 to 6%, 5 to 8%,

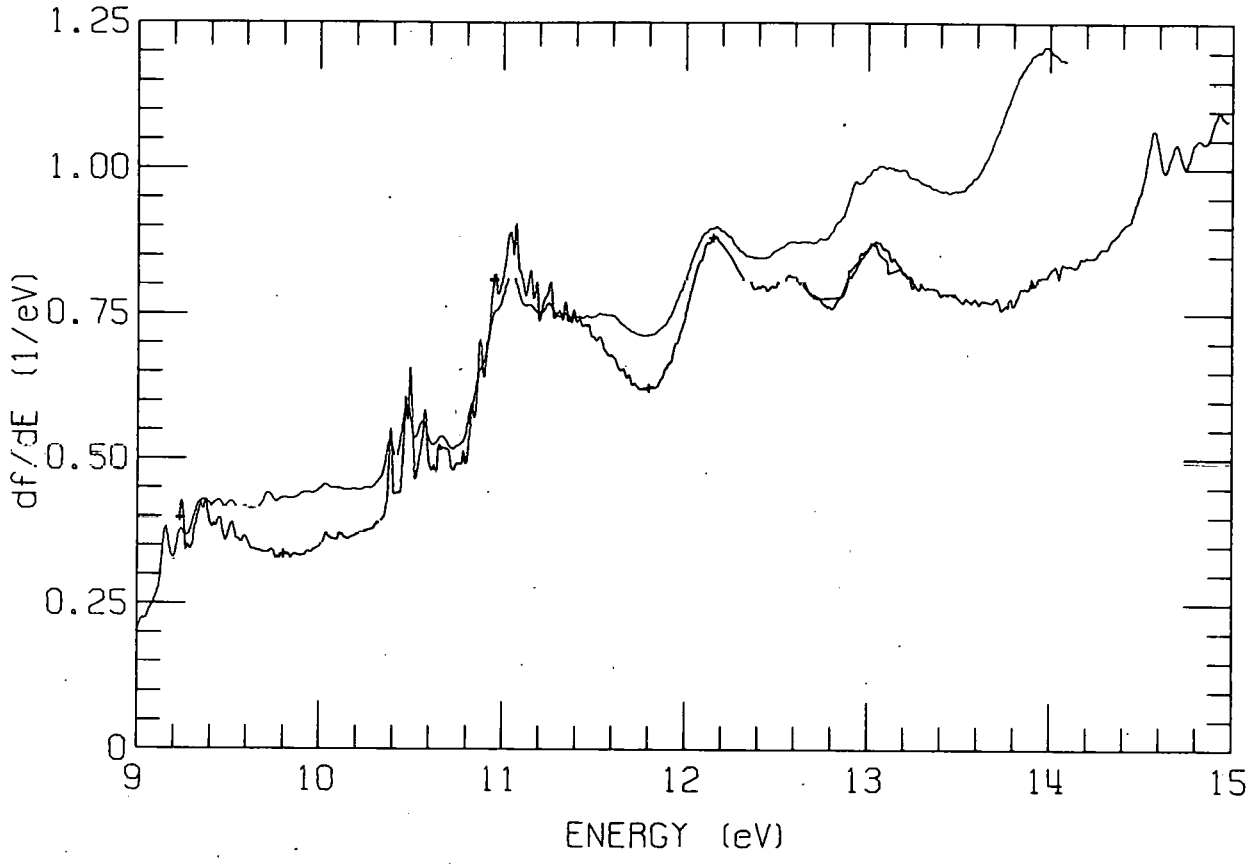

FIG. 4.--Oscillator-strength distribution for benzene from 9 to 15 eV. The present data are shown as a line with + marks on it, and the EELS data of Ref. 10 are shown as a line. The EELS data are above the present data except for a peak around 9.3 eV and some peaks between 10.4 and 11.4 eV.

and 6 to 16% for ethylene,[5] methanol and ethanol,[4] and benzene,[6] respectively, and the old data are shown in Figures 2 and 3 for three of these gases. We are investigating whether a difference in the calibration of the pressure gauge could explain these differences, or if they result from other effects, such as different corrections for scattered light, impure samples, or the photomultiplier detecting fluorescence of visible or ultraviolet light by the sample.

For the two alcohols and benzene, we compare our df/dE values with values measured by observing the electron energy-loss spectra (EELS) at zero-angle scattering for electrons with 100 eV of incident energy.[7–10] These comparisons are shown in Figures 2 and 4, and we show similar comparisons for n-hexane and methane in a companion report.[11] The agreement is best

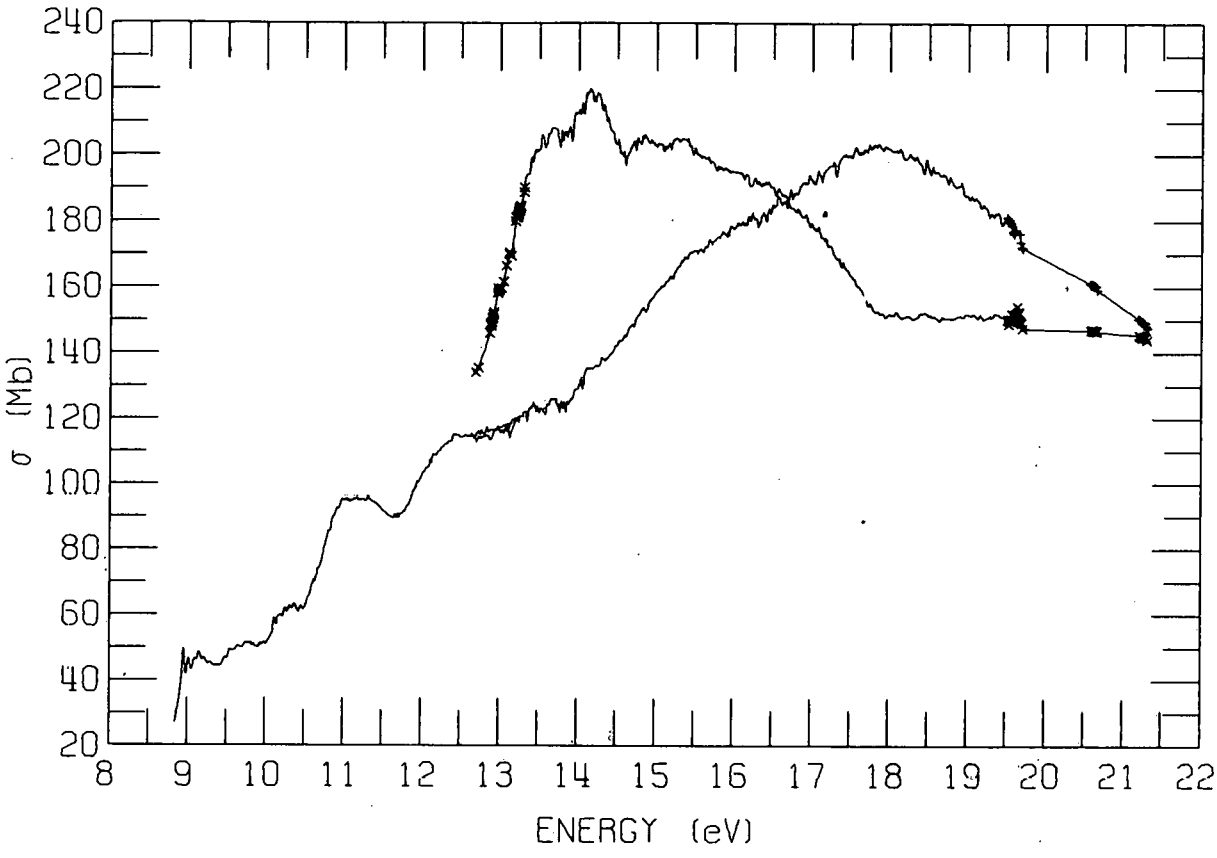

FIG. 5.--Absorption cross sections for toluene and carbon tetrachloride. The toluene data extend from 8.8 to 21.2 eV and the curves cross at 16.7 eV with the toluene lower at lower energies. For E > 19.5 eV, the individual points, connected by lines, are shown as +'s for toluene and X's for CCl_4, and the individual points are also shown for CCl_4 at E < 13.3 eV.

in the case of n-hexane,[11] where the relative shapes agree within 4% for energies from 10.5 to 14.7 eV. For the two alcohols, the relative shapes agree within 8% for energies from 10 to 15 eV. In these three cases, there is a tendency for the EELS data to become too large for E > 14 eV. In the case of benzene, the EELS data have been previously normalized[10] by comparison with optical data for the strong transition around 6.9 eV, and the EELS data are larger by as much as 30% (even for E < 13.6 eV). Figure 4 shows that the shapes differ considerably, so that lowering the EELS data by 10 to 20% would make the EELS data considerably smaller at some of the peaks — e.g., 9.4, 11.0, and 12.1 eV. These peaks are associated with Rydberg transitions, and it may be significant that the largest discrepancies (for E < 14 eV) in the

comparisons with the alcohols also occur in peaks associated with Rydberg transitions. Because of the nodal properties of the wavefunctions for Rydberg states with low principal quantum number, transitions to these states usually show a more rapid variation of the generalized oscillator strength with increasing momentum transfer than do transitions either to valence states or to ionization continua.[12-14] Thus, one might expect such states to show greater deviations between the optical df/dE value and the apparent df/dE obtained in an EELS experiment, which integrates over a range of momentum transfer. This difficulty will be accentuated for Rydberg states in series converging on higher ionization potentials (provided that the Rydberg state contributes a large fraction of the oscillator strength at that energy), because the small-momentum limit increases as the energy transfer becomes a larger fraction of the energy of the incident electrons.

In Figure 2, we compare with the absorption data reported by Ogawa and Cook,[15] and their values are somewhat larger, especially those for ethanol. For benzene, we have only shown σ values for $E > 12$ eV as reported by two other groups. There is a reasonable agreement with the values reported by Bunch et al.,[16] which show considerable scatter, but our values are definitely larger than those of Yoshino et al.[17] Comparison with other optical data for $E < 14$ eV can be made by comparing Figure 3, which compares with EELS data, with a corresponding figure in the article discussing the EELS data.[10]

Although some of the fine structure illustrated by the spectra is within the uncertainty in σ, much of the structure is real. For example, the ethylene spectrum shown in Figure 1 shows fine structure for energies from 12 to 16 eV that is likely the result of Rydberg series members converging to the vertical ionization potentials[18] at 14.70 and 15.89 eV, and the sharp structures in the neopentane spectrum between 15 and 17 eV appear to be associated with the vibrational members of the $n = 4$ and $n = 5$ members of a p-type Rydberg series converging on the vertical ionization potential reported[19] at 17.77 eV. The lower energy peaks appear to have an asymmetric Buetler-Fano line profile, and this area will be studied further.

The benzene spectrum shown in Figures 3 and 4 shows sharp features resolved as well as in the best synchrotron work,[20] and we plan work with still higher resolution. The toluene spectrum in Figure 5 shows a strong similarity to that of benzene.

The broad features in the spectra are also subject to interpretation. For example, Robin and Kuebler[21] have assigned the broad bands they find centered at E = 11.90, 13.45, and 18.8 eV in their EELS spectrum of methanol as the Rydberg transitions 1a" → 3s, 5a' → 3s, and 4a' → 3s, respectively. A comparison with Figure 2 suggests that they have failed to consider properly that the correction factor[7,22,23] that is required to convert EELS spectra into df/dE values will distort broad peaks to make the maxima appear at lower energies in the uncorrected EELS spectra. Thus we find the corresponding peaks to be around 12.1, 14.1, and > 19 eV. These shifts will only change the term values somewhat, but the shift of the peak they report at 15.5 eV to the value we find around 16.0 eV, makes their[21] tentative assignment as a 5a' → 3p Rydberg transition untenable. We also fail to observe the sharp feature they report at 12.91 eV, and this feature is likely to be caused by a nitrogen impurity.[24]

Similar assignments should also apply to the ethanol spectrum. This approach can be applied to the other spectra, and a more detailed analysis of both the sharp and the broad spectral features is under way in collaboration with D. E. Fowler.

We wish to thank D. E. Fowler for his help in preparing the figures, T. J. Kotek and J. Rundo for the use of their computer plotting program, R. H. Huebner for helpful discussions and the use of EELS data in digital form, and Y.-K. Kim for helpful discussions.

References

1. J. A. R. Samson. Techniques of Vacuum Ultraviolet Spectroscopy. John Wiley, New York, 1967, p. 267.
2. J. C. Person and P. P. Nicole. Radiological and Environmental Research Division Annual Report, July 1971–June 1972. ANL-7960, Part I, p. 76.
3. J. C. Person and P. P. Nicole. Radiological and Environmental Research Division Annual Report, July 1972-June 1973. ANL-8060, Part I, p. 158.

4. J. C. Person and P. P. Nicole. J. Chem. Phys. 55, 3390 (1971).
5. J. C. Person and P. P. Nicole. J. Chem. Phys. 49, 5421 (1968).
6. J. C. Person. J. Chem. Phys. 43, 2553 (1965).
7. R. H. Huebner and R. J. Celotta. Radiological and Environmental Research Division Annual Report, July 1971–June 1972. ANL-7960, Part I, p. 49.
8. R. H. Huebner, R. J. Celotta, S. R. Mielczarek, and C. E. Kuyatt. Abstracts, VIII ICPEAC, Belgarde, Yugoslavia, 16–20 July 1973, Ed. B. C. Čobić and M. V. Kurepa. Inst. Phys., Belgrade, 1973, p. 435.
9. R. H. Huebner, C. H. Fergurson, R. J. Celotta, and S. R. Mielczarek. Apparent oscillator strength distributions derived from electron energy-loss measurements: Methane and n-hexane. This report.
10. R. H. Huebner, R. J. Celotta, S. R. Mielczarek, and C. E. Kuyatt. Dipole oscillator-strength distributions derived for several hydrocarbons from electron energy-loss spectra. This report.
11. J. C. Person and P. P. Nicole. New determinations of the oscillator-strength distribution and the photoionization yields for methane and n-hexane. This report.
12. Y.-K. Kim, M. Inokuti, G. E. Chamberlain, and S. R. Mielczarek. Phys. Rev. Letters 21, 1146 (1968).
13. M. Krauss and S. R. Mielczarek. J. Chem. Phys. 51, 5241 (1969).
14. K. J. Miller. J. Chem. Phys. 51, 5235 (1969).
15. M. Ogawa and G. R. Cook. J. Chem. Phys. 28, 747 (1958).
16. S. M. Bunch, G. R. Cook, M. Ogawa, and A. W. Ehler. J. Chem. Phys. 28, 740 (1958).
17. M. Yoshino, J. Takeuchi, and H. Suzuki. J. Phys. Soc. Japan 34, 1039 (1973).
18. M. B. Robin. Higher Excited States of Polyatomic Molecules. Academic Press, New York, 1974, Vol. 1, p. 71.
19. A. E. Jonas, G. K. Schweitzer, F. A. Grimm, and T. A. Carlson. J. Electron. Spectry. 1, 29 (1972).
20. E. E. Koch and A. Otto. Vacuum ultraviolet and electron energy-loss spectroscopy of gaseous and solid organic compounds. To be published in Int. J. Radiat. Phys. Chem.
21. M. A. Robin and N. A. Kuebler. J. Electron Sepctry. 1, 13 (1972).
22. R. H. Huebner, R. J. Celotta, S. R. Mielczarek, and C. E. Kuyatt. J. Chem. Phys. 59, 5434 (1973).
23. E. N. Lassettre. Chemical Spectroscopy and Photochemistry in the Vacuum Ultraviolet, Ed. C. Sandorfy, P. J. Ausloos, and M. B. Robin. D. Reidel, Dordrecht, 1974, p. 43.
24. R. H. Huebner. Private communication, 1974.

NEW DETERMINATIONS OF THE OSCILLATOR-STRENGTH DISTRIBUTION AND THE PHOTOIONIZATION YIELDS FOR METHANE AND n-HEXANE*

James C. Person and Paul P. Nicole

Experimental data on the differential oscillator strength are presented for methane for energies E in the range of 12.8 and 40.8 eV and for n-hexane for $10.5 \leq E \leq 40.8$ eV. We also report the yield for ionization produced when the energy is deposited within the gas, which may include ionization by energetic photoelectrons, for $21.2 \leq E \leq 40.8$ eV.

The data in the literature on the absorption cross section σ show considerable disagreement even for the simplest alkane, and not much data are available for alkanes as large as hexane. As part of a program to determine accurate oscillator-strength distributions over a wide range of energy, we are measuring σ for methane and n-hexane, using monochromatic light.

We also measure ionization, and one goal is to determine the photoionization yield $\eta(E)$, the probability that absorption of a photon with an energy E produces an ion pair. Such data are especially timely for methane as an earlier estimate[1] of the dipole-matrix-element-squared for ionization M_i^2 has been called into question by recent electron-ion coincidence work in Amsterdam[2] that has suggested a lower value for M_i^2 and that η may be significantly less than unity for $E > 23$ eV.

The apparatus is described in a companion paper in this report.[3] Three light sources were used: the Hopfield continuum, the hydrogen many-lined spectrum, and a hollow-cathode lamp used with a low pressure of either helium or a helium-neon mixture to produce photons in the range $21.2 \leq E \leq 40.8$ eV. Research-grade materials were used for all the samples.

The value of σ is determined by assuming the Beer-Lambert relation and using the ratio of ion currents in the two chambers[3] to determine

$$I/I_0 = \exp(-\sigma n L_F) , \qquad (1)$$

*A preliminary version was presented at the IV International Conference on Vacuum-Ultraviolet Radiation Physics, Hamburg, July 22–26, 1974, and will be published by Vieweg-Pergamon.

where L_F is the length of the front chamber, n is the gas density, and I_0 and I are the photon fluxes entering and leaving the front chamber. Multiplication of the value of σ (in units of Mb = 10^{-18} cm^2) by 0.009112 gives the value of df/dE in units of eV^{-1}.

Figure 1 shows the measured df/dE values for methane for $12.75 \leq E \leq 40.81$ eV, with closely spaced points over most of the region from 13.21 to 20.59 eV. In addition to an estimated uncertainty of 2 to 4% in the calibration of the MKS Baratron pressure meter (the factory calibration was used), the data have an uncertainty of 1 to 2% for $14 < E < 19$ eV and 2 to 6% for the other energies. Figure 2 presents data in the energy range from 12 to 21 eV on an expanded scale in order to show the structure for $13.4 < E < 14.1$ eV

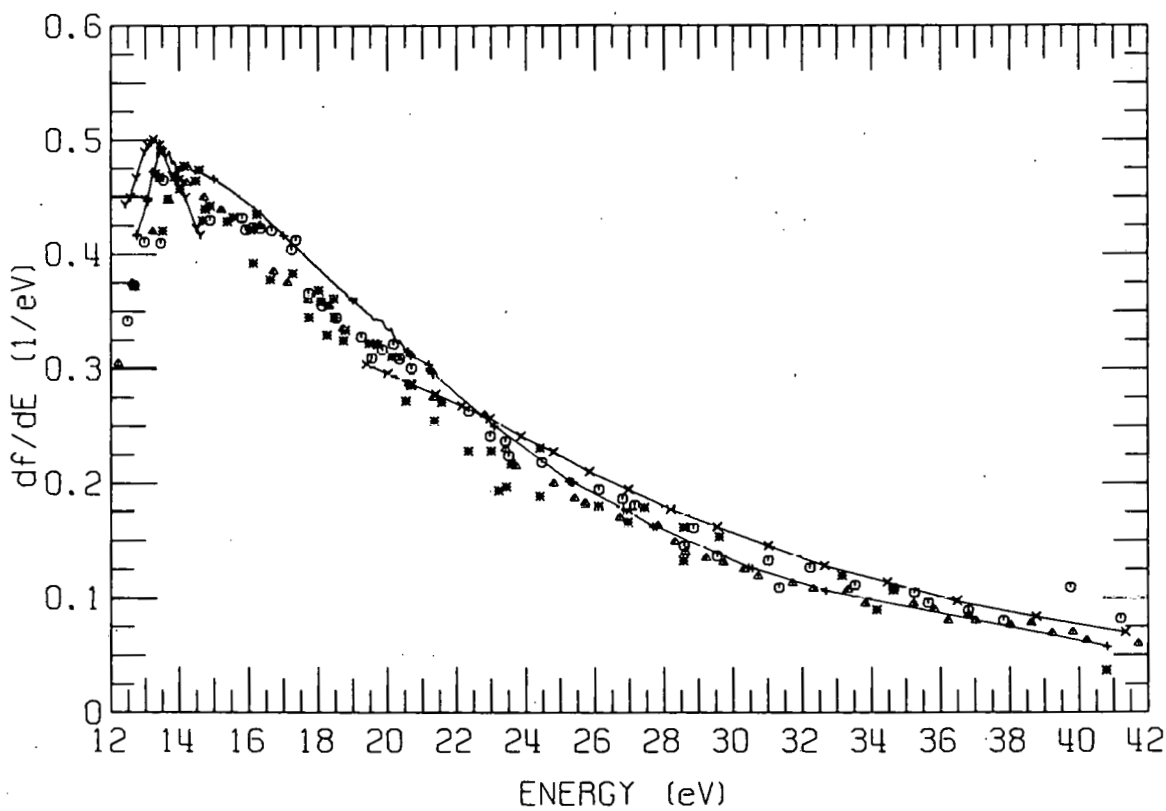

FIG. 1.--The oscillator-strength distribution for methane from 12 to 42 eV. The present df/dE values are shown as +'s connected by straight lines for $E < 13.21$ and $E > 20.59$ eV; for the energies between those limits the data points are closely spaced and only the line is shown with a few +'s. Some of the data of Ref. 5 are shown as a line connecting Y marks. The data of Refs. 2, 6, and 7 are plotted as triangles, *'s, and circles, respectively, while the data of Ref. 8 are shown as a line connecting X marks.

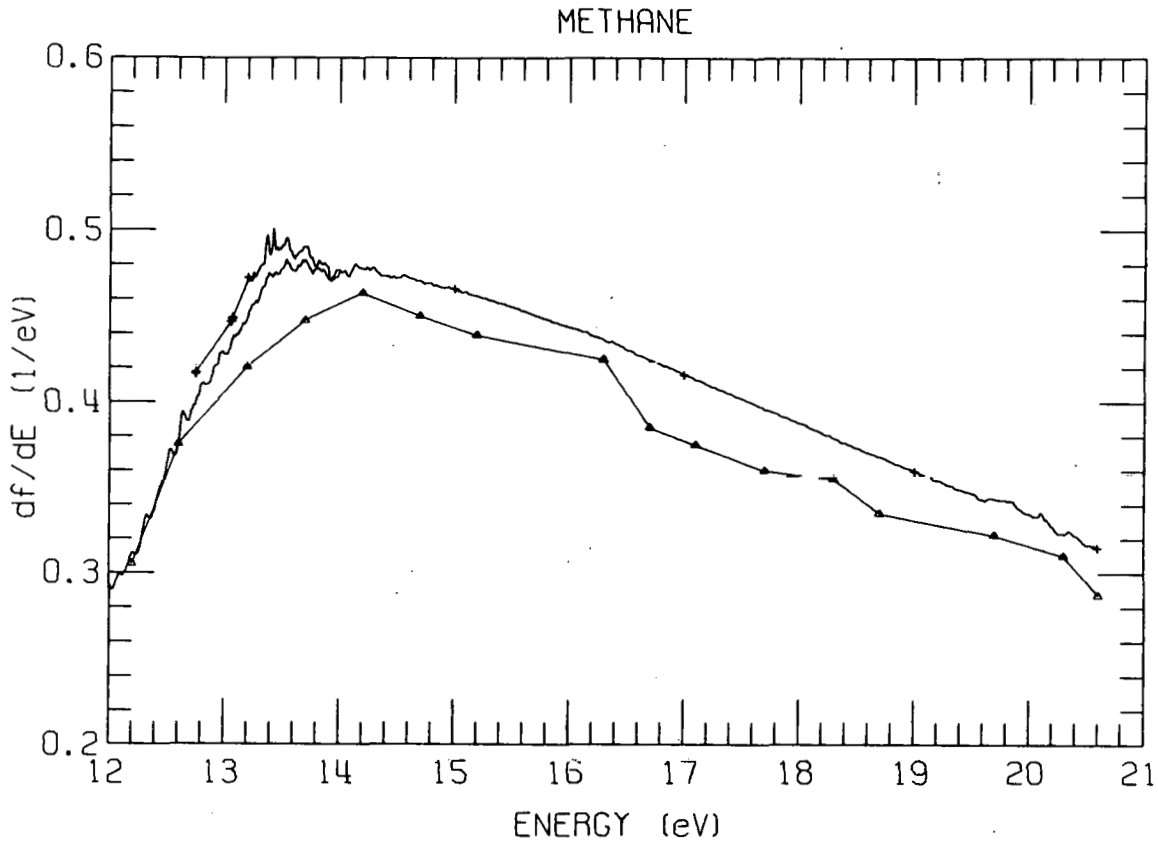

FIG. 2.--The oscillator-strength distribution for methane from 12 to 21 eV. The present data are shown as a line connecting +'s, but only a few of the points are shown for $13.21 < E < 20.59$ eV. The EELS data (Ref. 9 for $12 < E < 14$ eV) are shown as a line, and the triangles show the data of Ref. 2.

that is produced by Rydberg series converging on excited vibronic levels of the lowest electronic state of the ion. This state is split by the Jahn-Teller effect, and the progressions labeled c and d in the photoelectron spectrum[4] are likely candidates for the series limits.

Some of the data from other optical studies[5-8] are shown in Figure 1; our values tend to be larger for the lower energies, but most of the values are within 10% of those of Ditchburn,[6] Rustgi,[7] and Lee et al.[8] The latter group reports values that are above ours for higher energies. The electron-ion coincidence[2] work produced df/dE values that are in rather good agreement, although their values are lower for the lower energies, as is shown in more detail in Figure 2. Also plotted in Figure 2 are df/dE values[9] derived from electron energy-loss studies (EELS) at zero angle. These relative data were normalized by comparison with absolute EELS data,[10] and the agreement with our data is rather good.

Figure 3 shows the oscillator-strength distribution for n-hexane from 10.5 to 40.8 eV. The shape and the magnitude of the broad maximum is quite compatible with the trend shown by the smaller alkanes.[11] Figure 4 shows the comparison with other optical data,[12,13] and with the relative df/dE values from EELS.[9] The agreement with the EELS data is within 4% from 10.5 to 14.7 eV after normalization at one point, but we do not agree with the other optical data.

The value of $\eta_a I_0$, where η_a is the apparent ionization yield, is given by the sum of ion currents, after correction for photons that are not absorbed in either chamber; the value of I_0 is determined by use of a noble gas that, we assume, has $\eta_a = 1.0$. The value of η_a is related to η by

$$\eta_a = \eta + \eta_e \,, \tag{2}$$

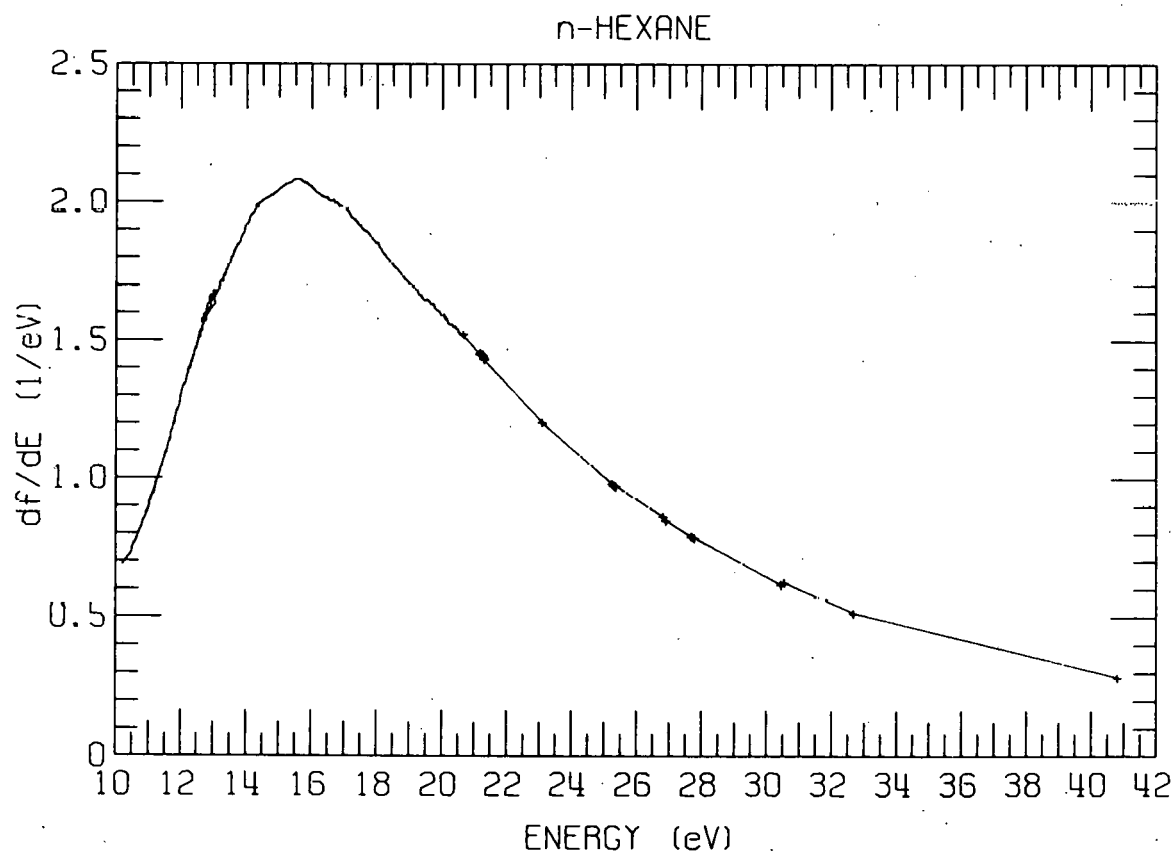

FIG. 3.--The oscillator-strength distribution for n-hexane from 10 to 41 eV. For E > 20.59 eV, +'s show the individual data points. There are two different determinations for energies around 13 eV.

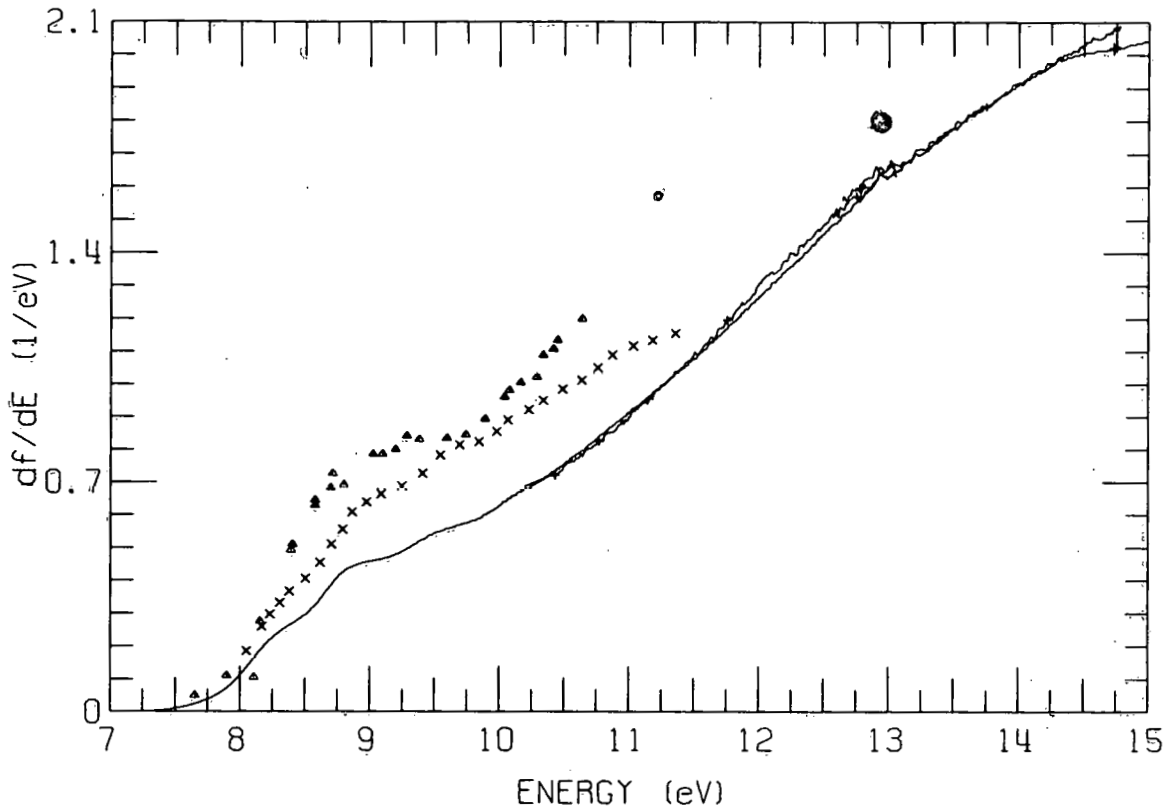

FIG. 4.--The oscillator-strength distribution for n-hexane from 7 to 15 eV. The present data are shown as a line with a few +'s on it from 10.5 to 15 eV. The EELS data of Ref. 9 are shown as a line with a normalization that has been multiplied by 0.73 in comparison with the one used in Ref. 9. The data of Ref. 12 are plotted as triangles and Ref. 13 data are shown as X's.

where η_e is the yield of additional ions produced by photoelectrons. As the kinetic energy of the photoelectron is $E - IP_j$, when the ion is produced at the jth ionization potential, it is obvious that

$$\eta_e = 0 \qquad \text{for } E < 2\,IP_1 \,. \tag{3}$$

Although $\eta_e > 0$ complicates measurement of η, the opportunity to study η_e presents an interesting method of learning about the low-energy behavior of the W value, the energy to produce an ion pair.

Even when $E > 2\,IP_1$, one can still obtain η by measuring η_a as a function of gas density and extrapolating to zero density. We have not yet worked at sufficiently low pressure to permit a reliable extrapolation, and the η_a values given in Table 1 are believed to be near the high-pressure limit, as we see

TABLE 1. Apparent Ionization Yields

E, eV	η_a	
	CH_4	C_6H_{14}
21.22	0.99 ± 0.02[a]	0.98 ± 0.02
23.09	1.00 ± 0.02[a]	1.02 ± 0.02
25.31	0.98 ± 0.04	1.10 ± 0.05
26.91	1.01 ± 0.03	
27.78	1.00 ± 0.03	1.23 ± 0.04
30.45	1.11 ± 0.05	1.34 ± 0.07
30.55	1.10 ± 0.05	1.34 ± 0.07
32.69	1.19 ± 0.07	1.40 ± 0.10
40.81	1.35 ± 0.10	1.6 ± 0.15

[a] For this energy, $\eta + \eta_a$.

little effect over the limited pressure range we have explored. For η studies at large E, redesign of the ionization chamber collecting plates would be desirable, as shown by Samson and Haddad.[14]

For the large E values, double ionization may occur, and this could make η greater than unity, as we measure the yield of single ionization plus twice the yield of double ionization. The energy required for double ionization IP^{+2} is reported for methane as 38.9 eV[15] and 40.7 eV,[16] and the ratio of $IP^{+2}/IP_1 = 2.8$ reported for three alkanes[15] can be used to predict $IP^{+2} \approx 28.5$ eV for n-hexane.

Note that $\eta_a = \eta$ for methane for E < 25 eV, and the combination of the low ionization yield near the ionization threshold[2,5] and the distribution of photoelectrons formed[4] suggest that η will be close to η until E > 28 eV or so. Thus, our η values at 23.1 eV and our η_a values at 25.3, 26.9, and 27.8 eV are in some disagreement with those of Backx and van der Wiel,[2] who find η values around 0.9 for these energies.

We wish to thank C. Backx and M. J. van der Wiel for communicating their results, D. E. Fowler for his help in preparing the figures, R. H. Huebner for providing df/dE values in digital form, and W. Jivery for use of the hollow-cathode lamp.

References

1. J. Berkowitz, M. Inokuti, and J. C. Person. Abstracts VIII ICPEAC, Belgrade, Yugoslavia, 16–20 July 1973. Ed. B. C. Čobić and M. V. Kurepa. Institute of Physics, Belgrade, 1973, p. 561.
2. C. Backx and M. J. van der Wiel, private communication, 1974.
3. J. C. Person and P. P. Nicole. Paper 17, this report.
4. J. W. Rabalais, T. Bergmark, L. O. Werme, L. Karlsson, and K. Seigbahn. Phys. Scripta 3, 13 (1971).
5. P. H. Metzger and G. R. Cook. J. Chem. Phys. 41, 642 (1964).
6. R. W. Ditchburgn. Proc. Roy. Soc. 229A, 44 (1955).
7. O. P. Rustgi. J. Opt. Soc. Am. 54, 464 (1964).

8. L. C. Lee, R. W. Carlson, D. L. Judge, and M. Ogawa. J. Quant. Spectry. Radiative Transfer 13, 1023 (1973).
9. R. H. Huebner, C. F. Fergurson, R. J. Celotta, and S. R. Mielczarek. Paper 14, this report.
10. W. R. Harshbarger and E. N. Lassettre. J. Chem. Phys. 58, 1505 (1973).
11. R. I. Schoen. J. Chem. Phys. 37, 2032 (1962).
12. B. A. Lombos, P. Sauvageau, and C. Sandorfy. J. Mol. Spectry. 24, 253 (1967).
13. J. W. Raymonda and W. T. Simpson. J. Chem. Phys. 47, 430 (1967).
14. J. A. R. Samson and G. N. Haddad. J. Opt. Soc. Am. 64, 47 (1974).
15. J. Appell, J. Durup, F. C. Fehsenfeld, and P. Fournier. J. Phys. B 7, 406 (1974).
16. R. Spohr, T. Bergmark, N. Magnusson, L. O. Werme, C. Nordling, and K. Siegbahn. Phys. Scripta 2, 31 (1970).

POTENTIAL BARRIER EFFECTS IN INNER-SHELL PHOTOABSORPTION SPECTRA OF ATOMS, MOLECULES, AND SOLIDS *

J. L. Dehmer

Advances in the field of potential barrier effects in the inner-shell photoabsorption spectra of atoms, molecules, and solids are reviewed.

In the last several years discrete levels extending up to 20 eV above inner-shell thresholds have been observed as intense peaks in inner-shell contributions to absorption spectra. These levels are not Rydberg states, and, in fact, when they are present, they seem to replace the normal Rydberg series and may even rob intensity from the continuum. There is now evidence that this phenomenon may be found in inner-shell spectra of atoms, molecules, and solids. The unifying concept which emerges from this array of observations is the presence of an effective potential barrier which hinders the escape of the photoelectron. This barrier produces highly localized states which are strong in inner-shell absorption spectra while excluding Rydberg and near-continuum states from overlapping with the inner shells from which excitation takes place. The purpose of this paper is to review recent progress in the area of potential barrier effects and to stress those aspects which unite the apparently unrelated observations in atoms, molecules, and solids.

The most familiar example of potential barriers in atomic physics is the centrifugal barrier occurring in the effective potential for electronic states with high ($\ell \geq 2$) angular momentum. This barrier results from the competition between the repulsive centrifugal potential and the attractive electrostatic potential acting on an electron in the field of an atomic ion. It was first described by Mayer[1] using the Thomas-Fermi model, and more recently by Rau and Fano[2] using the Hartree-Slater model.[3] These barriers partition the atomic potential into an inner well centered at $r \sim 1$ a.u., and an outer well centered at $r = \ell(\ell+1)$ a.u. In this two-well or bimodal potential, states

* Summary of an invited paper presented at the International Conference on X-Ray Processes in Matter, Helsinki, Finland, 29 July – 1 August 1974.

with total energy below or near the top of the barrier are partitioned into two classes. One class is referred to as "inner-well," states which are highly localized inside the potential barrier. The other class is referred to as "outer-well" states and are excluded from the inner well, being distributed diffusely outside the barrier. Examples[4,5] of both types of states are discussed.

Clearly the effect of this spatial segregation is most important in inner-shell absorption. Since the core orbitals are themselves localized in the inner-well region, their excitation selectively populates the inner-well final states, while transitions to the Rydberg and continuum states held outside the barrier are inhibited. Hence, inner-shell spectra will be dominated by transitions to inner-well states, and Rydberg structure and normal threshold behavior will be conspicuously absent. With this clue, one is able to find examples of potential barrier effects in spectra of a variety of materials.

Potential barrier effects in atomic spectra fall into four classes. The first class is exemplified by the $M_{IV,V}$ spectrum[6] of Xe. This spectrum represents intershell transitions exhibiting a delayed onset. To explain these terms, we focus on the 3d → f channel which will dominate this spectrum. In Xe, no nf subshell is bound in the inner well. Radial waves of f symmetry penetrate the potential barrier only above threshold in the continuous part of the spectrum, i.e., their penetration is delayed to higher energy. When this occurs, the 3d → εf cross section exhibits a broad peak or shape resonance in the cross section, a situation we characterize as delayed onset. When this barrier penetration occurs, the f-wave function inside the barrier resembles a 4f orbital in that it is located in the n = 4 shell. Thus the peak in the spectrum corresponds to the intershell transitions 3d → "4f." This cross section is reasonably well reproduced with a Hartree-Slater model[3] calculation.

A closely related class is represented by the $N_{IV,V}$ spectrum[7] of Xe, which can be characterized as an intrashell, 4d → "4f," set of transitions with a delayed onset. Superficially this type of spectrum resembles its intershell counterpart. There is one significant difference, however — the

Hartree-Slater model fails to reproduce the height, position, or shape of the experimental curve. The origin of this difficulty was first explained by Starace[8] in 1970, and is due to a strong exchange interaction between the excited electron and the 4d hole, which is neglected by the Hartree-Slater model. The magnitude of this interaction is as large as 1 a.u. near the peak in the Hartree-Slater cross section. This large magnitude derives from the extremely good spatial overlap between the 4d hole and 4f-like quasibound band of states causing the shape resonance in the cross section. Since Starace's work, other workers have used other methods to achieve agreement with experiment by incorporating this effect in their basis from the start or as an improvement on a one-electron scheme. Amusia[9] and Wendin[10] have used random-phase-approximation methods, and Kennedy and Manson[11] have used a Hartree-Fock scheme. This class of spectra we shall characterize as having delayed onset and strong intrashell exchange interaction.

The third and fourth classes involve atoms for which a bound inner-well state is available as a final state in the $\ell \rightarrow \ell + 1$ transitions. In this case the spectral range near the onset of this transition is dominated by transitions to this inner-well state since its overlap with the initial state is much greater than that of the higher members of the same series. Examples of this circumstance occur in the transition metal and rare earth elements, and are usually studied as thin films. However, we discuss these cases in terms of isolated atoms since the dominant photoabsorption mechanism involves only core levels and inner-well final states which are isolated from the environment of the atom. Indeed, this remark pertains to the first two classes as well, as can be seen by comparing the $N_{IV,V}$ spectra of gaseous and solid xenon.[7]

Examples of <u>intershell</u> transitions of this type are the $M_{IV,V}$ spectra of the rare earths.[12,13] In these spectra the dominant features are the $3d_{\frac{5}{2},\frac{3}{2}} \rightarrow 4f$ lines occurring <u>below</u> the $M_{IV,V}$ thresholds. These have been successfully treated theoretically by Sugar.[13,14]

The last class is represented by the $N_{IV,V}$ photoabsorption spectra of the lanthanides, and can be characterized as <u>intrashell</u> transitions dominated by excitation of an inner-well final state which is bound in the ground state,

namely the 4f subshell. These spectra, measured by several workers,[15-19] exhibit one or more intense lines above the $N_{IV,V}$ edge and many weak lines below the respective ionization threshold. The dramatic change from the analogous intershell $M_{IV,V}$ spectra was first interpreted[20] in the context of the Hartree-Slater model, which, as a first approximation, predicts the intershell and intrashell spectra to be qualitatively similar. However, in this representation, the exchange interaction between a 4f electron and the 4d hole again ranges up to 1 a.u. When taken into account, this interaction redistributes the levels of the dominant $4d^9 4f^{N+1}$ configuration over a 20-volt range. The optically allowed (in LS coupling) terms are raised above the ionization limit and give rise to the intense autoionizing peaks observed experimentally. Subsequent theoretical work[21-24] has succeeded in analyzing these spectra in detail.

Based on these four examples, it is possible to classify $\ell \rightarrow \ell + 1$ ($\ell > 0$) transitions for all atoms in the Periodic Table.[5]

The first example of resonant x-ray absorption by molecules emerged early in 1965 when LaVilla and Deslattes[25] measured and compared the K absorption spectra of the sulfur atom in H_2S and SF_6. This comparison is still the best known illustration of potential barrier effect in molecules. The H_2S spectrum shows a few lines of a Rydberg series which converge to the ionization limit with an average intensity in the discrete comparable to the intensity beyond the limit. In contrast to this "normal" behavior, the SF_6 spectrum is dominated by a very intense single peak which appears to replace the Rydberg series and to "rob" intensity from a 50-eV range of the continuum.

The strong similarity between this spectrum of SF_6 and the $M_{IV,V}$ spectra of the rare earths already suggests the presence of an effective barrier in the potential of the final state of photoionization of SF_6. A related experiment was performed by Zimkina and co-workers,[26,27] who looked at the region of the SF_6 spectrum near the sulfur $L_{II,III}$ edge and the fluorine K edge. In the former case, the spectrum is dominated by three large peaks, and there are no apparent Rydberg series. Because only even states will be populated by ionization of a sulfur 2p electron, the three peaks should represent one

inner-well state for the three symmetries, a_{1g}, t_{2g}, and e_g, which are formed from s and d waves centered on the sulfur. One assumes the g-wave contribution will be very small. Hence, this spectrum shows one strong peak each for all three allowed symmetries which can be constructed from s or d waves which are available to the electron ejected from a core level on sulfur.

About the time this tentative interpretation was proposed,[28] three important results were presented which prove this picture is quite sound: a) First Blechschmidt et al.[29] measured the sulfur $L_{II,III}$ spectrum of solid SF_6. It was identical to the gas phase data, demonstrating that the main peaks are truly inner-well states localized inside the molecule, and uncoupled from the molecule's environment. b) Nakamura et al.[30] repeated Zimkina's measurements in the immediate vicinity of the $L_{II,III}$ edge with higher sensitivity to discover two Rydberg series converging to the $L_{II,III}$ limits at 180.4 and 181.7 eV. This observation indicates that Rydberg states are populated in this process but are unusually weak, indicating they are excluded from overlapping with the sulfur core levels. c) Lastly, Gianturco et al.[31] tried to reproduce the SF_6 inner-shell spectra by considering the virtual orbitals of a Hartree-Fock LCAO calculation. Usually these unoccupied levels are disregarded as unrealistic, owing to the limited spatial region spanned by the basis set. However, in this case, the calculation succeeded amazingly well in reproducing the number and positions of the main peaks. This calculation, which generally confirmed our assignment, succeeded just because the peaks in the inner-shell spectra are inner-well states which occupy a region of space about the size of the molecule and, therefore, unlike more typical excited states, lie within the basis set space used to compute ground-state properties.

In all, the collected evidence[28] on some twenty or so molecules suggests that an effective potential barrier occurs on the outer rim of molecules where electrons accumulate on electronegative atoms, such as the F atoms in SF_6. The existence of a potential barrier in molecules was introduced by Barinskii,[32] Nefedov,[33] and Fomichev and Barinskii,[34] starting in late 1968. Since then, the concept has been used extensively in the interpretation[28,35] of molecular x-ray absorption spectra. Generally speaking, the

barrier is attributed to a net repulsion of the excited electron near the electronegative atoms in a highly coordinated molecule such as SF_6 or BF_3. The existence of a barrier in the case of BF_3 has been demonstrated by Cadioli et al.[36] However, the precise origin of the barrier has not been determined. It is commonly attributed to the requirement of orthogonality to occupied orbitals of the electronegative ligands and to exchange interaction with nonbonding electrons located on the periphery of the molecule. However, direct Coulomb interaction and centrifugal forces may contribute in part.

Therefore, although potential barrier effects in inner-shell photoabsorption of atoms and molecules are discussed in the same conceptual framework, relatively little is known about the potential barrier in the case of molecules. Elucidation of the anatomy of the molecular potential barrier is, therefore, an important outstanding problem in this area.

In the case of ionic crystals, each positive ion is surrounded by a "cage" of negative ions. If we ignore the remainder of the lattice for a moment, we have a situation bearing a strong resemblance to the molecule case we have just discussed. That is, in NaCl, each sodium atom is surrounded by six chlorine ions. In this "molecular" unit there exists all the ingredients of the effective potential barrier existing in SF_6. In the language of solid state physics, for a range of energies near the bottom of a conduction band, the final states may be either localized within the first layer of atoms or excluded from this volume. The former class constitutes a set of highly localized excitons or inner-well states. They exist in a quasimolecular environment and are most logically described in a real space representation using molecular symmetry. The outer-well states, in this context, are band states which are best represented in momentum space. Several recent papers[37–41] pertain to this rather new topic.

References

1. M. G. Mayer. Phys. Rev. 60, 184 (1941).
2. A. R. P. Rau and U. Fano. Phys. Rev. 167, 7 (1968).
3. F. Herman and S. Skillman. Atomic Structure Calculations. Prentice-Hall, Englewood Cliffs, N.J., 1963.

4. D. C. Griffin, K. L. Andrew, and R. D. Cowan. Phys. Rev. 177, 62 (1969).
5. J. L. Dehmer, unpublished.
6. R. D. Deslattes. Phys. Rev. Letters 20, 483 (1968).
7. R. Haensel, G. Keitel, P. Schreiber, and C. Kunz. Phys. Rev. 188, 1375 (1969).
8. A. F. Starace. Phys. Rev. A 2, 118 (1970).
9. M. Ya. Amusia, N. A. Cherepkov, and L. V Chernysheva. Zh. Eksp. Teor. Fiz. 60, 160 (1971) [Sov. Phys. — JETP 33, 90 (1971)], and references therein.
10. G. Wendin. J. Phys. B 6, 42 (1973), and references therein.
11. D. J. Kennedy and S. T. Manson. Phys. Rev. A 5, 227 (1972).
12. D. Ottewell, E. A. Stewardson, and J. E. Wilson, J. Phys. B 6, 2184 (1973), and references therein.
13. C. Bonnelle, R. C. Karnatak, and J. Sugar. Phys. Rev. A 9, 1920 (1974).
14. J. Sugar. Phys. Rev. A 6, 1764 (1972).
15. T. M. Zimkina, V. A. Fomichev, S. A. Gribovskii, and I. I. Zhukova. Fiz. Tverd. Tela. 9, 1447 (1967) [Sov. Phys. — Solid State 9, 1128 (1967)].
16. V. A. Fomichev, T. M. Zimkina, S. A. Gribovskii, and I. I. Zhukova. Fiz. Tverd. Tela. 9, 1490 (1967) [Sov. Phys. — Solid State 9, 1163 (1967)].
17. R. Haensel, P. Rabe, and B. Sonntag. Solid State Commun. 8, 1845 (1970).
18. T. M. Zimkina and S. A. Gribovskii. J. Phys. Paris 32 (Colloque C4), 282 (1971).
19. W. Gudat and C. Kunz. Phys. Rev. Letters 29, 169 (1972).
20. J. L. Dehmer, A. F. Starace, U. Fano, J. Sugar, and J. W. Cooper. Phys. Rev. Letters 26, 1521 (1971).
21. A. F. Starace. Phys. Rev. B 5, 1773 (1972).
22. J. Sugar. Phys. Rev. B 5, 1785 (1972).
23. J. L. Dehmer and A. F. Starace. Phys. Rev. B 5, 1792 (1972).
24. A. F. Starace. J. Phys. B 7, 14 (1974).
25. R. E. LaVilla and R. D. Deslattes. J. Chem. Phys. 44, 4399 (1966).
26. T. M. Zimkina and V. A. Fomichev. Dokl. Akad. Nauk USSR 169, 1304 (1966) [Sov. Phys. Dokl. 11, 726 (1966)].
27. T. M. Zimkina and A. C. Vinogradov. J. Phys. Paris 32 (Colloque C4), 3 (1971).
28. J. L. Dehmer. J. Chem. Phys. 56, 4496 (1972).
29. D. Blechschmidt, R. Haensel, E. E. Koch, U. Nielsen, and T. Sagawa. Chem. Phys. Letters 14, 33 (1972).
30. M. Nakamura, Y. Morioka, T. Hayaichi, E. Ishiguro, and M. Sasanuma. III International Conference on Vacuum Ultraviolet Radiation Physics. Phys. Soc. of Japan, Tokyo, 1971, Paper 1pA1-6.
31. F. A. Gianturco, C. Guidotti, and U. Lamanna. J. Chem. Phys. 57, 840 (1972).
32. R. L. Barinskii. International Symposium on X-Ray Spectra and the Structure of Matter, Kiev, USSR, September 1968, p. 222.

33. V. I. Nefedov. Zh. Strukt. Khim. 11, 299 (1970) [J. Struct. Chem. 11, 277 (1970)].
34. A. Fomichev and R. L. Barinskii. Zh. Strukt. Khim. 11, 875 (1970) [J. Struct. Chem. 11, 810 (1970)].
35. R. L. Barinskii and I. M. Kulikova. Zh. Strukt. Khim. 14, 372 (1973) [J. Struct. Chem. 14, 335 (1973)].
36. B. Cadioli, U. Pincelli, E. Tosatti, U. Fano, and J. L. Dehmer. Chem. Phys. Letters 17, 15 (1972).
37. T. Åberg and J. L. Dehmer. J. Phys. C 6, 1450 (1973).
38. C. Satoko and S. Sugano. J. Phys. Soc. Japan 34, 701 (1973).
39. A. B. Kunz, D. J. Mickish, and T. C. Collins. Phys. Rev. Letters 31, 756 (1973).
40. A. A. Maiste, A. M.-E. Saar, and M. A. Elango. JETP Letters 18, 97 (1973).
41. C. Satoko. Solid State Commun. 13, 1851 (1973).

COMMENT ON SOFT X-RAY ABSORPTION BY ALKALI HALIDE CRYSTALS*

T. Åberg† and J. L. Dehmer

Soft x-ray absorption spectra of alkali halides exhibit prominent peaks near the ionization threshold of alkali core orbitals. These experimental features, generally attributed to highly localized excitations, confined within the first layer of nearest neighbors, have been treated both from an atomic or molecular point of view and from a band structure point of view. The relationship between these two representations is discussed for the case of the Li^+ K-spectrum of LiF, recently treated by Kunz et al. (1973) using a Hartree-Fock band calculation.

*Abstract of a paper which appeared in J. Phys. C 7, L278 (1974).

†Laboratory of Physics, Helsinki University of Technology, 02150 Otaniemi, Finland.

PARTIAL PHOTOIONIZATION CROSS SECTIONS FOR Hg BETWEEN 600 AND 250 Å. EFFECT OF SPIN-ORBIT COUPLING ON THE $^2D_{\frac{5}{2}}/^2D_{\frac{3}{2}}$ BRANCHING RATIO OF Hg*

J. L. Dehmer and J. Berkowitz†

By means of photoelectron spectroscopy, we have measured the branching ratios for production of the $^2S_{\frac{1}{2}}$, $^2D_{\frac{5}{2}}$, and $^2D_{\frac{3}{2}}$ states of Hg^+ by photoionization of Hg in the wavelength range 600 Å to 250 Å. These branching ratios are combined with earlier measurements of the total photoionization cross section to produce partial photoionization cross sections for the above processes. These are shown in Figure 1. The wavelength dependence of the $^2D_{\frac{5}{2}}:{}^2D_{\frac{3}{2}}$ branching ratio exhibits a systematic deviation relative to the statistical value of 3:2 (Figure 2). That is, this ratio is greater than statistical where the respective partial cross sections are increasing with photon energy and is less than statistical when the partial cross sections are decreasing. This effect was previously predicted and is a consequence of spin-orbit coupling in the ionized subshell, in this case, the 5d subshell of Hg.

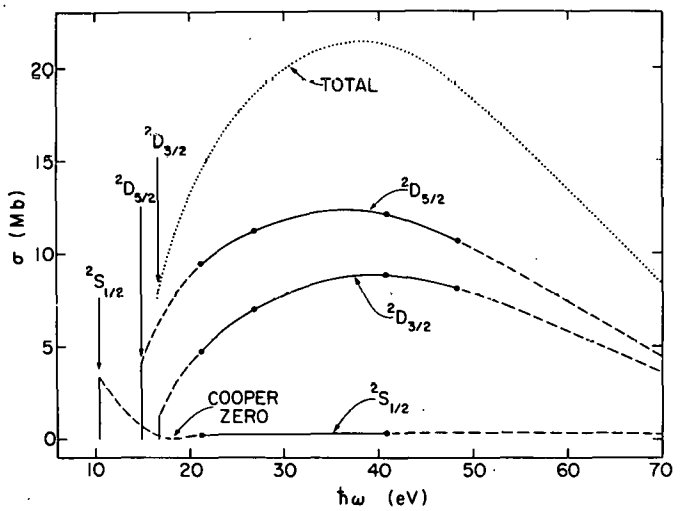

FIG. 1.--Partial photoionization cross sections for Hg.

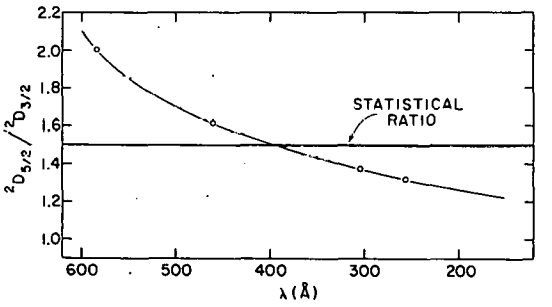

FIG. 2.--Wavelength dependence of $^2D_{\frac{5}{2}}:{}^2D_{\frac{3}{2}}$ branching ratio for mercury.

---

*Summary of a paper published in Phys. Rev. A 10, 484 (1974).

†Physics Division.

VALENCE SHELL EXCITATION ACCOMPANYING PHOTOIONIZATION IN MERCURY*

J. Berkowitz,† J. L. Dehmer, Y.-K. Kim, and J. P. Desclaux‡

The 584 Å photoelectron spectrum of mercury vapor exhibits weak peaks corresponding to formation of the excited $(5d)^{10}\ (6p)\ ^2P_{\frac{1}{2},\frac{3}{2}}$ ionic states, in addition to the one-electron transitions, which produce the $(5d)^{10}\ (6s)\ ^2S_{\frac{1}{2}}$ and $(5d)^9\ (6s)^2\ ^2D_{\frac{5}{2},\frac{3}{2}}$ states of Hg^+. Although the $^2P_{\frac{1}{2},\frac{3}{2}}$ states are forbidden by the usual shake-up mechanism, they can occur either by a "conjugate" shake-up process or by configuration interaction (CI) in the initial state. We present calculations which indicate that the latter is responsible for ~ 80% of the $^2P_{\frac{1}{2},\frac{3}{2}}$ intensity observed. The 304 Å photoelectron spectrum provides evidence for formation of additional excited ionic states which may have the configuration $(5d)^9\ (6p)^2$ and/or $(5d)^9\ 6s7s$. Our calculations show that the energies of these states are in the region of peaks experimentally observed. The $(5d)^9\ (6p)^2$ states can be formed by the initial-state CI mechanism, whereas the $(5d)^9\ 6s7s$ states are attainable via the shake-up process. The probabilities for these two transitions are comparable.

---

*Abstract of a paper published in J. Chem. Phys. 61, 2556 (1974). For a preliminary account, see Bull. Am. Phys. Soc. 19, 82 (1974).

†Physics Division.

‡Institut Max von Laue-Paul Langevin, Grenoble, France.

A GRAPHICAL ILLUSTRATION OF THE QUALITATIVE ASPECTS OF THE COOPER ZERO FOUND IN DIPOLE OSCILLATOR STRENGTH DISTRIBUTIONS

J. D Hanson* and J. L. Dehmer

One of the more outstanding spectral features of atomic dipole oscillator strength distributions is a deep minimum caused by a zero in the dipole matrix element for certain dipole-allowed excitation channels. This feature occurs in the photoabsorption spectra of many atoms and has become commonly known as the "Cooper zero." Here we illustrate the cause of the Cooper zero by plotting the wavefunctions and the integrand of the dipole matrix element for the $4p \rightarrow \epsilon d$ transitions in Kr which exhibits a zero at $\epsilon = 3.75$ Ryd.

The zero in partial photoabsorption cross sections caused by a change in sign in the dipole matrix element was first discussed by Seaton[1] in 1951 in connection with valence excitation in the alkali metals. Independently, Cooper[2] discovered the same phenomenon while studying the systematics of outer shell photoionization using the independent electron model. Cooper treated, among other cases, the rare gases, which exhibit a strong shape resonance in the same channel that at higher energy contains the zero matrix element. This combination of circumstances brought about the terms "Cooper maximum" and "Cooper zero" to denote this pair of spectral features. Subsequently, these terms have become commonly used by most workers in the field of photoabsorption phenomena.

The Cooper zero has been extensively documented[3] in experimental and theoretical studies in the past decade. Moreover, the cause for this phenomenon is well understood in terms of cancellation in the dipole matrix element produced by a final state node traversing the outer loop of the initial state wavefunction as the final state energy increases. However, although the zero is caused by a final state node, this requires a subsidiary circumstance to prevail, namely the presence of a node in the initial state. This has apparently prompted the view[4] that it is the initial state node which plays

*Appointee, Undergraduate Research Participation Program, Fall 1974, from Kalamazoo College, Kalamazoo, Michigan 49001.

the primary role in the cancellation which causes the zero. Specifically, it is stated in Ref. 4 that "At higher photoelectron energies [in the 4d → εf channel of Hg], the continuum orbital starts to overlap the nodes of the bound orbital, cancellation occurs, the dipole matrix element decreases and finally changes sign." To clarify this, we have prepared a plot of the integrand of the dipole matrix element, together with the pertinent wavefunctions, to illustrate the cause of the Cooper zero in the 4p → εd channel in Kr. A similar illustration of the origin of the Cooper maximum was given by Manson and Cooper.[5]

In the independent electron approximation, the partial cross section for the process 4p → εd in Kr is given by

$$\sigma_{4p \rightarrow \epsilon d} = \frac{16\pi\alpha a_0^2 (\epsilon - \epsilon_{4p})}{3} R^2_{4p \rightarrow \epsilon d} . \qquad (1)$$

The Cooper zero in this channel is caused by a change in sign of the radial dipole matrix element $R_{4p \rightarrow \epsilon d}$ defined by

$$R_{4p \rightarrow \epsilon d} = \int_0^\infty P_{4p}(r)\, r\, P_{\epsilon d}(r)\, dr , \qquad (2)$$

where P_{4p} and $P_{\epsilon d}$ are solutions of the radial Schroedinger equation

$$\left[\frac{d^2}{dr^2} + V(r) + E - \frac{\ell(\ell+1)}{r^2} \right] P_{E\ell}(r) = 0 , \qquad (3)$$

where r is in Bohr units and E is in Rydberg units. The radial wavefunctions P_{4p} and $P_{\epsilon d}$ are normalized in the standard way to unity and to unit energy range, respectively. In the present example, V(r) is a Hartree-Slater potential taken from the tabulation of Herman and Skillman.[6]

Figure 1 contains a plot of the quantities P_{4p}, $P_{\epsilon d}$, and $P_{4p}\, r\, P_{\epsilon d}$ at three values of ϵ = 1.0, 3.75, and 4.40 Ryd. The plot for ϵ = 1.0 represents the situation at the Cooper maximum. The integrand function is composed of four main bumps. (We disregard the very small positive hump occurring below $r \sim 0.2\ a_0$). The first one, extending from near the nucleus out to $r \sim 0.75\ a_0$

is generated by the nearly coincident initial and final state nodes outside the n=3 shell (i.e., outside the first loop in the ϵd function, and second loop in the 4p function). The second contribution is dominant at this energy and causes the net negative dipole matrix element. It is bounded at $r \sim 3.2\ a_0$ by the second node in the final state wavefunction, whose movement with energy will play a dominant role in producing the net zero in the matrix element. The next two humps, produced by successive nodes in the final state wavefunction are already appreciable at this energy, but do not dominate the integrand until the kinetic energy is higher.

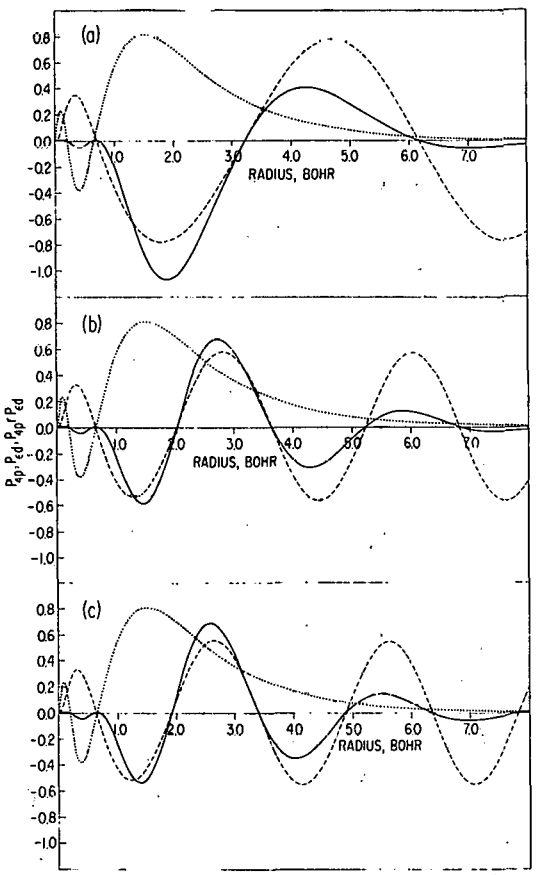

FIG. 1.--Plot of P_{4p} (...), $P_{\epsilon d}$ (---), and $P_{4p}\, r\, P_{\epsilon d}$ (—) for Kr at kinetic energies of ϵ = 1.0 Ryd (a), 3.748 Ryd (b), and 4.4 Ryd (c).

Note that the hump bounded by initial state nodes plays a very minor role in the net integral, and that this role does not change over the energy range pertinent to a discussion of the Cooper zero. This results from the relative insensitivity of the nodal structure of the final state in the atomic core in this energy range.

Between ϵ = 1.00 and ϵ = 3.75 Ryd, the second node of the final state moves from $r \sim 3.2\ a_0$ to $r \sim 2.0\ a_0$. This shift diminishes the second main hump in the integrand and makes the next hump dominant. At this energy, a near perfect cancellation occurs between the positive and negative contributions to the integrand, causing a zero in the dipole matrix element. Note also that although the main qualitative cause of the Cooper zero can be most simply understood by focussing on the motion of the second node of the ϵd wavefunction through the outer loop in the 4p wavefunction, the successive nodes

play a non-negligible role. From Figure 1 it is clear that actually the cancellation in the integrand involves contributions from several humps in the integrand caused by successive nodes in the final state.

The final set of curves in Figure 1 illustrates the situation at $\epsilon = 4.40$ Ryd, where a slight shrinking of the radii of the final state nodes have shifted the balance so that the net matrix element is now positive. As the final state energy continues to increase, the integral increases, reaching a maximum at $\epsilon \sim 8$ Ryd, whereupon it begins a monotonic decrease toward zero. However, for reasons not clear from a graphical-type argument, we see no further zeros (at least for $\epsilon < 500$ Ryd).

References

1. M. J. Seaton. Proc. Roy. Soc. (London) A208, 418 (1951).
2. J. W. Cooper. Phys. Rev. 128, 681 (1962).
3. U. Fano and J. W. Cooper. Rev. Mod. Phys. 40, 441 (1968).
4. T. E. H. Walker and J. T. Waber. J. Phys. B 7, 674 (1974).
5. S. T. Manson and J. W. Cooper. Phys. Rev. 165, 126 (1968).
6. F. Herman and S. Skillman. Atomic Structure Calculations. Prentice-Hall, Inc., Englewood Cliffs, New Jersey, 1963.

THEORY OF ANGULAR DISTRIBUTION OF PHOTOELECTRONS EJECTED FROM GAS-PHASE TARGETS*

Dan Dill†

The angular distribution $d\sigma/d\Omega$ of photoelectrons ejected by electric dipole interaction from isolated randomly oriented atomic or molecular targets is restricted (Yang's theorem) to the general form

$$\frac{d\sigma}{d\Omega} = \frac{\sigma}{4\pi} [1 + \beta P_2 (\cos\theta)] ;$$

σ is the integrated cross section, β is the asymmetry parameter, and θ is the ejection angle measured from the electric vector of the incident light. The goal of the study of angular distribution is to usilize β — obtained either by measurement or by direct calculation — as a probe both of static (e.g., symmetry) information on the initial and final target state, and of dynamic information on the photoionization process itself. To extract such information involves essentially unravelling geometry from dynamics in the theoretical analysis of β. This unravelling has yielded a general formulation of angular distribution theory, in terms of the angular momentum transferred in the photoionization process. The formulation provides a unified framework within which specific treatments of photoelectron angular distributions can be understood. Further, it reduces the general problem of the evaluation of a small number of dynamical parameters which characterize the unique properties of any particular system; geometrical parameters common to all systems have been evaluated once and for all. Finally, it has provided new insight into dynamical information uniquely probed by angular distribution studies, notably anisotropic interaction experienced by the electron as it departs the target.

---

*Abstract of invited talk for the Annual Meeting of the American Physical Society Division of Electron and Atomic Physics, December 2–4, 1974, Chicago.

†Appointee, Faculty Research Participation Program, Center for Educational Affairs, Argonne National Laboratory. Permanent address: Department of Chemistry, Boston University, Boston, Massachusetts 02215.

EFFECTS OF ANISOTROPIC ELECTRON-ION INTERACTIONS IN ATOMIC PHOTOELECTRON ANGULAR DISTRIBUTIONS*

Dan Dill,† Anthony F. Starace,‡ and Steven T. Manson§

The photoelectron asymmetry parameter β in LS-coupling is obtained as an expansion into contributions from alternative angular momentum transfers j_t. The physical significance of this expansion of β is shown to be that 1) the electric dipole interaction transfers to the atom a characteristic single angular momentum $j_t = \ell_0$, where ℓ_0 is the photoelectron's initial orbital momentum, whereas 2) angular momentum transfers $j_t \neq \ell_0$ indicate the presence of anisotropic (i.e., term-dependent) interaction of the outgoing photoelectron with the residual ion. For open-shell atoms the photoelectron-ion interaction is generally anisotropic; photoelectron phase shifts and electric dipole matrix elements depend on both the multiplet term of the residual ion and the total orbital momentum of the ion-photoelectron final-state channel. Consequently, β depends on the term levels of the residual ion and contains contributions from all allowed values of j_t. These findings contradict the independent particle model theory for β, which ignores final-state electron-ion interaction and to which our expressions reduce in the limiting cases for which only $j_t = \ell_0$ is allowed, namely 1) spherically symmetric atoms [e.g., closed-shell atoms] and 2) open-shell atoms for which the electron-ion interaction is isotropic [e.g., very light elements]. Numerical calculations of the asymmetry parameters and partial cross sections for photoionization of atomic sulfur are presented to illustrate the theory and to demonstrate the information on electron-ion dynamics that can be obtained from the theoretical and experimental study of β for open-shell atoms.

---

*Abstract of paper submitted to Phys. Rev. A.

†Appointee, Faculty Research Participation Program, Center for Educational Affairs, Argonne National Laboratory. Permanent address: Department of Chemistry, Boston University, Boston, Massachusetts 02215.

‡Behlen Laboratory of Physics, The University of Nebraska, Lincoln, Nebraska 68508.

§Department of Physics, Georgia State University, Atlanta, Georgia 30303. Consultant, RER Division, Argonne National Laboratory.

ANGULAR DISTRIBUTION OF PHOTOELECTRONS FROM HALOGEN ATOMS*

Steven T. Manson,† Anthony F. Starace,‡ and Dan Dill§

Calculations of the cross section and asymmetry parameter for photoionization of the outer p subshell of F, Cl, and Br have been carried out. Numerical Hartree-Fock discrete and continuum wavefunctions were employed.(1) The halogens were chosen for study because they are the likeliest group of open-shell atoms to be experimentally investigated.(2) The electron-ion interaction is found to be anisotropic for Cl and Br as exhibited by the differing phase shifts of the continuum wavefunctions in the various final-state channels. Consequently, we find, as in sulfur,(3) that the asymmetry parameters for Cl and Br 1) depend on the final state ionic term level and 2) have contributions from all allowed angular momentum transfer.

References

1. D. J. Kennedy and S. T. Manson. Phys. Rev. A 5, 227 (1972).
2. J. Berkowitz, Physics Division, private communication.
3. D. Dill, S. T. Manson, and A. F. Starace. Phys. Rev. Letters 32, 971 (1974).

*Abstract of a paper to be presented at the Annual Meeting of the American Physical Society, Division of Electron and Atomic Physics, Chicago, 2–4 December 1974.

†Georgia State University. Consultant, Argonne National Laboratory.
‡University of Nebraska.
§Boston University. Consultant, Argonne National Laboratory

SPECTROSCOPY AND COLLISION THEORY*

U. Fano† and Dan Dill‡

We outline and restate the main concepts and formulas that have been employed since 1969 in a group of extensive studies of spectral data. Seaton's Multichannel Quantum Defect Theory, complemented by the concept of eigenchannels of the short-ranged electron-core interaction, has served mostly as a tool for semiempirical analysis. Reference is made to extension of the treatment to negative ions, and to the direct ab initio calculation of the eigenchannel parameters which should constitute a new interface for comparison of theory and experiment. Illustrative results are presented, as well as a guide to relevant literature.

*Abstract of an invited paper presented at the IVth Conference on Ultraviolet and X-Ray Spectroscopy of Astrophysical and Laboratory Plasmas (Colloquium

No. 27 of the International Astrophysical Union), Cambridge, Massachusetts, 9–11 September 1974.

†Department of Physics, The University of Chicago, Chicago, Illinois 60637.
‡Appointee, Faculty Research Participation Program, Center for Educational Affairs, Argonne National Laboratory. Permanent address: Department of Chemistry, Boston University, Boston, Massachusetts 02215.

ELECTRON-MOLECULE SCATTERING AND MOLECULAR PHOTOIONIZATION USING THE MULTIPLE-SCATTERING METHOD*

Dan Dill† and J. L. Dehmer

We have adapted the multiple-scattering method to treat unbound electronic states of molecules in the independent electron approximation. An inhomogeneous linear system is derived whose solution yields the K matrix for the electron-molecule interaction. Using the K matrix, we derive continuum electronic wavefunctions by imposing boundary conditions corresponding to electron-molecule scattering and molecular photoionization, i.e., the wavefunctions satisfy the so-called outgoing-wave and incoming-wave normalization, respectively. These wavefunctions are then used to obtain expressions for elastic scattering and photoionization differential cross sections.

---

*Abstract of an article published in J. Chem. Phys. 61, 692 (July 1974).
†Consultant, Argonne National Laboratory. Permanent address; Department of Chemistry, Boston University, Boston, Massachusetts 02215.

PRELIMINARY RESULTS ON APPLICATION OF THE MULTIPLE-SCATTERING TECHNIQUE TO ELECTRON-MOLECULE SCATTERING AND MOLECULAR PHOTOIONIZATION: THE Π_g RESONANCE IN e-N_2 SCATTERING

J. L. Dehmer and Dan Dill*

We have performed a prototype calculation of the well-known 2.5-eV shape resonance in e-N_2 scattering to test the usefulness of the multiple-scattering method for electronic continuum molecular wavefunctions. The results of this demanding test are very encouraging.

We will not dwell here on the formal development or philosophy of the multiple-scattering approach to molecular wavefunctions in the electronic continuum. Both are described in detail elsewhere.[1,2] Here, instead, we describe very preliminary prototype calculations designed to indicate the ability of this new approach to reproduce well-known characteristics of real systems.

We have chosen to compute the energy dependence of the Π_g eigenphase sum for elastic e-N_2 scattering. This makes an ideal test case for two reasons: a) in this scattering channel for N_2 there is a distinct shape resonance at an electron energy of 2.5 eV, which has been exhibited in both experiment[3] and theoretical calculations;[4,5] b) the combination of diatomic geometry and low kinetic energy is most susceptible to the main weakness of the present version of the multiple-scattering approach — the muffin-tin approximation. Moreover, aside from this possible trouble area, this resonance has proved elusive to other approaches. It is known[6] that spherically averaged representation of the e-N_2 potential using the Slater exchange approximation fails to reproduce this resonant behavior because the potential is too attractive, binding a discrete Π_g state. The single-center expansion of Sawada, Ganas, and Green[7] also produces behavior indicating that the shape resonance has been "pulled" into the discrete.

In the present calculation an approximate e-N_2 potential was prepared using the re-expansion-of-atomic-charge-distribution method of Johnson et al.†

*Consultant. Permanent address: Department of Chemistry, Boston University, Boston, Massachusetts 02215.

†It is recommended that the reader consult Ref. 8 for a detailed account of the application of the multiple-scattering method to the electronic structure of molecules.

To best describe the short-range N_2^--like potential, two $N^{-\frac{1}{2}}$ $(1s^2 2s^2 2p^{3.5})$ charge distributions were superimposed with a separation of 1.0977 Å. The long-range potential was taken to be the monopole term of the polarizability expansion. These two were joined at their crossing point. To learn the sensitivity of the calculation to the strength of the statistical exchange approximation used, we scaled this contribution to the potential between $\alpha = 0.5$ and $\alpha = 1.0$ (the Slater value[9]). This range includes the Kohn-Sham value[10] of $\alpha = 2/3$. The resulting eigenphase sums are shown in Figure 1. Note the transition from a bound Π_g state at $\alpha = 1$ to sharp resonant behavior at $\alpha \sim 0.6$ (i.e., rapid increase in eigenphase sum by $\sim \pi$). The curve $\alpha = 0.6$ agrees with the most recent work of Burke[4] and coworkers, and is believed to represent the physical situation very well. Note this behavior occurs near the Kohn-Sham[10] value of $\alpha = 2/3$. Also notable is the smooth, artifact-free behavior of the curves. This shows the discontinuities in the model potential are averaged out.

A more detailed report is being prepared which includes the effect of using a self-consistent field version of the potential described above, and also treats all scattering channels and the resulting total, differential, and momentum transfer cross sections.

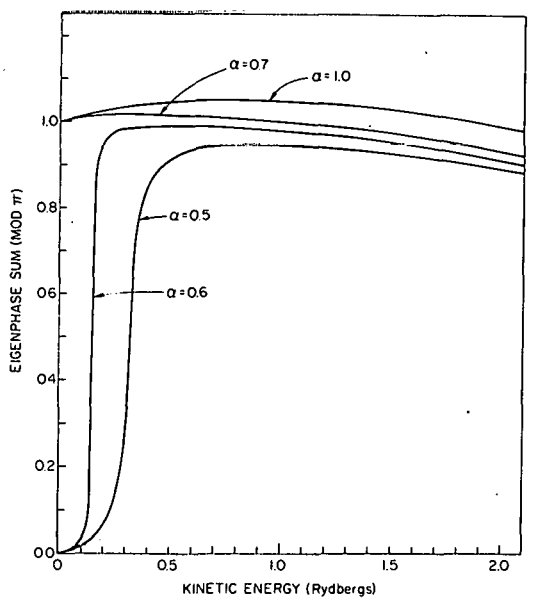

FIG. 1.--Eigenphase sum for the $^2\Pi_g$ channel in e^--N_2 scattering. Curves are labeled by the value of the coefficient of the Slater exchange term used.

We wish to emphasize that this type of application is the most dubious limit of applicability of the multiple-scattering approach. It is best suited for studying spectral properties extending over large energy ranges, such as extended fine structure in inner-shell photoionization cross sections. Convergence is expected to be faster in this multicenter representation than for single-center representations so that higher kinetic energies are more easily studied. Moreover, complex molecules are easily treated by multiple-scattering methods, while convergence propertics of single-center models remain untested. Also, highly coordinated molecules and small molecules with disparate atomic sizes (HCl, H_2O, etc.) should be far better represented by the muffin-tin model than homonuclear diatomics. Therefore, the outlook is good for the model, even in its present form. Naturally an eventual improvement of the treatment of the core region is desirable.

References

1. J. L. Dehmer and D. Dill. Argonne National Laboratory Radiological and Environmental Research Division Annual Report, July 1972–June 1973. ANL-8060, Part I, pp. 110–157.
2. Dan Dill and J. L. Dehmer. J. Chem. Phys. 61, 692 (1974).
3. D. E. Golden. Phys. Rev. Letters 17, 847 (1966).
4. P. G. Burke and N. Chandra. J. Phys. B 5, 1696 (1972).
5. M. Krauss and F. H. Mies. Phys. Rev. A 1, 1592 (1970).
6. P. Bagus, IBM Research Laboratory, San Jose, California. Private communication.
7. T. Sawada, P. S. Ganas, and A. E. S. Green. Phys. Rev. A 9, 1130 (1974).
8. K. H. Johnson. Scattered-Wave Theory of the Chemical Bond. Advances in Quantum Chemistry, Ed. P. O. Löwdin. Academic Press, New York, 1973, Vol. 7, p. 143.
9. J. C. Slater. Phys. Rev. 81, 385 (1951).
10. W. Kohn and L. J. Sham. Phys. Rev. A140, 1133 (1965).

SYSTEMATICS OF FESHBACH RESONANCES IN THE MOLECULAR HALOGENS*

David Spence

Using an electron-transmission spectrometer[1] we locate the energetically lowest-lying Feshbach resonances in the molecular halogens F_2, Cl_2, Br_2, and I_2. A typical spectrum of the derivative of the electron current transmitted through a bromine target is shown in Figure 1. These resonances are associated with Rydberg states and have symmetry $(X^2\Pi_g)(ns\sigma)^2[^2\Pi_{\frac{1}{2},\frac{3}{2}}]$, where n = 3, 4, 5, 6 for F_2, Cl_2, Br_2, and I_2, respectively. The binding energy of the lowest pair of nsσ electrons to the ground-state positive-ion core decreases monotonically as the size of the molecules increases from 4.45 ± 0.05 eV in fluorine to 3.57 ± 0.05 eV in iodine, as tabulated in Table 1 and shown graphically in Figure 2. A simple qualitative theoretical argument, based on atomic model, satisfactorily describes the decrease in the binding energy as being due to increasing core "size" as the principal quantum number of the Rydberg electron increases from 3 to 6 from F_2 to I_2. This increasing core size moves the extrema of the largest loops of the radial wavefunction to the lowest ns Rydberg electrons shown in Figure 3 to larger distances from the ion core, thus reducing their binding energy accordingly.

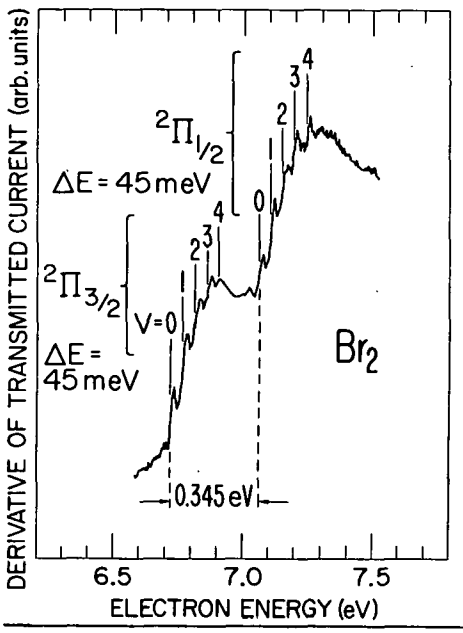

FIG. 1.--Derivative of the transmitted electron current vs. electron energy in molecular bromine. The two bands of resonances derived from the addition of a pair of nsσ electrons to the $^2\Pi_{\frac{3}{2}}$ and $^2\Pi_{\frac{1}{2}}$ components of the $X^2\Pi_g$ positive ion core. The separation of the two bands, 0.345 eV, is indicated by the horizontal arrows.

*Summary of a paper which appeared in Phys. Rev. A 10, 1045 (1974).

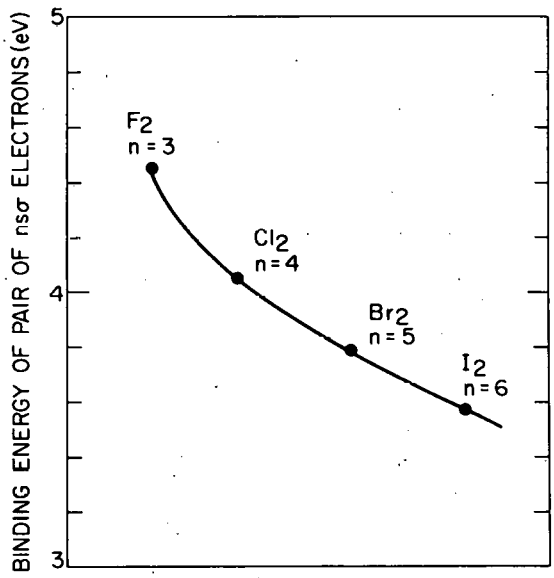

FIG. 2.--Binding energies of the lowest pair of nsσ electrons to ground-state positive-ion cores for the molecular halogens. The binding energy of the nsσ pair decreases monotonically by almost 1 eV as the molecular size increases from fluorine to iodine.

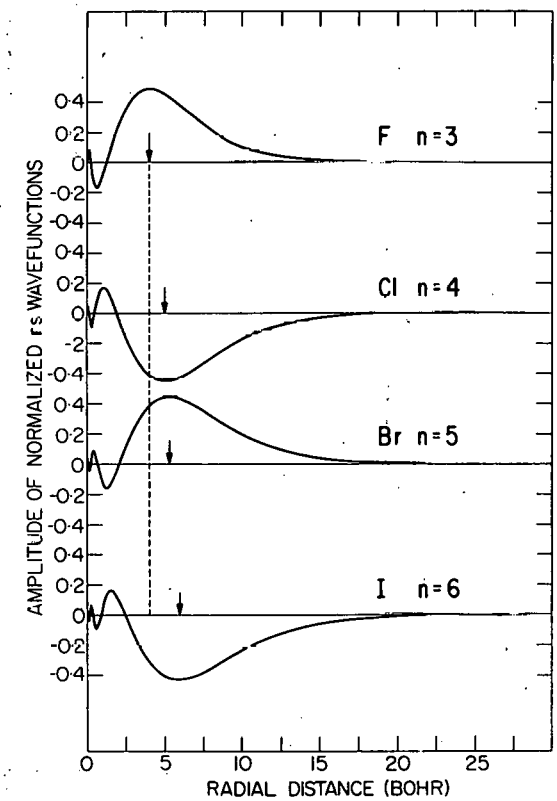

FIG. 3.--Hartree-Slater radial wavefunctions for the lowest ns Rydberg electrons in F, Cl, Br, and I. The radial coordinates of the extrema of the largest loops are indicated by the arrows, and show the increase in size of the electron orbit from F through Cl and Br to I.

TABLE 1. Ionization Potentials and Lowest Observed Feshbach Resonances in the Molecular Halogens, together with the Binding Energies of the Lowest Pair of nsσ Electrons to the Positive Ion Core in These Molecules

Molecule	Ionization potential, eV		Resonance energy, eV	Resonance Principal quantum number	$(ns\sigma)^2$ binding energy, eV
	Potts and Price [2]	Comford et al. [3]	Present experiment		
F_2	15.70	15.7	11.25	3	4.45
Cl_2	11.51	11.49	7.46	4	4.05
Br_2	10.51	10.51	6.72	5	3.79
I_2	9.35 (v) 9.33 (a)	9.34	5.78 (v) 5.65 (a)	6	3.57

(v) = vertical.
(a) = adiabatic.

References

1. L. Sanche and G. J. Schulz. Phys. Rev. A 6, 69–86 (1972).
2. A. W. Potts and W. C. Price. Trans. Farad. Soc. 67, 1242 (1971).
3. A. B. Comford, D. C. Frost, C. A. McDowell, J. L. Ragle, and I. A. Stenhouse. J. Chem. Phys. 54, 2651 (1971).

ELECTRON-TRANSMISSION SPECTROSCOPY IN MOLECULAR CHLORINE*

David Spence

Using the technique of electron-transmission spectroscopy,[1] we locate a vibrational progression of resonances with spacing 0.080 eV in the total cross section for scattering of electrons by molecular chlorine, as shown in Figure 1. The first member of this series occurs at 7.48 ± 0.05 eV. From measured vibrational spacings and Franck-Condon factors of this progression, which are tabulated in Table 1, and using calculated quantum defects, we determine the configuration of these resonant states to be $[X^2\Pi, Cl_2^+](4s\sigma_g)^2$ $[^2\Pi]$. The lowest Rydberg state in chlorine, with which this progression is associated, is located at about 8.0 eV and has configuration $[X^2\Pi, Cl_2^+]4s\sigma_g$ $[^{1,3}\Pi]$.

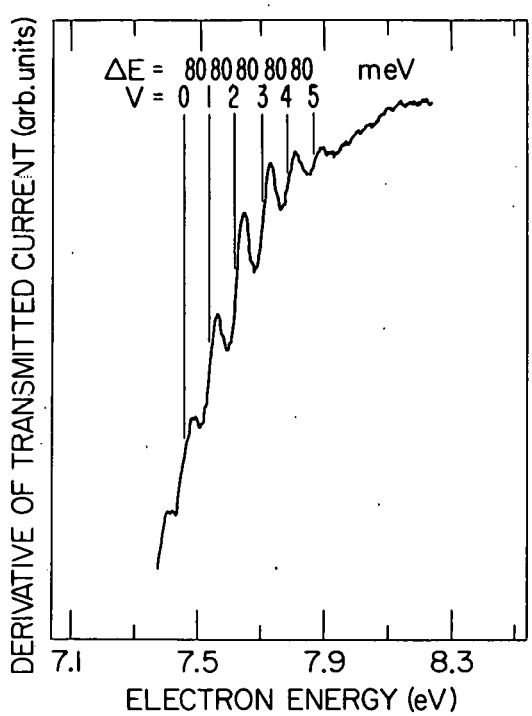

FIG. 1.--Derivative of a transmitted electron current through a target of molecular chlorine as a function of incident electron energy. The band of resonances derives from the additive of two nsσ electrons to the $X^2\Pi_g$ positive ion core.

*Abstract of a paper presented at the Chicago Meeting of the American Physical Society, 4–7 February 1974.

TABLE 1. Comparison of Vibrational Intensities Observed for Progressions of Feshbach Resonances in the Present Experiments with the Appropriate Vibrational Intensities Observed for the Molecular Chlorine ($X^2\Pi$) Positive Ion States

Vibrational quantum numbers	Vibrational intensities		
	Negative ion system	Positive ion system	
	Present experiment	Potts and Price[2]	Cornford et al.[3]
	$Cl_2(\Sigma_g^+, v=0) \rightarrow Cl_2^-(v)$	$Cl_2(^1\Sigma_g^+, v=0) \rightarrow Cl_2^+(X^2\Pi, v)$	
0	0.42	0.46	0.39
1	0.89	0.88	0.91
2	1.00	1.00	1.00
3	0.83	0.74	0.63
4	0.50	0.36	0.23
5	0.19	0.16	0.11

References

1. L. Sanche and G. J. Schulz. Phys. Rev. A 6, 69 (1972).
2. A. W Potts and W. C. Price. Trans. Farad. Soc. 67, 1242 (1971).
3. A. B. Cornford, D. C. Frost, C. A. McDowell, J. L. Rayle, and I. A. Stenhouse. J. Chem. Phys. 54, 2651 (1971).

ELECTRON-TRANSMISSION SPECTROSCOPY IN THE ACID HALIDES*

David Spence and Tetsushi Noguchi

Using an electron-transmission spectrometer[1] we have made the first measurements of the energies of Feshbach resonances in the acid halides HF, HCl, HBr, and HI. These resonances, which consist of two electrons bound to a positive ion core, are associated with Rydberg states of the neutral molecule. Each acid halide exhibits several isolated resonances and bands of resonances with the positive ion cores in either the ground or excited states. These resonances are correlated with known Rydberg parent states, thus allowing determination of the resonance electron configuration and the electron affinities of the Rydberg states.

Reference

1. L. Sanche and G. J. Schulz. Phys. Rev. Letters 26, 943 (1971).

*Abstract submitted for the Chicago Meeting of the Division of Electron and Atomic Physics, American Physical Society, 2–4 December 1974.

TOTAL CROSS SECTIONS FOR DOUBLE EXCITATION IN He BY ELECTRON IMPACT*

David Spence

By modulating the amplitude of the trapping potential in a trapped electron apparatus we have made the first measurements of the total cross section for excitation by electron impact of the $(2s^2)^1S$ and $(2s2p)^3P$ doubly excited states in helium from threshold to 7 eV. These cross sections are made "absolute" by normalization to the known 2^3S cross section. The $(2s^2)^1S$ cross section peaks to a value 3×10^{-20} cm^2 at threshold, has a subsidiary peak in the region of the $(2s2p^2)^2D$ resonance and then decreases monotonically. The $(2s2p)^3P$ cross section has a minor peak of magnitude 2×10^{-20} cm^2 at threshold, then rises to a broad maximum of magnitude 3×10^{-20} cm^2 4.0 eV above its threshold.

*Abstract submitted for the Chicago Meeting of the Division of Electron and Atomic Physics, American Physical Society, 2–4 December 1974.

ELECTRON CORRELATION EFFECTS NEAR THRESHOLD FOR ELECTRON-IMPACT IONIZATION OF HELIUM*

David Spence

Using a modification of the trapped-electron technique,[1] we have measured the total intensity of electrons inelastically scattered from helium as a function of both incident and final energies near the ionization threshold. We find that a "cusp," first observed by Cvejanovic and Read,[2] which appears in the scattered electron intensity at the ionization threshold for electrons of near-zero final energy, decreases in visibility as the energy of the scattered electrons increases. This effect is illustrated in Figure 1 where we have plotted the inelastically scattered current as a function of incident energies for fixed final energies of 0.07 eV, 1.0 eV, and 2.0 eV. For scattered-electron energies greater than about 2.0 eV, the intensity is smooth through the ionization threshold, as shown for clarity in Figure 2. The physical reason for the cusp is the formation of states with two excited and strongly correlated

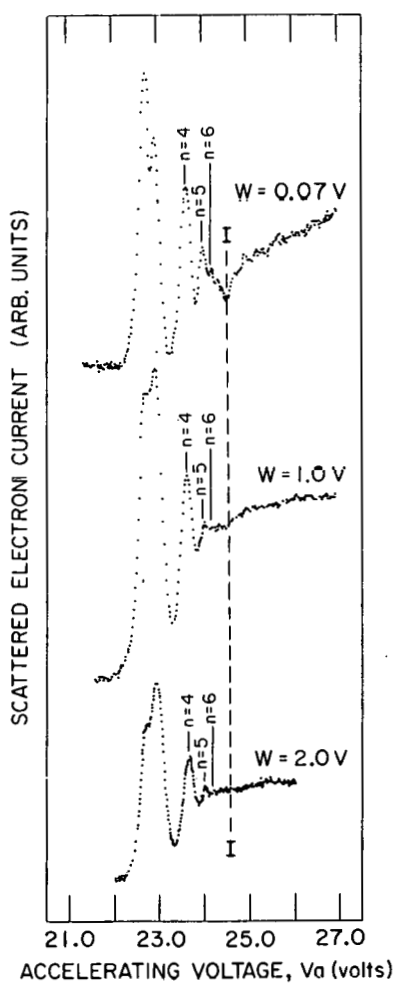

FIG. 1.--Spectra showing total yield of scattered electrons from He with final energies eW as a function of the incident energy $e(V_a + W)$. The ionization threshold is marked I.

*Expanded abstract of a manuscript submitted to Phys. Rev. Letters.

electrons.[3] These experiments define the range of excess energies above the ionization threshold for which correlation effects are important, and hence measure the energy range of validity of the Wannier law of threshold ionization.[4]

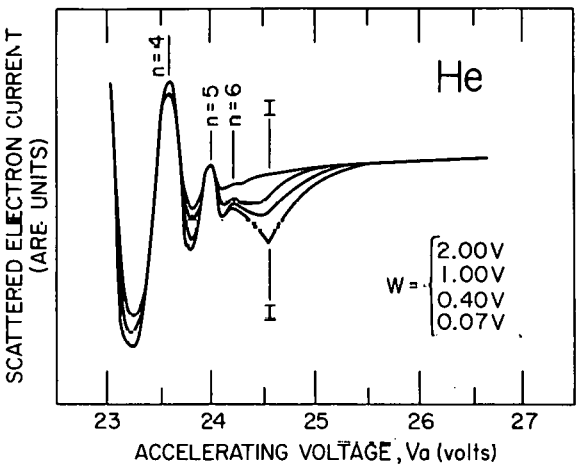

FIG. 2.--Comparison of spectra of scattered electron intensities as a function of incident energy $e(V_a + W)$ for different values of final energy eW. The ionization threshold is marked I.

References

1. G. J. Schulz. Phys. Rev. 112, 150 (1958).
2. S. Cvejanovic and F. H. Read. J. Phys. B 14, 1841 (1974).
3. U. Fano. J. Phys. B 14, L401 (1974).
4. G. H. Wannier. Phys. Rev. 90, 817 (1953).

SEARCH FOR LOW-LYING RESONANCES IN ELECTRON SCATTERING BY ATOMIC HYDROGEN*

David Spence and Mitio Inokuti

Measurements of the transmission of an energy-selected electron beam through atomic hydrogen fail to indicate any resonance below 9.5-eV electron energy. The negative result, shown graphically in Figure 1, contradicts recent suggestions by Rudkjøbing[1,2] and by Van Rensbergen[3,4] that some diffuse interstellar absorption bands might be attributable to preionizing transitions in the hydrogen negative ions. A bulk of reliable theoretical data,[5-7] however, justifies our finding.

*Summary of a paper which appeared in J. Quant. Spectry. Radiative Transfer 14, 953–957 (1974).

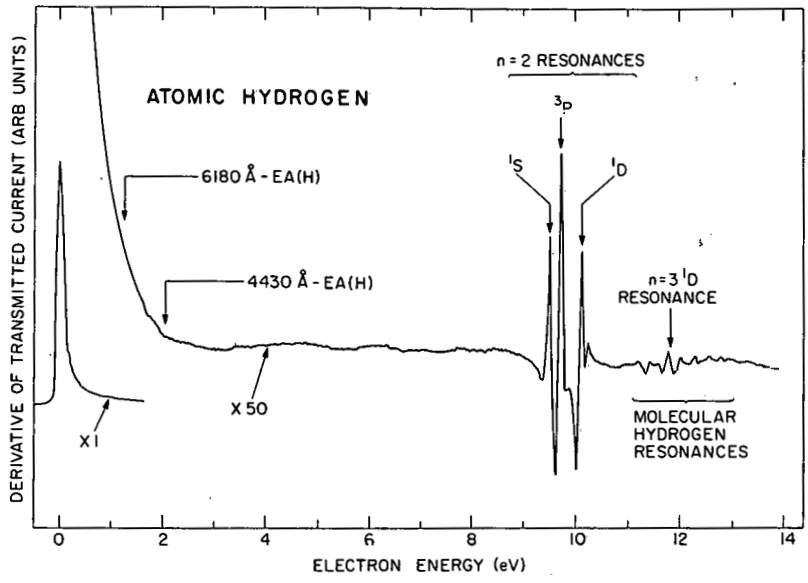

FIG. 1.--A plot of the derivative of the current transmitted through atomic hydrogen as a function of electron energy. The arrows at low energies indicate the energies at which resonances would occur if preionization transitions in H^- were responsible for the 6180 Å and 4430 Å interstellar absorption bands. The arrows in the region of 10 eV indicate the positions of several resonances predicted theoretically in which both electrons are in n = 2 orbitals. Higher-lying structures are due predominantly to resonances in molecular hydrogen, which constitute a small percentage of the target gas.

References

1. M. Rudkjøbing. Astrophys. Space Sci. 6, 157 (1970).
2. M. Rudkjøbing. J. Quant. Spectry. Radiative Transfer 13, 1479 (1973).
3. W. Van Rensbergen. J. Quant. Spectry. Radiative Transfer 11, 1125 (1971).
4. W. Van Rensbergen. J. Quant. Spectry. Radiative Transfer 12, 1105 (1972).
5. C. Schwartz. Phys. Rev. 124, 1468 (1961).
6. R. L. Armstead. Phys. Rev. 171, 91 (1968).
7. M. Inokuti and Y.-K. Kim. Phys. Rev. 173, 154 (1968).

MEASUREMENTS OF THE $H^-(3p^2)\ ^1D$ STATE BY ELECTRON-TRANSMISSION SPECTROSCOPY*

David Spence

Using an electron-transmission spectrometer we measure structures in the total cross section for e-H scattering, a typical spectrum shown in Figure 1. In the center trace, where the dissociation is about 90%, the series of resonances between 11.0 + 13.0 eV are molecular in origin, with the exception of the large deflection at 11.86 eV which we attribute to the $H^-(3p^2)\ ^1D$ state. Increasing the dissociation to essentially 100% removes all molecular structures leaving one isolated resonance in this energy region, as shown in the lower curve. Also marked on the lower curve are the theoretical locations of several resonance states in which both electrons have principal quantum number of 3. From a series of 26 measurements of spectra of the type shown in Figure 1, we find the energy of the $(3p^2)\ ^1D$ state of H^- to be 11.860 ± 0.030 eV above the ground state of atomic hydrogen. This result is compatible with measurements of autoionizing states of H^- obtained from ion-neutral collision experiments,[1] which yield the energy of this state to be 11.860 ± 0.040 eV and from measurements of structures in the 12-2p excitation cross section,[2]

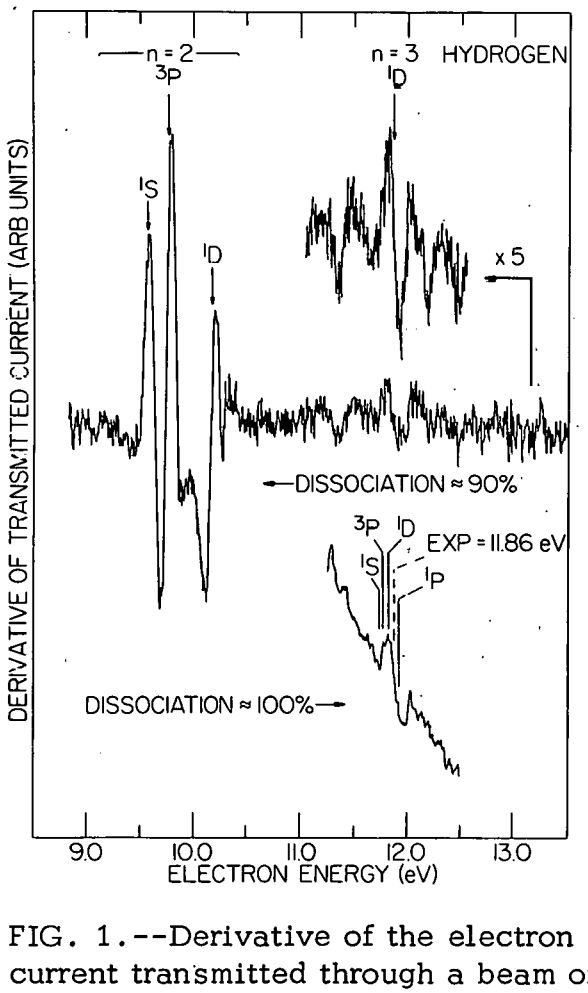

FIG. 1.--Derivative of the electron current transmitted through a beam of partially dissociated hydrogen.

*Abstract of a paper submitted for publication in J. Phys. B. Atom. and Molec. Phys.

which yield a value 11.89 ± 0.020 eV. The experimental results, however, are in significant disagreement with the theoretical value[3] of 11.819 eV for the energy of the $H^-(3p^2)\ ^1D$ state.

References

1. J. S. Riseley, A K. Edwards, and R. Geballe. Phys. Rev. A 9, 1115–1129 (1974).
2. J. W. McGowan, J. F. Williams, and E. K. Curley. Phys. Rev. 180, 132–138 (1969).
3. P. G. Burke. Advances in Atomic and Molecular Physics, Ed. D. R. Bates and I. Esterman. Academic Press, New York, 1965, Vol. 4, pp. 173–219.

INTRODUCTION TO THE SYMPOSIUM ON THE JESSE EFFECT AND RELATED PHENOMENA*

Mitio Inokuti

Nearly a quarter of a century ago Jesse discovered that a minute amount of contaminants greatly enhances the total ionization of helium gas by alpha particles. The discovery has stimulated many workers to study the role of metastable and other excited species in gaseous mixtures, a subject that now has numerous ramifications and applications. The present Symposium was conceived for reviewing the current understanding of the Jesse effect and its microscopic mechanisms, which include collisions and quenching of excited atoms, Penning ionization, properties of diatomic rare-gas molecules, photoionization, and transport of resonance radiations. Related macroscopic phenomena concern gaseous discharges and vacuum ultraviolet lasers.

---

*Abstract of a paper presented at the Symposium on the Jesse Effect and Related Phenomena, Gatlinburg, Tennessee, November 9–10, 1973, and published in Radiat. Res. 59 (1974).

PHOTOIONIZATION AND THE JESSE EFFECT: A COMPARISON OF YIELDS AND ISOTOPE EFFECTS*

James C. Person

The comparison of the ionization yield from the Jesse effect η_J and the photoionization yield η_P, as first made by Platzman,[1-5] is updated, with the major results given in Tables 1–3. The majority of examples snow $\eta_J \approx \eta_P$ and most of the other η_J values are about 10 to 20% lower than the η_P values. Isotope effects are also compared, and the η_J data are used to estimate the fraction of ionization via direct ionization. This is a large fraction for most cases, provided that the branching yield for competitive preionization ρ is as large as 1.4. However, it is a small fraction in most cases if $\rho \leq 1.2$. The general tendency for part of the data to show $\eta_J \approx \eta_P$ and part to show η_J values 10 to 20% smaller could be rationalized either by some contributions from metastable Jesse precursors with $\eta_M < \eta_P$ or by contributions from molecular excited states as Jesse precursors, with these states tending to

TABLE 1. Ionization Yields with Helium as Parent Gas

Additive gas	η_J	η_J[a]	η_P		
			21.2 eV[b]	21.2 eV[c]	19.8 – 21.2 eV
H_2	0.92[d]	0.93 – 0.98	1.00	1.00	
N_2	0.89[d]	0.91 – 0.96	0.98	1.00	0.96 – 1.00[f]
O_2	0.9 [d]		0.95	1.00	0.93 – 1.00[f]
CO		0.84 – 0.87	0.96	0.97	0.97 – 0.98[g]
CO_2	0.87[d]	0.88 – 0.92	1.00	1.00	0.99 – 1.00[g]
CH_4	0.83[e]	0.81 – 0.83	0.96	1.00	
C_2H_6	0.80[e]		0.90	0.98	
C_2H_4	0.78[e]		0.98		
C_6H_6	0.81[e]				0.88 – 1.05[h]

[a] Calculated from data of Ref. 13; [b] Refs. 22, 23; [c] Ref. 21; [d] Refs. 1,3; [e] Ref. 6; [f] Ref. 12; [g] Ref. 14; [h] Ref. 15.

*Based on a paper presented at the Symposium on the Jesse Effect and Related Phenomena, Gatlinburg, Tennessee, November 9–10, 1973. Abstract of paper in Radiat. Res. 59, 408–421 (1974).

TABLE 2. Ionization Yields with Neon as Parent Gas

Additive gas	η_J	η_J [a]	η_P	
			16.7 + 16.8 eV [b]	16.6 – 16.8 eV
H_2	0.83 [c]	0.84 – 0.92	0.94	
N_2		0.79 – 0.87	0.90	
H_2O	0.55 [d]		0.72	0.72 – 0.74 [e]
CO_2		0.77 – 0.79	0.87	
CH_4	1.00 [d]		1.00	
C_2H_6	0.93 [d]		1.00	
$n\text{-}C_4H_{10}$	0.91 [d]		1.00	
C_2H_2	0.77 [c]		0.92	
C_2H_4	0.78 [d]		0.98	
C_6H_6	0.72 [d]			0.95 – 1.01 [f]

[a] Calculated from data of Ref. 13; [b] Refs. 22,23; [c] Refs. 1,3; [d] Ref. 6; [e] Ref. 18; [f] Ref. 15.

TABLE 3. Ionization Yields with Argon as Parent Gas

Additive gas	η_J [a]	η_J [b]	η_J [c]	η_P [d]	η_P [e]	η_P
Ethane			0.08	0.05	0.02 – 0.08	
Propane		0.26 – 0.29	0.31	0.25	0.23 – 0.25	
c-Propane		0.31 – 0.34	0.41		0.53 – 0.51	
n-Butane	0.32	0.33 – 0.36	0.35	0.32	0.36 – 0.43	0.35 – 0.43 [f]
i-Butane		0.30 – 0.32	0.44		0.34 – 0.41	
Acetylene		0.64 – 0.73	0.87	0.80	0.77 – 0.84	0.69 – 0.88 [g]
Ethylene	0.24	0.23 – 0.25	0.24	0.20	0.23 – 0.17	0.18 – 0.26 [f]
Propene		0.23 – 0.24	0.23		0.23 – 0.25	0.24 [g]
Butene-1		0.39 – 0.42	0.31		0.30 – 0.37	
Benzene	0.39	0.36 – 0.39		0.47		0.46 [h]
Ethanol		0.22 – 0.23		0.20		0.22 – 0.25 [i]
Acetone		0.16 – 0.17		0.21		0.22 – 0.23 [j]
Methyl iodide		0.48 – 0.51		0.74		

[a] Calculated from data of Ref. 6; [b] Calculated from data in Table I of Ref. 16; [c] Data from from Ref. 16 using $\beta_1 = 0.0106$ from Ref. 17; [d] Data for argon resonance lamp with LiF window, Refs. 19, 22; [e] Data for monochromatic argon resonance light, Ref. 17; [f] Data for seven E_P values from 11.56 to 11.78 eV, Ref. 10; [g] Data for seven E_P values from 11.56 to 11.78 eV, Ref. 8; [h] Datum for $E_P = 11.64$ eV, Ref 7, revised by NO values of Ref. 20; [i] Data for seven E_P values from 11.56 to 11.78 eV, Ref. 9; [j] Data for seven E_P values from 11.56 to 11.78 eV, Ref. 11.

transfer smaller energies. The cases with η_{JD}/η_{JH} larger than η_{PD}/η_{PH} would be more consistent with the former explanation, if the competitive preionization process is approximately independent of the mode of excitation, but several cases exhibited approximately equal isotope ratios and would be consistent with either explanation. In addition, we have suggested that a systematic variation of chamber geometry may provide a test for the importance of vacuum ultraviolet radiation in the decay of the Jesse precursors.

References

1. R. L. Platzman. J. Phys. Radium 21, 853 (1960). Engl. translation: Argonne National Laboratory Radiological Physics Division Semiannual Report, January through June 1960. ANL-6199, p. 6.
2. R. L. Platzman. Radiat. Res. 17, 419 (1962).
3. R. L. Platzman. Vortex 23, 372 (1962).
4. R. L. Platzman. J. Chem. Phys. 38, 2775 (1963).
5. W. P. Jesse and R. L. Platzman. Nature 195, 790 (1962).
6. W. P. Jesse. J. Chem. Phys. 41, 2060 (1964).
7. J. C. Person. J. Chem. Phys. 43, 2553 (1965).
8. J. C. Person and P. P. Nicole. J. Chem. Phys. 53, 1767 (1970).
9. J. C. Person and P. P. Nicole. J. Chem. Phys. 55, 3390 (1971).
10. J. C. Person and P. P. Nicole. J. Chem. Phys. 49, 5421 (1968).
11. J. C. Person and P. P. Nicole. Argonne National Laboratory Radiological Physics Division Annual Report, July 1969–June 1970. ANL-7760, Part I, p. 97.
12. R. E. Huffman. Can. J. Chem. 47, 1823 (1969).
13. C. E. Klots. J. Chem. Phys. 46, 3468 (1967).
14. R. B. Cairns and J. A. R. Samson. J. Geophys. Res. 70, 99 (1965).
15. M. Yoshino, J. Takeuchi, and H. Suzuki. J. Phys. Soc. Japan 34, 1039 (1973).
16. G. S. Hurst, T. E. Bortner, and R. E. Glick. J. Chem. Phys. 42, 713 (1965).
17. C. E. Klots. J. Chem. Phys. 56, 124 (1972).
18. D. H. Katayama, R. E. Huffman, and C. L. O'Bryan. J. Chem. Phys. 59, 4309 (1973).
19. P. Ausloos and S. G. Lias. Radiat. Res. Rev. 1, 75 (1968).
20. K. Watanabe, F. W. Matsunaga, and H. Sakai. Appl. Opt. 6, 391 (1967).
21. S. W. Bennett, J. B. Tellinghuisen, and L. F. Phillips. J. Phys. Chem. 75, 719 (1971).
22. R. E. Rebbert and P. Ausloos. J. Res. Nat. Bur. Stands., Sect. A, 75, 481 (1971).
23. P. Ausloos. Mol. Photochem. 4, 39 (1972).

ROTATIONAL EFFECT IN THE IONIZATION OF A HIGHLY EXCITED ATOM BY COLLISION WITH A POLAR MOLECULE.

Michio Matsuzawa*

If the collisional ionization is chiefly due to energy transfer from the polar-molecule rotation to an electron in a high Rydberg state of the atom, then theory predicts that the cross section averaged over a thermal distribution of rotational states should show step-like structure as a function of the energy of the Rydberg state. This structure has been experimentally detected, and it can be considered as direct evidence of the rotational effect in the collisional ionization.

Recently I[1-3] proposed a mechanism for the collisional ionization of an atom in a high Rydberg state with a polar molecule in which a Rydberg electron becomes ionized by gain of energy from rotational de-excitation of the polar molecule in a rotationally excited state at thermal energies, namely,

$$A^{**}(n,\ell) + M(J) \rightarrow (A^{+} + e) + M(J') \quad . \qquad (1)$$

Here n and ℓ are the principal quantum number and the angular momentum of the Rydberg electron, and J is the rotational quantum number of the polar molecule. This mechanism explains the relative dependence of the ionization cross sections for various combinations of an atom and a polar molecule.[3]

The present article points out that the step-like structure in the n dependence of the cross section for process (1) is theoretically predicted from the proposed mechanism, provided the rotational states of the polar molecule are populated according to thermal distribution.[4] This step-like structure, if experimentally detected, can be considered as direct evidence of the rotational effect.

Using the Born approximation with a point-dipole interaction between an electron and the polar molecule, I write the collisional ionization cross section for process (1) as[3]

*Visiting Scientist, October 1972–March 1974. Present address: The University of Electro-Communications, Chofu-shi, Tokyo.

$$\sigma_i(n, J \rightarrow J-1) = \frac{8\sqrt{2}\pi}{3} \left(\frac{\mu}{E} \right)^{\frac{1}{2}} D^2 \frac{J}{2J+1} I_d(n, \epsilon_0) \ . \qquad (2)$$

Here μ is the reduced mass of the colliding system $A^{**} + M$, D is the dipole moment of the polar molecule, and E is the energy of the relative motion. The notation $I_d(n, \epsilon_0)$ signifies

$$I_d(n, \epsilon) = \int_0^\infty \frac{dF_n(Q, \epsilon)}{d\epsilon} \, dQ \ .$$

Here $dF_n(Q, \epsilon)/d\epsilon$ is the form factor density of the atom in Rydberg states n per unit range of energy ϵ of the ejected electron, and ϵ_0 is the difference between the rotational excitation energy 2BJ and the binding energy of the Rydberg electron

$$\epsilon_0 = 2BJ - E_n \ , \qquad (3)$$

and B is the rotational constant of the polar molecule. (Here and in what follows, atomic units are used unless otherwise specified.)

Experimentally, it is very difficult to specify the particular rotational state of the polar molecule at thermal energies. Hence, the experiment is carried out under a condition in which the polar molecule has a thermal distribution over rotational states. Then the average of expression (2) over the rotational states of the polar molecule yields for a linear rigid rotor under the usual experimental condition an n-dependent ionization cross section

$$\sigma_i(n) = \frac{8\sqrt{2}\pi}{3} \left(\frac{\mu}{E} \right)^{\frac{1}{2}} D^2 I_{rot}(n) \ . \qquad (4)$$

Here $I_{rot}(n)$ denotes the average of a quantity $[J/(J+1)] \, I_d(n, \epsilon_0)$ over the rotational states, namely,

$$I_{rot}(n) = \frac{\sum_{J=J_0}^{\infty} \{J/(2J+1)\} I_d(n, \epsilon_0) \cdot (2J+1) \exp\{-BJ(J+1)/kT\}}{\sum_{J=0}^{\infty} (2J+1) \exp\{-BJ(J+1)/kT\}} \ . \qquad (5)$$

Here J_0 is the smallest rotational quantum number which satisfies $\epsilon_0 \geq 0$ at given E_n.

Figure 1 is a plot of the calculated quantity $I_{rot}(n)$ vs. E_n for the H^{**} + HF system. $I_d(n, \epsilon_0)$ was evaluated with the recent data on $dF_n(Q, \epsilon)/d\epsilon$ of the H atom[4] and molecular constants of HF given by Herzberg.[5] It should be noted that step-like structures appear at every binding energy that satisfies the relation $E_n = 2BJ(J = 1, 2, \ldots)$. This step comes from the fact that the polar molecule with rotational quantum number J can only ionize high Rydberg states with the binding energy $E_n \leq 2BJ$.

Chupka[6] has experimentally detected this step-like structure in Kr^{**} + HF and Kr^{**} + HCl systems. By mass spectroscopy he observed SF_6^- ions produced by photons of fixed wavelengths in mixtures of SF_6 and Kr. The partial pressure of Kr was about 2×10^{-4} Torr, and that of SF_6 was about 1×10^{-4} Torr. The SF_6^- ions result from the process

$$Kr^{**} + SF_6 \rightarrow Kr^+ + SF_6^- , \qquad (6)$$

where Kr^{**} denotes a Rydberg state of Kr excited by photons. When a small amount (corresponding to a partial pressure less than 10^{-5} Torr) of a dipolar gas, e.g., HF, is introduced, then there is a competition between process (6) and the process

$$Kr^{**} + HF(J) \rightarrow Kr^+ + e + HF(J') . \qquad (7)$$

In the experiment the electron resulting from process (7) is quickly accelerated by an applied electric field and is not captured by SF_6. Figure 2 shows the influence of HF on the SF_6^- production. The step-like structure occurs at photon wavelengths corresponding to the rotational states that begin to contribute to process (7), in agreement with the theoretical prediction (Figure 1). Figure 3 shows the similar effect of HCl.

There is some quantitative discrepancy between experiment and theory as to the n dependence in the interval between one step and another. This may be attributed to the simplified treatment, namely, the Born approximation with a point-dipole interaction for the rotational de-excitation of the polar molecule

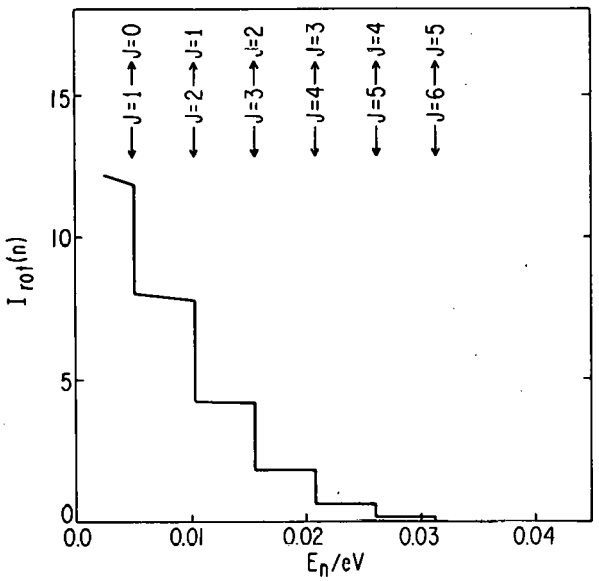

FIG. 1.--Step-like structure in the n dependence of the collisional ionization cross section for $H^{**} + HF$ system. The arrows denote the positions of $E_n = 2BJ(J=1,2,3,\ldots)$, where $2B = 0.00519$ eV. The rotational constant B of a HF molecule is adopted from Ref. 5.

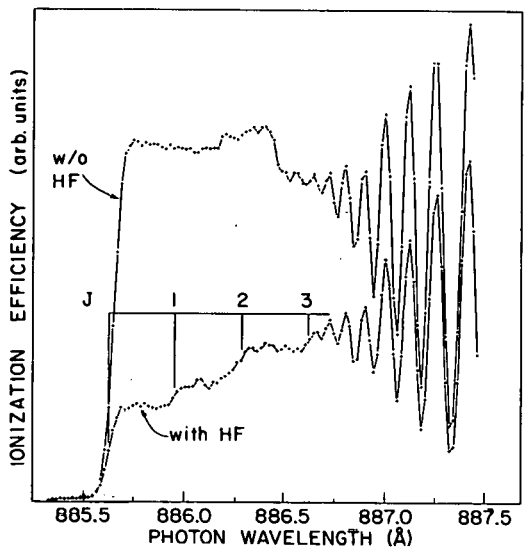

FIG. 2.--The number of SF_6^- ions produced in Kr-SF_6 mixtures with and without HF by photons of mixed wavelengths. (Courtesy of W. A. Chupka)

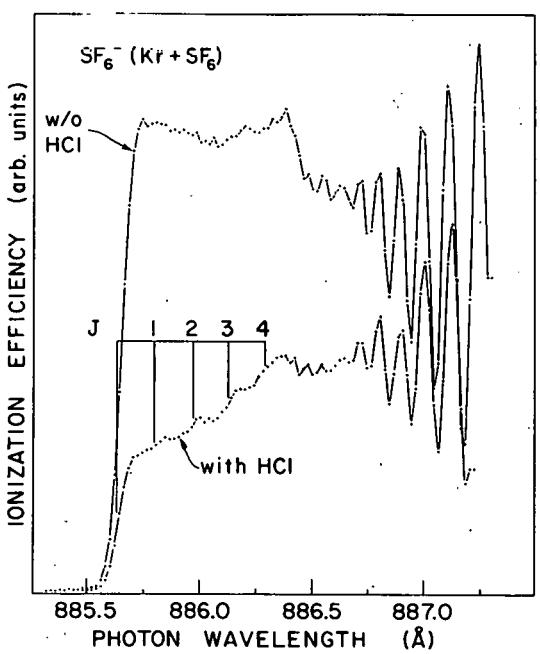

FIG. 3.--The number of SF_6^- ions produced in Kr-SF_6 mixtures with and without HCl by photons of fixed wavelengths. (Courtesy of W. A. Chupka)

by the electron impact (see also discussion in Ref. 3). I maintain that the detection of this step-like structure is clear-cut evidence for the proposed mechanism in the collisional ionization.

Acknowledgement

I wish to thank Dr. W. A. Chupka of the Physics Division for numerous discussions and especially for supplying Figures 2 and 3 prior to publication.

References

1. M. Matsuzawa, J. Chem. Phys. 55, 2685 (1971).
2. M. Matsuzawa. J. Chem. Phys. 58, 2679 (1973).
3. M. Matsuzawa. J. Electr. Spectry. 4, 1 (1974).
4. M. Matsuzawa. Phys. Rev. A 9, 241 (1974).
5. G. Herzberg. Molecular Spectra and Molecular Structure. I. Spectra of Diatomic Molecule. Van Nostrand, New York, 1950, 2nd ed., p. 536.
6. W. A. Chupka. Bull. Am. Phys. Soc. 19, 70 (1974).

IONIZATION OF A MERCURY ATOM BY COLLISION WITH AN EXCITED ARGON MOLECULE

Michio Matsuzawa*

The cross section for the ionization process $Ar_2^*(1250\ \mathring{A}) + Hg \rightarrow 2Ar + Hg^+ + e$ is evaluated by the use of data on the photoionization of a mercury atom and on the emission spectra of an excited argon molecule.

It is well known that a small amount of impurity greatly increases the ionization produced by charged particles in noble gases. This is called the Jesse effect[1] and is usually attributed to excitation transfer by a metastable noble-gas atom to an impurity. In He contaminated with a trace of Ar, the metastable helium atom He^m gives rise to ionization according to the process

$$He^m + Ar \rightarrow He + Ar^+ + e\ , \qquad (1)$$

which is usually known as Penning ionization. Recently, Hurst and coworkers[2] have investigated the Jesse effect in various noble gases contaminated with other gases, and pointed out that an atom A^* excited by optically allowed transitions and a molecule A_2^* also produce ionization by excitation transfer processes analogous to (1), namely,

$$A^* + B \rightarrow A + B^+ + e \qquad (2)$$

and

$$A_2^* + B \rightarrow 2A + B^+ + e\ . \qquad (3)$$

Recently Jesse[3] investigated the pressure effect of the W value in argon admixed with mercury and found that the kinetics were quite different from the results obtained with contaminants in He. This seems to suggest an important role of excited species other than the metastable atom.

For elucidation of this finding, we need the cross sections of processes (2) and (3). Actually, Process (2) has been theoretically treated by many authors so far.[4–6] The purpose of the present report is to evaluate theoretically the cross section for a particular example, (3),

*Visiting Scientist, October 1972–March 1974. Present address: The University of Electro-Communications, Chofu-shi, Tokyo.

$$Ar_2^*(1250\ \text{Å}) + Hg \rightarrow 2Ar + Hg^+ + e\ , \qquad (4)$$

which may be useful for the understanding of the result described in Ref. 3.

Katsuura's treatment[4] of process (2) with a slight modification yields the expression for the ionization cross section σ for process (3),

$$\sigma = 18.14\ [(\hbar v)^{-1} \int \mu_e^2(E)\mu_i^2(E)\, dE]^{2/5} \qquad (\text{in cm}^2)\ , \qquad (5)$$

where $\mu_i(E)$ and $\mu_e(E)$ are the dipole matrix elements for the photoionization

$$B + h\nu \rightarrow B^+ + e\ , \qquad (6)$$

and for the emission

$$A_2^* \rightarrow 2A + h\nu\ , \qquad (7)$$

respectively. Here $E = h\nu$ is the excitation energy in the photoionization (6), or the de-excitation energy in the emission process (7) and v is the velocity of relative motion. Expression (5) is derived under the following assumptions:

i) straight-line trajectory for the relative motion,

ii) rotating-atom approximation, and

iii) multipole expansion of the interaction between A_2^* and B.

Details of the derivation of the formula (5) are given in the Appendix.

The squared matrix element $\mu_i^2(E)$ for $Hg \rightarrow Hg^+ + e$ can be evaluated from the experimental data[7-9] on the photoionization of mercury using the relation

$$\sigma_{ph} = 4\pi^2 E(\hbar c)^{-1}\ \mu_i^2(E) \qquad (\text{in cm}^2)\ .$$

The data of Refs. 8 and 9, which report relative values, are normalized to the data of Ref. 7 at photon energy E = 11 eV. The consistency of these data is tested in Figure 1. Agreement among these data is not so good in the high energy region of the peak at E = 11 eV. The values of the curve tentatively drawn in Figure 1 are used for the evaluation of the ionization cross section.

The energy dependence of the squared matrix element $\mu_e^2(E)$ for Ar_2^* can also be evaluated from the data on the emission spectra of Figure 18 of Ref. 10. The structures at 1100 Å and 1300 Å are removed because these may come from other excited species. The absolute value of $\mu_e^2(E)$ can be deter-

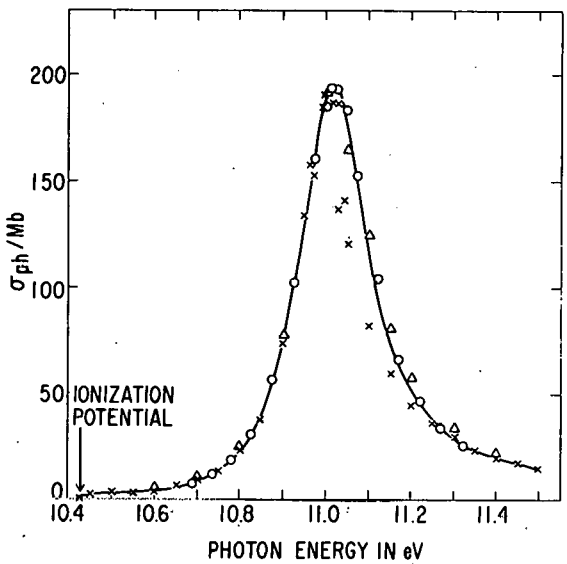

FIG. 1.--The photoionization cross section of σ_{ph} of mercury. The circles represent the data of Ref. 7, the crosses those of Ref. 8, and the triangles those of Ref. 9.

mined from the measurement of the emission lifetime τ. However, there is controversy about the measured absolute value of the lifetime of the 1250 Å emission of the excited argon molecule. Thornard and Hurts[11] obtained 2.8 μsec for this emission. There are two spectrally unresolvable molecular states ($^1\Sigma_u^+$, $^3\Sigma_u^+$), which decay independently to the molecular ground state ($^1\Sigma_g^+$). The authors of Ref. 12 contend that the 2.8-μsec lifetime is probably associated with the $^3\Sigma_u$ state of the excited argon molecule. Recently Koehler et al.[13] measured the lifetime of this emission and obtained 6 nsec for the $^1\Sigma_u^+ - {}^1\Sigma_g^+$ emission and 30 nsec for the $^3\Sigma_u^+ - {}^1\Sigma_g^+$ emission.

For the time being, we will employ the result of Ref. 11. Then there is a relation between τ and the optical oscillator-strength density $df/d\lambda$,

$$\frac{1}{\tau} = 6.670_2 \times 10^{15} \int \frac{1}{\lambda^2} \frac{df}{d\lambda} d\lambda \qquad (\lambda \text{ in Å}) ,$$

where $df/d\lambda$ is given in terms of the quantity $\phi(p,\lambda)$ measured in Ref. 10 as

$$df/d\lambda = N\lambda^2 \phi(p,\lambda) \qquad (\lambda \text{ in Å}) .$$

Here N is a normalization factor. The value $\tau = 2.8$ μsec gives $N = 2.91 \times 10^{-27}$. Then we get

$$|\mu_e(E)|^2 = 0.70 \times 10^{-32} \lambda^5 \phi(p,\lambda) \qquad (\text{in a.u.}) ,$$

where λ is measured in Å. The data obtained for $\mu_e^2(E)$ and $\mu_i^2(E)$ are shown in

Figure 2. Using these data, we get

$$\int \mu_i^2(E)\,\mu_e^2(E)\,dE = 0.460 \times 10^{-4} \qquad \text{(in a.u.)} .$$

For thermal velocity ($v = 1.35 \times 10^{-4}$ a.u. at 300°K), we have for process (4)

$$\sigma = 11.8 \text{ a.u.} \sim 3\ \mathring{A}^2 , \tag{8}$$

based on the result of Ref. 11. If we adopt the 6-nsec lifetime for the 1250 Å emission and use the same line profile, the calculated cross section should be multiplied by a factor of $(2.8 \times 10^3/6)^{2/5} \sim 12$. Then we get

$$\sigma = 137 \text{ a.u.} \sim 40\ \mathring{A}^2 . \tag{9}$$

Finally, we should make some comments on these final results. There is ambiguity about how the curves are drawn in Figure 1 and how the structures at 1100 Å and 1300 Å are removed from Figure 18 of Ref. 10. However, the final result is rather insensitive to this ambiguity because of power 2/5 in the expression (5). The assumption ii), namely the rotating-atom approximation, gives the cross section for process (2) only about 20% larger than that without this approximation.[6] This result may not be directly applied to process (4). However, the error from this approximation can be considered at most within a factor of two. It should be noted that assumptions i) and iii) can be well justified if the resulting cross section is found large. The value 3 $\mathring{A}^2$ of the cross section is not large, so that one suspects that this absolute value may not be highly reliable. In the calculation leading to $\sigma = 40\ \mathring{A}^2$, the assumptions

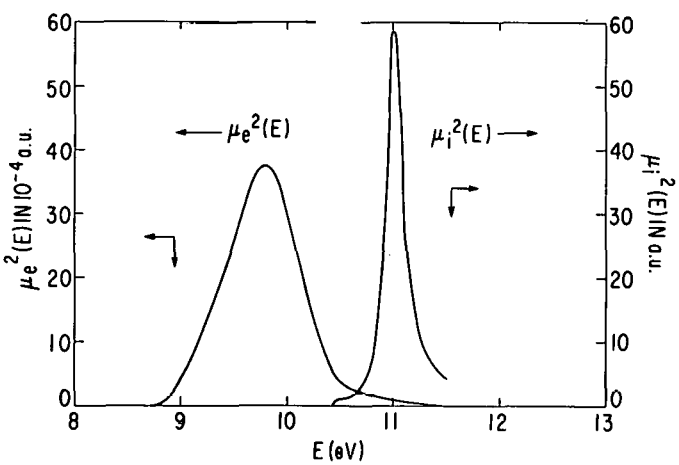

FIG. 2.--The dipole moments $\mu_i^2(E)$ and $\mu_e^2(E)$. The left-hand scale applies to $\mu_e^2(E)$, and the right-hand scale to $\mu_i^2(E)$. The scale of $\mu_c^2(E)$ is normalized to give the emission lifetime of 2.8 μsec.

i) and iii) become better satisfied, and the final result (9) is more reliable.

At present there seem to be no clear-cut grounds as to which values we should adopt for the lifetime of the 1250 Å emission. However, we cannot eliminate the possibility that there may exist different excited species in two experiments[11,13] because of different experimental conditions. For analysis of experiment on the Jesse effect, one should probably use the result (8) because of the similarity of the experimental conditions between Refs. 3 and 11.

APPENDIX

The initial state of the colliding system in process (3) is designated by the wavefunction ϕ, which is the product $\phi(A_2^* | \vec{r}_a)\, \phi(B | \vec{r}_b)$ of the eigenfunction of an excited molecule and that of the ground-state atom, where $\vec{r}_a$ and $\vec{r}_b$ represent the position vectors of the electrons. In the final state, the molecule A_2 is in the repulsive ground state and the atom B is excited to the continuum. Thus the wavefunction of the final state $\psi_{\epsilon E_d}$ is given by $\phi(2A | \vec{r}_a)\, \phi(B_+ + e | \vec{r}_b)$. Here ϵ and E_d are the energies of the ionized electron and of the dissociating motion of the atoms in the repulsive potential, respectively. We assume that these wavefunctions are real and orthonormalized as

$$\langle \phi | \phi \rangle = 1 ,$$

$$\langle \psi_{\epsilon E_d} | \psi_{\epsilon' E_d'} \rangle = \delta(\epsilon - \epsilon')\, \delta(E_d - E_d') ,$$

and

$$\langle \phi | \psi_{\epsilon E_d} \rangle = 0 .$$

Under assumptions i) and ii), one can write the total wavefunction ψ as follows

$$\psi = C_i(T)\, \phi \exp(-i E_i t/\hbar) + \iint d\epsilon\, dE_d\, C_f(\epsilon, E_d, t)\, \psi_{\epsilon, E_d} \exp(-i E_f t/\hbar) . \tag{A-1}$$

Here E_i and E_f are the total energies of the initial and final states. Substitution of this expression into the time-dependent Schrödinger equation gives the following set of coupled differential equations:

$$i\hbar v\, dCi/dx = \int dE_d \int d\epsilon\, C_f(\epsilon, E_d)\, \langle \phi | V | \psi_{\epsilon, E_d} \rangle \exp[-i(E_f - E_i)x/\hbar v] .$$

$$i\hbar v\, d\, C_f(\epsilon, E_d)/dx = C_i \langle \psi_{\epsilon, E_d} | V | \phi \rangle \exp[i(E_f - E_i)x/\hbar v] , \qquad \text{(A-2)}$$

where V is the interaction between the atom and the molecule. From assumption i) (straight-line trajectory), one may consider that the excited A_2 molecule or the center of mass of the dissociating molecule travels with constant speed v parallel to and at a distance R_0 from the x axis, while the atom B is located at the origin. Thus we have changed the variable t to x using the relation $x = vt$. Further, we have neglected $\langle \phi | V | \phi \rangle$ and $\langle \psi_{\epsilon, E_d} | V | \psi_{\epsilon, E_d} \rangle$ because they are short-ranged. The equations (A-2) with the initial condition $C_f(\epsilon, E_d) = 0$ at $-\infty$ yield

$$dCi(x)/dx = -(\hbar v)^{-2} \int d\epsilon \int dE_d \langle \phi | V(\vec{R}) | \psi_{\epsilon, E_d} \rangle \int_{-\infty}^{x} dx'\, C_i(x')$$

$$\times \langle \psi_{\epsilon, E_d} | V(\vec{R'}) | \phi \rangle \exp[-i(E_i - E_f)(x - x')/\hbar v] . \qquad \text{(A-3)}$$

Here $\vec{R}$ is the positive vector of A_2 relative to B, and one gets the relation $R^2 = R_0^2 + v^2 t^2$. The exponential function $\exp[-i(E_i - E_f)(x - x')/\hbar v]$ is a rapidly varying function except for $x \cong x'$. Thus the main contribution to the integral over x' comes from the region $x \sim x'$. Hence, we get

$$dCi(x)/dx \cong -\pi(\hbar v)^{-1} C_i(x) \int d\epsilon \int dE_d \left| \langle \phi | V(\vec{R}) | \psi_{\epsilon, E_d} \rangle \right|^2 \delta(E_i - E_f) . \qquad \text{(A-4)}$$

Here we have made use of the relation

$$\int_{-\infty}^{x} e^{-iy(x - x')} dx' = -i\, P(1/y) + \pi\delta(y) \qquad \text{(A-5)}$$

and neglected the energy dependence of $\langle \phi | V | \psi_{\epsilon, E_d} \rangle$. Thus the cross section for (3) is written as

$$\sigma = 2\pi \int_0^{\infty} P(R_0) R_0 dR_0 ,$$

where

$$P(R_0) = 1 - \exp\left\{\frac{-2\pi}{\hbar v}\int_{-\infty}^{\infty} dx \int d\epsilon \left|\langle\phi|V(R)|\psi_{\epsilon,E_d}\rangle\right|^2_{E_i=E_f}\right\} . \quad (A-6)$$

Here $P(R_0)$ is the probability of excitation transfer by collision of A_2^* with B at an impact parameter R_0.

If we make use of the multipole expansion of $V(\vec{R})$ (assumption iii) and retain only the leading term, namely, dipole-dipole interaction under assumption ii, we have

$$\langle\psi_{\epsilon,E_d}|V|\phi\rangle = -2\mu_e(E_d)\mu_i(\epsilon)R^{-3} . \quad (A-7)$$

Thus we get the expression for process (3)

$$\upsilon = 18.14\,[(\hbar v)^{-1}\int d\epsilon\,\mu_e^2(E_d)\mu_i^2(\epsilon)\big|_{E_i=E_f}]^{2/5} . \quad (A-8)$$

The initial and final state energies E_i and E_f are given by

$$E_i = E_{A_2^*}$$

and

$$E_f = \epsilon + E_d + I_B ,$$

where $E_{A_2^*}$ is the excitation energy relative to A+A, I_B is the ionization potential of the atom B relative to the ground state. Thus the condition $E_i = E_f$ yields

$$E = E_{A_2^*} - E_d = I + \epsilon .$$

The energy E can be interpreted as the transition energy in the photoionization (6) or in the emission (7). Hence, the change of variable ϵ to E gives the final expression (5) for the collisional ionization (3) in the text.

References

1. W. P. Jesse and J. Sadauskis. Phys. Rev. 100, 160 (1954).
2. J. E. Parks, G. S. Hurst, T. E. Stewart, and H. L. Weidner. J. Chem. Phys. 57, 5467 (1972).
3. W. P. Jesse. Final Report of Research on the Ionization of Gases and the Average Energy to Make an Ion Pair. Submitted to the Chicago Operations Office, U.S. Atomic Energy Commission on contract AT(11-1)-329 (1972). Unpublished.

4. K. Katsuura. J. Chem. Phys. 42, 3771 (1965).
5. T. Watanabe and K. Katsuura. J. Chem. Phys. 47, 800 (1967).
6. T. Watanabe. Radiation Chemistry II, Advances in Chemistry Series No. 82, Ed. R. F. Gould. Am. Chem. Soc., Washington, D.C., 1963, p. 176.
7. R. Lincke and B. Streddle. Z. Physik 238, 168 (1970).
8. J. Berkowitz and C. Lifshitz. J. Phys. B 1, 439 (1968).
9. B. Brehm. Naturforsch. 21a, 196 (1966).
10. T. E. Stewart, G. S. Hurst, T. E. Bortner, J. E. Parks, F. W. Martin, and H. L. Weinder. J. Opt. Soc. Am. 60, 1290 (1970).
11. N. Thornard and G. S. Hurst. Phys. Rev. A 5, 1110 (1973).
12. D. C. Lorents and R. E. Olson. Excimer Formation and Decay Processes in Rare Gases, Stanford Research Institute Semiannual Technical Report No. 1. Unpublished.
13. H. A. Koehler, L. J. Ferderber, D. L. Redhead, and P. J. Ebert. Phys. Rev. A 9, 768 (1974).

SPECTRAL PROPERTIES OF ATOMIC IONS: A NEW PROJECT

J. W. Cooper,* J. L. Dehmer, U. Fano,† Mitio Inokuti, Yong-Ki Kim, S. T. Manson,‡ and C. E. Theodosiou§

We have initiated an attempt at elucidation of the systematics of the spectra of atomic ions, including highly stripped ions.

Our new collaborative efforts aim at a theoretical survey of basic spectral data, e.g., energy levels and oscillator strengths of atomic positive ions in general. With the advent of intense heavy-ion accelerators and of the beam-foil spectroscopy, analyses of those spectral data now form a new branch of basic radiation physics. Furthermore, the physics of some highly stripped ions plays an important role in controlled thermonuclear research, specifically in plasma diagnostics and in the understanding of atomic contamination of plasmas.

Our extensive experience in theoretical spectroscopy of neutral atoms leads us to stress the following two points of view.

a) Extensive and diverse observable data can be usefully represented in terms of limited sets of physically significant numerical parameters (e.g., phaseshifts, oscillator strength densities, amplitude ratios of wavefunctions at the nucleus and at infinity). The variation of such parameters along the periodic system and along isoelectronic sequences generally lends itself to easy and instructive mapping.

b) "Relativistic" effects — often understood as the differences of computational results based on Dirac and Schroedinger equations, respectively — can be usefully resolved into contributions of separate physical effects which

*National Bureau of Standards, Washington, D.C. 20234.

†Department of Physics, The University of Chicago, Chicago, Illinois 60637 Appointee, Faculty Research Participation Program, Center for Educational Affairs, Argonne National Laboratory.

‡Department of Physics, Georgia State University, Atlanta, Georgia 30303. Consultant, RER Division, Argonne National Laboratory.

§Department of Physics, The University of Chicago, Chicago, Illinois 60637.

correspond, e.g., to different terms in the Pauli approximation of the relativistic equation. Such are the spin-orbit interactions and the influence of the kinetic energy term $p^4/8m^3c^2$, where p is the electron momentum, m is the electron mass, and c is the light speed. Each of these effects can then be studied from the point of view of a). A limitation to the above picture arises because the effects of relativity on different electrons do not remain independent but must be evaluated self-consistently;[1] one of the initial tasks will be to extend our approach to this phenomenon.

Our idea now is to consider the practical applicability of these points of view to an estimation of relevant characteristics of the unknown spectra of highly stripped ions. More specifically, we should estimate values and trends of the few most important parameters throughout the periodic system, and then see how dependably one can interpolate further values, and predict from them the spectral data of practical interest.

Initial tasks would probably include:

1) Mapping of zero-energy phaseshifts over the whole "surface" (Z,σ) (Z = atomic number, σ = order of the spectrum). These parameters yield, among other things, the order in which subshells are filled. The Z dependence alone has been studied[2,3] for $\sigma = 1$.

2) (Z,σ) mapping of phaseshift splits due to spin-orbit interactions. This mapping has been done[4] for $\sigma = 1$ only.

3) (Z,σ) mapping of the effect of $p^4/8m^3c^2$, extending the recent work[5] which was also limited to $\sigma = 1$ only.

A considerable share of our early activities should consist of analyzing, interpreting, and correlating data already available from various sources. For example, we should examine the scaling properties, if any, of the ionization potentials tabulated by Kelly and Harrison[6] for all (Z,σ) with $Z \leq 36$.

References

1. Yong-Ki Kim and J. P. Desclaux. Paper 43 this report.
2. S. T. Manson. Phys. Rev. 182, 97 (1969).
3. J. L. Dehmer and R. P. Saxon. Argonne National Laboratory Radiological and Environmental Research Division Annual Report, July 1973–

June 1974. ANL-8060, Part I, p. 102.
4. J. L. Dehmer. Phys. Rev. A 7, 4 (1973).
5. U. Fano, C. E. Theodosiou, and J. L. Dehmer. Paper 42 this report.
6. R. L. Kelly and D. E. Harrison, Jr. Atomic Data 3, 177 (1971).

ELECTRON OPTICS OF ATOMIC FIELDS*

U. Fano,† C. E. Theodosiou,† and J. L. Dehmer

We present a unified discussion and illustrations of the electron-optical aspect of electron penetration into, or escape from, the inner region of atoms. Both processes may focus or defocus the amplitudes of wavefunctions and shift their phases, as manifested in countless phenomena ranging from level shifts to β-decay rates. A background survey begins by discussing the Fermi-Segrè formula for hyperfine splittings and emphasizes the interplay of hydrogenic and WKB approximations. The phase-amplitude method, which determines amplitude ratios and phase shifts directly, proves useful for interpreting the systematics of these parameters along the periodic system. Survey calculations have been carried out throughout the periodic system using Hartree-Slater potential fields of: a) $\alpha_\ell(0)/\alpha_\ell(\infty)$, the ratio of the wavefunction's amplitude at r = 0 to that outside the atom (Figure 1); b) $d\,\delta_\ell/dE\,|_{E=0}$, the energy derivative of the phase shift at E = 0 (Figure 2); c) The $\delta_\ell(E=0)$ and $\alpha_\ell(0)/\alpha_\ell(\infty)$ induced by either a unit perturbation localized near r = 0 or a relativistic correction. The paper provides only general discussions and rather crude solutions, intended to serve purposes of orientation in surveying problems and in checking results, while standard methods

*Summary of paper to be submitted for publication. Part of this work was presented at the Chicago Meeting of the Division of Electron and Atomic Physics, American Physical Society, December 2–4, 1974.

†Department of Physics, The University of Chicago, Chicago, Illinois 60637.

seem preferable for working out specific applications accurately.

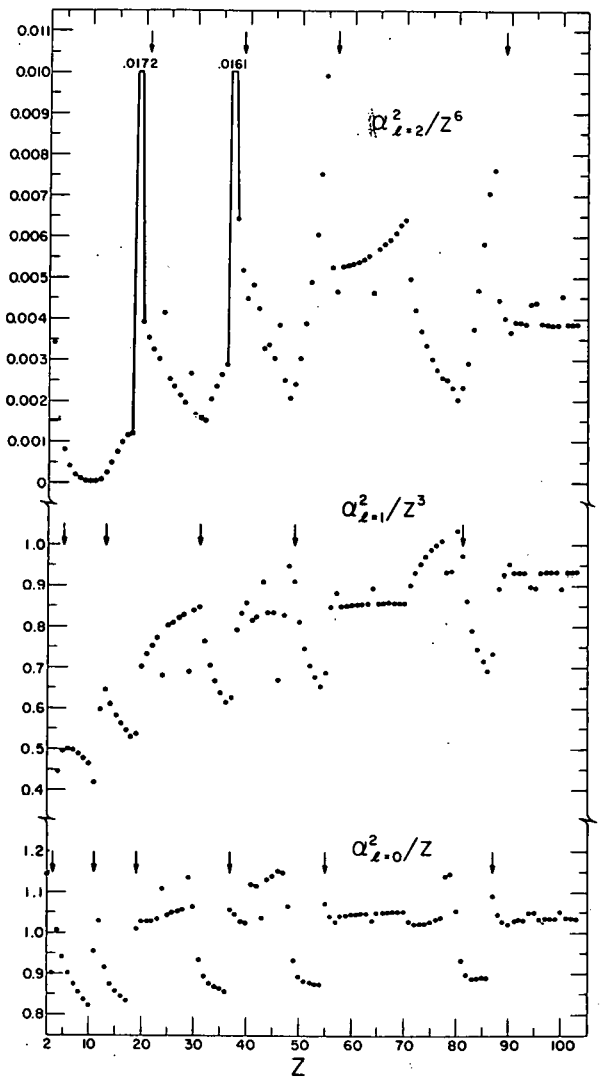

FIG. 1.--Reduced values of the amplitude function α^2_ℓ at r = 0 as a function of atomic number Z.

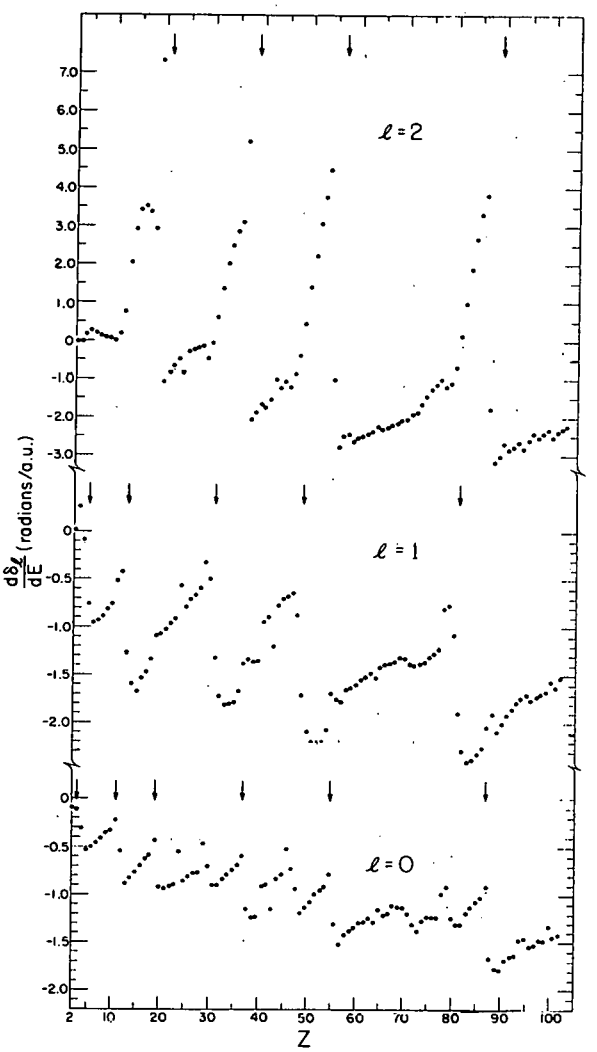

FIG. 2.--Energy derivative of the asymptotic phase shift $d\delta_\ell/dE$ at E = 0 as a function of atomic number Z.

RELATIVISTIC EFFECTS IN OUTER SHELLS OF ATOMS*

Yong-Ki Kim and J. P. Desclaux†

The contraction of the inner orbitals due to relativistic effects changes the outer orbitals through the self-consistency requirements of the atomic field. The relativistic $\langle r \rangle$ for the 6s orbitals of Hg and Au are ~15% smaller than the nonrelativistic results, whereas the relativistic $\langle r \rangle$ for the 5d orbitals are ~3% larger. Consequently, the f values calculated from the relativistic wavefunctions show a substantial departure from the nonrelativistic values. For instance, the f values for the resonance transitions of Hg are:

Transition	Experiment[1]	Nonrelativistic Hartree-Fock	Relativistic Hartree-Fock
$6^1S_0 \rightarrow 6^1P_1$	1.11 ± 0.10	3.03	1.99

The introduction of a limited configuration interaction in the outer shells reduces the relativistic f value to 1.53

Reference

1. A. Skerbele and E. N. Lassettre. J. Chem. Phys. 53, 2708 (1970).

*Abstract of a paper to be presented at the Annual Meeting of the Division of Electron and Atomic Physics, American Physical Society, Chicago, 2–4 December 1974.

†Institut Max von Laue-Paul Langevin, Grenoble, France.

STANDING-WAVE MODIFICATION OF REGGE TRAJECTORIES AND ITS APPLICATION TO ATOM-ATOM AND ION-ATOM SCATTERING AT THERMAL ENERGIES*

Smio Tani† and Mitio Inokuti

We consider the global behavior of the phase shift $\delta(k,\ell)$ as a function of linear momentum k and angular momentum ℓ. The loci of points at which $\delta(k,\ell) = \pi/2 \pmod{\pi}$ represent essential features of an interaction potential. In a series of examples, we illustrate close relations of these loci to 1) the strength of the interaction potential, 2) the presence of glory undulation in the total cross section, 3) the orbiting effect due to penetration through the centrifugal barrier at low energies, and 4) the domain in which semiclassical approximations are valid. On certain theoretical grounds, one may consider this new method to be a standing-wave modification of the direct-channel Regge trajectory approach. An application to the $He-Li^+$ scattering is presented (see Figure 1). The data are based on the Sutherland potential defined in our earlier work.(1) Each contour is labeled with an integer n. Positive-n contours are looped and chiefly characterize the attractive part of the interaction potential; in contrast, negative-n contours extend to infinity and chiefly characterize the repulsive part. The broken curve shows where the energy becomes equal to the height of the centrifugal barrier. Notice the close approach of the contours with n = 1 and 2, for example, reminiscent of an avoided crossing of molecular terms. In the vicinity of such a region, the phase shift $\delta(k,\ell)$ changes by π either as a function of k for fixed ℓ (a resonance) or as a function of ℓ for fixed k, and therefore may bring about a structure in the scattering cross section.

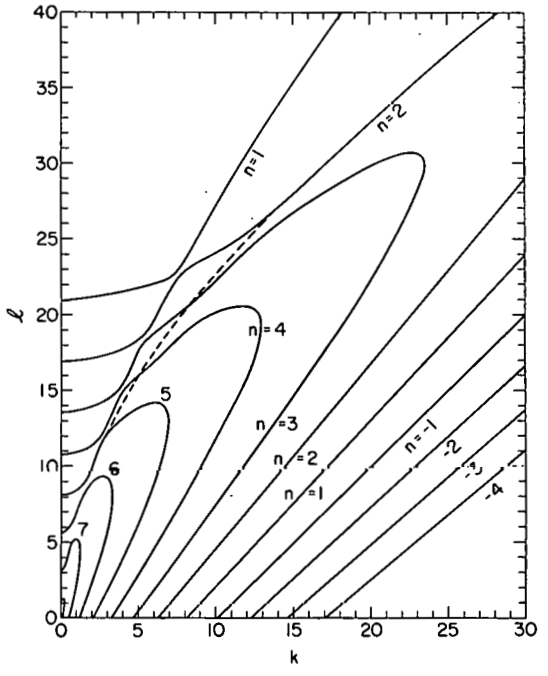

FIG. 1.--The loci of points at which $\delta(k,\ell) = \pi/2 \pmod{\pi}$ for the $He-Li^+$ scattering.

Reference

1. S. Tani and M. Inokuti. J. Chem. Phys. 54, 2265 (1971).

*Summary of a paper published in J. Chem. Phys. 61, 4422 (1974).

†Physics Department, Marquette University, Milwaukee, Wisconsin 53233. Consultant, RER Division, Argonne National Laboratory.

LOW-ENERGY PHASE SHIFTS IN THE SUTHERLAND MODEL FOR THE Li SCATTERING

Venkata S. Krishna* and Smio Tani*†

We present some numerical results that illustrate effects of barrier penetration and orbiting.

We investigated the low-energy phase shifts in the Li^+-He scattering, using a Sutherland-model potential. The loci of points where the phase shift is equal to $\pi/2$ (mod π) have been plotted in Figure 1 of the preceding article.[1] We noticed characteristic patterns of the trajectories at several points, e.g., at about k = 8 and $\ell = 23$.

It is important to understand the meaning of such a pattern and to know how it influences the cross sections. We have calculated both the quantal and the WKB (semiclassical) phase shifts in the vicinity of such a pattern. The results for linear momentum k = 8 and k = 9 are shown in Figures 1 and 2. The classical deflection angles Θ are also shown in the lower part of each graph.

An orbiting[2] occurs when the value of energy is equal to the height of the centrifugal barrier. The loci of such values of ℓ and k were shown by a broken line in Figure 1 of the preceding paper.[1] For k = 8, this occurs at $\ell_0 = 20.28$, and the quantal phase shift makes an abrupt change by an amount nearly equal to π. For k = 9 the classical orbiting occurs at $\ell_0 = 21.54$, but an abrupt change in quantal phase shift is absent there.

Another abrupt change in the phase shift occurs slightly below $\ell = 23$ for k = 8, and slightly above $\ell = 23$ for k = 9. Such an abrupt change should be associated with the first mentioned characteristic pattern. When the phase shift is plotted as a function of k for fixed ℓ, a sharp resonance will be revealed as a sharp rise of the phase shift in a narrow interval. When the phase shift is plotted as a function of ℓ for fixed k (as is done in Figures 1 and 2), it is

*Physics Department, Marquette University, Milwaukee, Wisconsin 53233.
†Consultant, RER Division, Argonne National Laboratory.

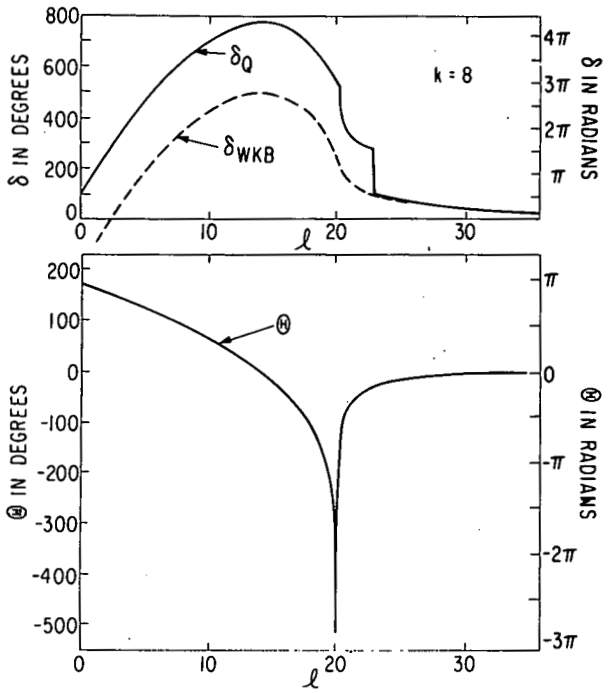

FIG. 1.--Phase shift δ and classical deflection angle Θ for k = 8 plotted against ℓ. The solid curve labeled δ_Q represents the quantal phase shift, and the broken curve δ_{WKB} represents the WKB phase shift.

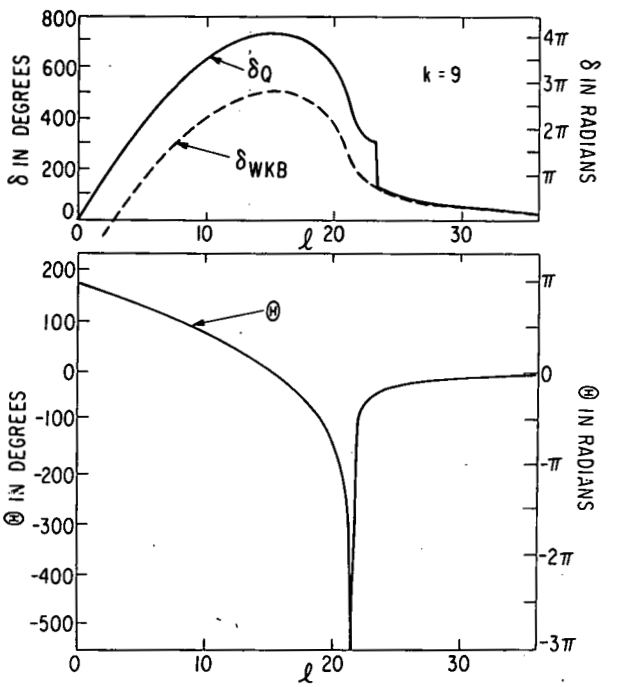

FIG. 2.--Phase shift δ and classical deflection angle Θ for k = 9 plotted against ℓ. The solid curve labeled δ_Q represents the quantal phase shift, and the broken curve δ_{WKB} phase shift.

likely that sharp resonance will be revealed as a sharp drop of the phase shift.

If the drop of the phase shift is infinitely sharp and exactly equal to π, it will cause no change in the cross sections. Since this is not precisely the case, there will be some influence on the cross sections. Thus it is interesting to compare differential cross sections derived from the quantal and classical phase shifts.

References

1. S. Tani and M. Inokuti. Standing-Wave Modification of Regge Trajectories and Its Application to Atom-Atom and Ion-Atom Scattering of Thermal Energies. This report.
2. K. W. Ford and J. A. Wheeler. Ann. Phys. (N.Y.) 7, 259 (1959).

SEARCH FOR LONG-LIVED DOUBLY-CHARGED NEGATIVE IONS

W. A. Chupka,* David Spence, and C. M. Stevens†

In recent years there have been three experiments[1-3] reported which purport to have detected long-lived ($\geq 10^{-5}$ sec) doubly-charged negative ions in free space. In all of these experiments, two of which use an electron bombardment source[1,3] and the third[2] a Penning ionization source, the results are open to the criticism in that the observed ion peaks may be experimental artifacts.[4] In view of the fundamental importance of the possible existence of long-lived double-charged negative ions and of their practical application (e.g., in high-energy accelerators), we have attempted to verify the existence of such ions. We have used a 100" radius double-focusing mass spectrometer of such a design that artifact peaks (caused, for example, by collisional dissociation of a diatomic ion into an atomic ion plus neutral), cannot occur. We have repeated the electron-impact experiments over a range of pressures and electron currents which spans the two earlier experiments[1,3] for the gaseous targets I_2, HI, CF_3Cl, CH_3I, and mixtures of H_2 plus I_2. We find no evidence of any doubly-charged atomic halogen ions. Whereas earlier experiments[1,3] claimed values of doubly-charged/singly-charged species ($x^{=}/x^{-}$) of 10^{-1} to 10^{-2}, we set lower limits of $x^{=}/x^{-}$ of $< 10^{-11}$.

Changes have been made in our Penning ion source which should allow us to duplicate the pressures and elements of the earlier experiments.[2] However, it seems very likely that the earlier reports of long-lived double-charged negative ions produced by electron impact are in error. Our conditions of flight time and electric field strength in the source region do not differ sufficiently from those of the earlier electron-impact work to offer a plausible explanation for our lack of observation of doubly-charged negative ions.

*Physics Division, Argonne National Laboratory.

†Chemistry Division, Argonne National Laboratory.

The only positive result of our experiments was the detection of the negative ion HI^- from our Penning ionization source. This ion has not previously been observed.

References

1. W. K. Stuckey and R. W. Kiser. Nature 211, 963 (1960).
2. H. Baumann, E. Heinicke, H. J. Kaiser, and K. Bethge. Nucl. Instr. Methods 95, 389 (1971).
3. J. E. Ahnell and W. S. Koski. Nature 245, 30 (1973).
4. J. H. Fremlin. Nature 211, 1453 (1966).

CALCULATION OF RELATIVE RATES FOR NEUTRAL AND IONIC INHIBITION IN HYDROCARBON FLAMES*

David Spence and E. T. McHale†

In a previous report[1] it was suggested on purely qualitative grounds that inhibition of hydrocarbon flames by lanogenated hydrocarbons was predominantly of an ionic nature. Putting these arguments on a quantitative basis forces us to rewrite this conclusion.

Many halogenated organic compounds exhibit a chemical inhibiting effect on hydrocarbon flames. Most mechanisms for the inhibition of such flames involve only neutral species, although several authors have been concerned with the possible role played by negative ions in the inhibition process.[2–4] The most comprehensive semiquantitative description of the possible role of ions in flame inhibition by halogenated hydrocarbons is that given by Mills.[4] In this model, the halogenated hydrocarbon undergoes dissociative electron attachment to form a negative halogen ion and a free radical, a typical such reaction being $e + CF_3Br \rightarrow Br^- + CF_3$. Mills proposed that the negative ion and/or free radical so formed then reacts with flame-free radicals O, OH, and/or H in reactions of the type $CF_3 + H \rightarrow CF_3H$ (recombination) and $Br^- + H \rightarrow HBr + e^-$ (associative electron detachment). The ionic inhibition mechanism is thus:

$$RX + e \xrightarrow{k_1} X^- + R \qquad \text{(dissociative attachment)} \qquad (1)$$

$$X^- + H \xrightarrow{k_2} HX + e \qquad \text{(associative detachment)}\ , \qquad (2)$$

where X^- is a halogen ion and R is a radical.

Mills, however, was unable to give convincing quantitative arguments in support of this model. Reaction-kinetic calculations, based on experimental data from Ref. 5 and other studies, are presented which support the case that

---

*A full account of this work will appear in Combustion and Flame.

†Atlantic Research Corporation, Alexandria, Virginia 22314.

an ionic inhibition mechanism cannot compete with neutral inhibition processes of the type

$$RX + H \xrightarrow{k_3} R + HX \qquad (3)$$

at electron densities found in flames. The calculations are based on the assumption that removal of H atoms is sufficient to effect flame inhibition.

Data are available which allow a comparison of the rates of the coupled ionic reactions (1) and (2) with the direct neutral inhibition step (3). Considering first reaction (2), from the known binding energies[6] of the molecules XOH and XO and the electron affinities[7] of X, we can calculate that the activation energies for the reactions $X^- + OH(O) \rightarrow XOH(XO) + e$ are much too high for these to be significant at the temperatures of interest, being typically 1.5 to 2 eV.

In the case of $X^- + H$, the rate constant k_2 for associative detachment will have no exponential term and may be given[8] approximately by

$$k_2 = 2\pi e(\alpha/\mu)^{\frac{1}{2}} , \qquad (4)$$

where e is the electronic charge, α is the polarizability of the H atom, and μ is the reduced mass of the $H + X^-$ system. This rate, known as the polarization rate constant, yields values of k_2 of approximately 2.0×10^{-9} cm^3 sec^{-1} and is virtually the same for all species of X^-. The reactions $Cl^- + H \rightarrow HCl + e$ and $F^- + H \rightarrow HF + e$ have been studied experimentally at room temperature by Fehsenfeld et al.[9] using a flowing afterglow. The measured specific reaction rates are $1.0 (\pm 0.2) \times 10^{-9}$ cm^3 sec^{-1} and $1.6 (\pm 0.2) \times 10^{-9}$ cm^3 sec^{-1}, respectively, very close to the polarization rate constant. Although these measurements were taken at room temperature, Herzenberg[10] has shown that associative detachment rates will be insensitive to a temperature below several thousand degrees K.

The rate of reaction (1) is governed by the steady-state electron density in a flame. Using Eqs. (1) and (2), and making the assumption that under inhibited conditions, the concentration of X^- is in steady state

$$-\frac{d[X^-]}{dt} = 0 = k_1[RX][e^-] - k_2[X^-][H] \qquad (5)$$

and

$$[e^-] = \frac{k_2[H]\,[X^-]}{k_1[RX]} \quad . \tag{6}$$

Consider as a numerical example the case of 1% of CF_3Br inhibiting an atmospheric pressure CH_4-air flame. Using measured values of the cross section for negative ion production in CF_3Br at 1200°K from Ref. 5, we can calculate k_1 from

$$k_1 = \sigma\hat{v}\,N \text{ cc/mol sec} \quad , \tag{7}$$

where $\sigma = 9.8 \times 10^{-15}$ cm^2, $\hat{v} = 1.9 \times 10^7$ cm/sec is the average velocity of an electron at 1200°K, and N is Avogadro's number. Estimates of the value of [H] in a methane-air flame can be obtained from the data of Fenimore and Jones[11] and yield values between $\approx 5 \times 10^{14}$ and $\approx 5 \times 10^{16}$ atoms/cc, depending on whether the flame is lean or rich. For a stoichiometric mixture, $[H] \approx 5 \times 10^{15}$ atoms/cc, a value of $k_2 = 1.2 \times 10^{15}$ cm^3/mol sec, cited earlier, is taken. Inserting these values into Eq. (6) yields

$$[e^-] = 10^{-3}\,[X^-] \quad . \tag{8}$$

Since the total concentration of negative charges in a flame is equal to the concentration of positive ions, the electron concentration in an inhibited flame is reduced to about one-thousandth of the positive ion concentration. The concentration of positive ions in a stoichiometric methane-air flame at 1 atmosphere is about 5×10^{11} ions/cc,[12] and hence, in an inhibited flame the electron concentration is about 5×10^8 electrons/cc.

We can now compare the effectiveness of inhibition by an ionic mechanism to that by a neutral route by examining the ratio of the rates for reactions (1) and (3):

$$\frac{\text{Rate (3)}}{\text{Rate (1)}} = \frac{k_3[H]}{k_1[e^-]} \quad , \tag{9}$$

where $[e^-]$ is the electron density in the inhibited flame determined above and the measured k_3 is $10^{15.64}\exp(-17{,}450/RT)$ cc/mol sec.[13]

For CF_3Br inhibiting an atmospheric pressure, methane-air flame we find at 1200°K

$$\frac{\text{Rate (3)}}{\text{Rate (1)}} = 3 \times 10^2 \ . \qquad (10)$$

It is clear that in this case the ionic mechanism is insignificant compared to the neutral mechanism in the inhibition process. Similar calculations for the comparatively poor inhibitor SF_6, where attachment cross sections are very high and neutral reaction rates rather slow, (and must be regarded as the limiting case for the maximum effect of ionic inhibition), show that the ratio of rate (3) to rate (1) is 7:1. It should be noted, however, that SF_6 is generally not regarded as a chemical inhibitor, since its effect on flames can be accounted for by its physical action alone.

The assumption, mentioned earlier, that removal of H atoms causes flame inhibition, is generally accepted. (This does not exclude the possibility that direct removal of other species, e.g., O or OH, also occurs in inhibited flames.) While the present study does not prove or disprove this assumption, it can be pointed out that reaction (3) is competitive with the branching reaction

$$H + O_2 \xrightarrow{k_{10}} OH + O \ . \qquad (11)$$

The rate coefficient of the latter is $10^{14.35} \exp(-16{,}800/RT)$ cc/mol sec.[14] The ratio of reaction (3) to (11) is 1200°K and 1% CF_3Br addition is thus computed to be

$$\frac{\text{Rate (3)}}{\text{Rate (11)}} = 0.76 \ . \qquad (12)$$

At the 1% level, CF_3Br would only produce moderate inhibition of a CH_4-air flame. At the 5% level, where extinguishment occurs, the ration of rate (3) to rate (11) is 3.8 .

The foregoing calculations suggest that ions play no significant role in inhibiting flames. The numerical estimates clearly establish that neutral inhibition reactions are far more important than ionic processes.

References

1. D. Spence. Argonne National Laboratory Radiological and Environmental Research Division Annual Report, July 1972–June 1973. ANL-8060, Part I, p. 222.
2. E. C. Creitz. J. Res. Nat. Bur. Stand. 65A, 389 (1961).
3. T. J. Lee. J. Phys. Chem. 67, 360 (1963).
4. R. M. Mills. Combustion and Flame 12, 513 (1968).
5. D. Spence and G. J. Schulz. J. Chem. Phys. 58, 1800 (1973).
6. Joint Army-Navy-Air Force Thermochemical Tables, 2nd Ed., NRDS-NBS No. 37 (1971).
7. R. S. Berry and C. W. Reimann. J. Chem. Phys. 38, 1540 (1963).
8. E. E. Ferguson. Advances Electronics Electron Phys. 24, 1 (1968).
9. F. C. Fehsenfeld, C. J. Howard, and E. E. Ferguson. J. Chem. Phys. 58, 5841 (1973).
10. A. Herzenberg. Phys. Rev. 160, 806 (1967).
11. C. P. Fenimore and G. W. Jones. J. Phys. Chem. 65, 2200 (1961).
12. H. F. Calcote. Proc. 8th Int. Symp. on Combustion. Williams and Wilkins, Baltimore, 1962, p. 184.
13. A. G. Trotman-Dickenson and G. S. Milne. Table of Biomolecular Gas Reactions. NSRDS-NBS No. 9 (1967), p. 12.
14. D. L. Baulch, D. D. Drysdale, and A. C. Lloyd. High Temperature Reaction Rate Data, Vol. 3. The University, Leeds, England, April 1969.

PUBLICATIONS BY THE STAFF OF THE RADIATION PHYSICS SECTION FOR THE PERIOD JULY 1973 THROUGH JUNE 1974

Major Papers

J. Berkowitz, J. L. Dehmer, K. Shimada, and M. Szwarc. Photoelectron Spectroscopic Studies of (α-Naphthyl)-$(CH_2)_4$-(α-Naphthyl) Vapor: Open Chain or Cyclic Conformation? J. Electron Spectry. 2, 211–214 (1973).

J. Berkowitz, J. L. Dehmer, and T. E. H. Walker. PES of High Temperature Vapors. IV. The Cesium Halides. Effect of Spin-Orbit Interaction on the Photoelectron and Mass Spectra of Alkali Halides. J. Chem. Phys. 59, 3645–3653 (1973).

J. Berkowitz, J. L. Dehmer, K. Shimada, and M. Szwarc. Addendum to Photoelectron Spectroscopic Studies of (α-Naphthyl)-$(CH_2)_4$-(α-Naphthyl) Vapor: Open Chain or Cyclic Conformation? J. Electron Spectry. 3, 164–165 (1974).

J. Berkowitz, J. L. Dehmer, and T. E. H. Waber. On the Photoelectron Spectra of Alkali Halide Vapors. J. Electron Spectry. 3, 323–325 (1974).

R. H. Huebner, R. J. Celotta, S. R. Mielczarek, and C. E. Kuyatt. Electron Energy-Loss Spectroscopy of Acetone Vapor. J. Chem. Phys. 59, 5434–5443 (1973).

R. H. Huebner, W. F. Frey, and R. N. Compton. Threshold Electron Excitation of Azulene. Chem. Phys. Letters 23, 587–591 (1973).

Shobu Kaneko and Mitio Inokuti. Atomic Polarizability. Butsuri (Bull. Phys. Soc. Japan) 28, 825–835 (1973). Published in Japanese.

Shobu Kaneko and Mitio Inokuti. Effects of Error in the Unperturbed Wavefunction on Electric Polarizabilities and Shielding Factors of Atoms. Chem. Phys. Letters 23, 275–277 (1973).

Yong-Ki Kim and P. S. Bagus. Generalized Oscillator Strengths for the Resonance Transitions in Alkaline-Earth Atoms. Phys. Rev. A 8, 1739–1747 (1973).

Yong-Ki Kim. Comments on the Distorted-Wave Born-Approximation Cross Sections for the 2^1P Excitation of He. Phys. Rev. A 9, 1462–1464 (1974).

Michio Matsuzawa. Form Factors of the Hydrogen Atom in Excited States. Phys. Rev. A 9, 241–250 (1974).

Michio Matsuzawa. Ionization of Long-Lived Highly Excited Atoms by Collision with Molecules. II. J. Electron Spectry. 4, 1–12 (1974).

P. Pyykkö, E. Pajanne, and Mitio Inokuti. Hydrogen-Like Relativistic Corrections for Electric and Magnetic Hyperfine Integrals. Int. J. Quantum Chem. 7, 785–806 (1973).

David Spence and G. J. Schulz. Cross Sections for Production of O_2^- and C^- by Dissociative Electron Attachment in CO_2: An Observation of the Renner-Teller Effect. J. Chem. Phys. 60, 216–220 (1974).

David Spence. Core Excited Resonances in Hydrogen. J. Phys. B. Atomic Mol. Phys. 7, L87–90 (1974).

Smio Tani and Mitio Inokuti. Modification of the Variation-of-Parameters Method and Integration of the Schroedinger Equation. J. Comput. Phys. 11, 409–422 (1973).

T. E. H. Walker, J. Berkowitz, J. L. Dehmer, and J. T. Waber. Nonstatistical Ratios of Photoionization Cross Sections for States Split by Spin-Orbit Coupling. Phys. Rev. Letters 31, 678–681 (1973).

Abstracts of Conference Papers

J. Berkowitz, J. L. Dehmer, Y.-K. Kim, and J. P. Desclaux. Valence Shell Excitation Accompanying Photoionization in Hg. Bull. Am. Phys. Soc. 19, 82–83 (1974).

J. Berkowitz, Mitio Inokuti, and J. C. Person. Dipole Strengths for Ionization of Molecules. Comparison of High-Energy Electron-Impact Data with Photoabsorption Data. 8th Int. Conf. on Physics of Electronic and Atomic Collisions, Belgrade, Yugoslavia, July 16–20, 1973. Abstracts of Papers, pp. 561–562.

J. L. Dehmer, J. Berkowitz, and Yong-Ki Kim. $^2D_{5/2}$:$^2D_{3/2}$ Branching Ratios for Zn, Cd, and Hg at 584 Å. 8th Int. Conf. on Physics of Electronic and Atomic Collisions, Belgrade, Yugoslavia, July 16–20, 1973. Abstracts of Papers, pp. 555–556.

J. L. Dehmer, Mitio Inokuti, and R. P. Saxon. Systematics of Partial Dipole Oscillator-Strength Distributions and their Moments for Atoms of the First and Second Row. 8th Int. Conf. on Physics of Electronic and Atomic Collisions, Belgrade, Yugoslavia, July 16–20, 1973. Abstracts of Papers, pp. 567–568.

J. L. Dehmer and Dan Dill. Calculation of Continuum Molecular Wavefunction Based on the Multiple Scattering Model. Bull. Am. Phys. Soc. 18, 1531 (1973).

J. L. Dehmer and J. Berkowitz. Wavelength Dependence of the $^2D_{5/2}$:$^2D_{3/2}$ Branching Ratio of Hg between 584 Å and 256 Å. Bull. Am. Phys. Soc. 19, 82 (1974).

R. H. Huebner, R. J. Celotta, S. R. Mielczarek, and C. E. Kuyatt. Oscillator Strength Values Derived from Electron Energy-Loss Spectra of Molecules. 8th Int. Conf. on Physics of Electronic and Atomic Collisions, Belgrade, Yugoslavia, July 16–20, 1973. Abstracts of Papers, p. 435.

Yong-Ki Kim, Mitio Inokuti, and R. P. Saxon. Slow Electrons Ejected from Rare Gas Atoms by Fast Charged Particles. 8th Int. Conf. on Physics of Electronic and Atomic Collisions, Belgrade, Yugoslavia, July 16–20, 1973. Abstracts of Papers, p. 688.

Yong-Ki Kim. Dipole Contribution in Energy Distribution of Secondary Electrons. Bull. Am. Phys. Soc. 19, 70 (1974).

Michio Matsuzawa. Ionization of Highly Excited Atoms by Collision with Molecules. 8th Int. Conf. on Physics of Electronic and Atomic Collisions, Belgrade, Yugoslavia, July 16–20, 1973. Abstracts of Papers, pp. 605–606.

Michio Matsuzawa. Step-Like Structure in the n-Dependence of Collisional Ionization of a Highly Excited Atom A** by a Polar Diatomic Molecule M. Bull. Am. Phys. Soc. 19, 69–70 (1974).

Michio Matsuzawa. n and ℓ Dependence of Electron Transfer from a Highly Excited (n,ℓ) Atom to SF_6. Bull. Am. Phys. Soc. 19, 160 (1974).

R. P. Saxon, Mitio Inokuti, and J. L. Dehmer. Systematics of the Total Cross Section for Inelastic Scattering of Fast Charged Particles by Atoms of the First and Second Row. 8th Int. Conf. on Physics of Electronic and Atomic Collisions, Belgrade, Yugoslavia, July 16–20, 1973. Abstracts of Papers, pp. 302–303.

David Spence and W. A. Chupka. Resonances in the Scattering of Electrons by Atomic Oxygen. Bull. Am. Phys. Soc. 18, 1505 (1973).

David Spence. Electron Transmission Spectroscopy in Molecular Chlorine. Bull. Am. Phys. Soc. 19, 71 (1974).

David Spence and G. J. Schulz. Cross Sections for Production of O_2^- and C^- by Dissociative Electron Attachment in Carbon Dioxide. 8th Int. Conf. on Physics of Electronic and Atomic Collisions, Belgrade, Yugoslavia, July 16–20, 1973. Abstracts of Papers, p. 467.

T. E. H. Walker, J. L. Dehmer, and J. Berkowitz. He I Photoelectron Spectra of the Cesium Halide Vapors. 8th Int. Conf. on Physics of Electronic and Atomic Collisions, Belgrade, Yugoslavia, July 16–20, 1973. Abstracts of Papers, pp. 559–560.